

Aus dem Comprehensive Pneumology Center (CPC) /
Institute of Lung Biology and Disease (ILBD)
Helmholtz Zentrum München

Kommissarischer Direktor: Dr. Önder Yildirim

Adaptive mitochondrial regulation of the proteasome



Dissertation
zum Erwerb des Doktorgrades der Naturwissenschaften
an der Medizinischen Fakultät der
Ludwig-Maximilians-Universität zu München

vorgelegt von

Thomas Meul

aus Rosenheim

2020

Mit Genehmigung der Medizinischen Fakultät
der Universität München

Betreuerin: Prof. Dr. rer. nat. Silke Meiners

Zweitgutachter: PD Dr. rer. nat. Kai Hell

Dekan: Prof. Dr. med. dent. Reinhard Hickel

Tag der mündlichen Prüfung: 25.02.2021

Eidesstattliche Versicherung

Ich, Thomas Friedrich Wilhelm Meul, erkläre hiermit an Eides statt, dass ich die vorliegende Dissertation mit dem Thema

„Adaptive mitochondrial regulation of the proteasome“

selbstständig verfasst, mich außer der angegebenen keiner weiteren Hilfsmittel bedient und alle Erkenntnisse, die aus dem Schrifttum ganz oder annähernd übernommen sind, als solche kenntlich gemacht und nach ihrer Herkunft unter Bezeichnung der Fundstelle einzeln nachgewiesen habe.

Ich erkläre des Weiteren, dass die hier vorgelegte Dissertation nicht in gleicher oder in ähnlicher Form bei einer anderen Stelle zur Erlangung eines akademischen Grades eingereicht wurde.

München, 25.03.2021

Thomas Meul

Ort, Datum

Unterschrift



Table of contents

Eidesstattliche Versicherung	II
Table of contents	IV
Summary	VIII
Zusammenfassung	X
1 Introduction	1
1.1 Protein homeostasis in the cell	1
1.2 The proteasome system	3
1.2.1 Proteasome structure and function	3
1.2.2 Regulation of 20S activity.....	7
1.2.3 Regulation of 26S proteasome activity and assembly	9
1.3 Mitochondria – key metabolic organelles	15
1.3.1 Structure and function.....	15
1.3.2 TCA cycle and oxidative phosphorylation	17
1.3.3 Mitostress signaling.....	21
1.3.4 Mitochondrial models of respiratory chain dysfunction.....	22
1.4 Mitochondria-to-proteasome signaling	23
2 Aims	27
3 Materials	29
3.1 Antibodies	29
3.1.1 Primary antibodies.....	29
3.1.2 Secondary Antibodies	30
3.2 Oligonucleotides	30
3.2.1 Primers for quantitative RT-PCR.....	30
3.2.2 siRNAs	31
3.3 Cell culture	31
3.3.1 Cell lines.....	31
3.3.2 Primary human lung fibroblasts.....	31
3.3.3 Primary human skin fibroblasts	31
3.3.4 Cell culture media.....	32
3.4 Drugs and treatments	32

3.5	Enzymes	32
3.6	Kits	32
3.7	Markers	33
3.8	Buffer formulations	33
3.9	Reagents	34
3.10	Chemicals	35
3.11	Consumables	36
3.12	Technical devices and further equipment	36
3.13	Software	37
4	Methods	39
4.1	Cell culture	39
4.1.1	Cultivation of mammalian cells.....	39
4.1.2	Cell harvest.....	39
4.1.3	Treatment of cells.....	40
4.1.4	Cell proliferation assay.....	41
4.1.5	Measurement of nascent protein synthesis.....	41
4.1.6	siRNA mediated gene silencing.....	42
4.2	Protein biochemistry	42
4.2.1	Protein extraction from cells.....	42
4.2.2	Bicinchoninic acid (BCA) assay.....	43
4.2.3	Western blot analysis.....	43
4.2.4	Native gel electrophoresis.....	44
4.2.5	Proteasome activity assay with luminescent substrates.....	44
4.2.6	Labeling of active proteasome complexes with activity-based probes (ABPs)	45
4.3	Mass spectrometry analysis	46
4.3.1	Proteomics screen	46
4.3.2	Phosphoproteomics screen	47
4.3.3	Metabolomics screen.....	48
4.4	Nucleic acid biochemistry	48
4.4.1	Quantitative real-time RT-PCR.....	48
4.4.2	Bulk mRNA sequencing.....	49
4.5	Characterization of mitochondria	49
4.5.1	Isolation of functional mitochondria	49
4.5.2	Electron microscopy.....	50
4.5.3	Quantification of mitochondrial volume.....	50
4.6	Statistical analysis	51

5	Results.....	53
5.1	Mutator MEFs with chronic mitochondrial dysfunction maintain functions required for cellular viability	53
5.2	Proteasome activity and assembly is impaired in mutator MEFs with chronic mitochondrial dysfunction	55
5.3	Respiratory chain complex I deficiency leads to diminished aspartate biosynthesis in mutator MEFs.....	58
5.4	Aspartate deficiency causes global cellular alterations in mutator MEFs including protein synthesis.....	65
5.5	Aspartate supplementation activates proteasome activity and protein synthesis in mutator MEFs.....	68
5.6	Aspartate supplementation induces 26S proteasome complex assembly by the expression of specific proteasome assembly factors	75
5.7	Aspartate activates several signaling pathways in mutator MEFs including mTOR.....	80
5.8	Aspartate induced mTOR signaling is linked to reactivation of proteasome activity and assembly in mutator MEFs.....	83
5.9	Defective complex I function drives metabolic adaption of the proteasome in human cells.....	87
5.10	Pharmacological inhibition of respiratory chain complex I in murine and human cells phenocopies chronic conditions in mutator cells.....	88
5.11	Immunoproteasome dependent antigen presentation is induced in mutator MEFs with complex I deficiency	93
6	Discussion	99
6.1	Respiratory chain complex I deficiency causes metabolic reprogramming and impaired aspartate biosynthesis	99
6.2	Downregulation of protein synthesis and impaired 26S proteasome function in respiration defective cells.....	102
6.3	26S proteasome assembly is reactivated by aspartate mediated induction of protein synthesis in cells with complex I deficiency	105
6.4	Aspartate activates proteasome assembly via expression of specific assembly factors.....	109
6.5	Reactivation of 26S proteasome assembly and activity depends on aspartate induced mTORC1 signaling in mutator MEFs.....	112

6.6	Chronic mitochondrial dysfunction in mutator MEFs induces immunoproteasome expression and MHC I antigen presentation.....	114
7	Concluding remarks.....	117
8	References	119
	List of abbreviations	135

Summary

Cellular proteostasis describes all processes, which are involved in synthesis, folding and degradation of proteins. The balance between protein translation and degradation is strictly regulated in the cell to ensure its viability. For this purpose, the activity of the protein synthesis and degradation machinery can be adapted according to cellular needs. Disturbance of proteostasis leads for example to accumulation of misfolded or damaged proteins in the cell and is linked to aging and conformational diseases (proteinopathies) such as neurodegenerative, cardiovascular and pulmonary diseases. The ubiquitin-proteasome system plays a central role for the balanced protein turnover in the cell as it is responsible for the degradation of up to 80 % of all cellular proteins. The proteasome is a large protein complex, with catalytically active cleavage sites located within the 20S core proteasome. Ubiquitin-dependent degradation of folded proteins is mainly performed by the 26S proteasome, which is formed by the assembly of 20S core particle and 19S regulatory particles. Assembly and activity of the 26S proteasome are fine-tuned according to cellular needs such as growth and differentiation. Regulation of protein synthesis via the mammalian target of rapamycin (mTOR) has for example direct effects on 26S proteasome function. As 26S proteasome function is strictly dependent on energy in form of ATP, mitochondria – the powerhouses of the cell – are also involved in the regulation of protein degradation by the proteasome. Additionally, reactive oxygen species (ROS), which are mainly produced by dysfunctional mitochondria, negatively influence 26S proteasome assembly and activity. However, mitochondria are not only the main source of cellular ATP and ROS but also provide important metabolites and precursors generated by the tricarboxylic acid cycle (TCA), which are involved in central cellular processes such as proliferation.

While a variety of regulatory mechanisms for protein translation and 26S proteasome mediated protein degradation have already been described, a metabolic regulation of cellular proteostasis mediated by mitochondria has not been demonstrated so far. Therefore, the main focus of the present study was to dissect a possible connection between mitochondrial metabolism and cellular proteostasis. For that three different models for mitochondrial respiratory chain dysfunction were used: mouse embryonic fibroblasts (MEFs) derived from the so-called mtDNA mutator mouse model, primary human skin fibroblasts with a mutation in the ND5 subunit of respiratory chain complex I and primary human skin

and lung fibroblasts treated with the complex I inhibitor and anti-diabetic drug metformin. The different models are all characterized by respiratory chain complex I deficiency in the absence of increased ROS production. Cells maintained cellular viability and did not show signs of severe stress despite respiratory chain dysfunction. Mitochondrial complex I deficiency in mutator MEFs caused metabolic reprogramming of the TCA cycle resulting in diminished aspartate biosynthesis. Reduced aspartate levels caused downregulated proteostasis as both protein translation and 26S proteasome assembly and activity was decreased in respiration deficient cells but could be rescued by supplementation of aspartate. Furthermore, aspartate supplementation induced mTORC1 mediated protein synthesis and mTORC1-dependent transcriptional activation of defined proteasome assembly factors, which were involved in activation of 26S proteasome assembly and activity in cells with complex I deficiency. Similar data were obtained in ND5 mutant skin fibroblasts and upon metformin treatment. In contrast to diminished proteasome function, chronic respiratory chain impairment in mutator MEFs led to strongly induced immunoproteasome expression and activity. Upregulation of the immunoproteasome was accompanied by increased MHC class I antigen presentation during chronic mitochondrial dysfunction representing a so far unknown stress response which may probably serve to alert the immune system. This finding requires further analysis.

These results thus uncover a novel concept of how mitochondrial metabolism adaptively adjusts protein synthesis and degradation by the proteasome to the metabolic condition of the cell. These data extend the knowledge about proteasomal regulation in the cell and have therapeutic implications for diseases and drug-targeted mitochondrial reprogramming.

Zusammenfassung

Die zelluläre Proteostase beschreibt alle Prozesse, die an der Synthese, Faltung und dem Abbau von Proteinen beteiligt sind. Das Gleichgewicht zwischen Proteintranslation und -abbau wird in der Zelle streng reguliert, um ihre Lebensfähigkeit zu gewährleisten. Zu diesem Zweck kann die Aktivität der Proteinsynthese- und Abbaumaschinerie entsprechend den zellulären Bedürfnissen angepasst werden. Eine Störung der Proteostase führt z.B. zur Akkumulation fehlgefalteter oder beschädigter Proteine in der Zelle und wird mit Alterung und Proteinfehlfaltungskrankheiten (Proteinopathien) wie neurodegenerativen, kardiovaskulären und Lungenerkrankungen in Verbindung gebracht. Das Ubiquitin-Proteasom-System spielt eine zentrale Rolle für einen ausgeglichenen Proteinumsatz in der Zelle, da es für den Abbau von bis zu 80 % aller zellulären Proteine verantwortlich ist. Das Proteasom ist ein großer Proteinkomplex mit katalytisch aktiven Untereinheiten, die sich innerhalb des 20S-Kern-Proteasoms befinden und die Spaltung von Proteinen in Peptide durchführen. Der Ubiquitin-abhängige Abbau gefalteter Proteine erfolgt hauptsächlich durch das 26S-Proteasom, das durch den Zusammenbau von 20S-Kern-Proteasom und 19S-Regulator gebildet wird. Assemblierung und Aktivität des 26S-Proteasoms sind auf die zellulären Bedürfnisse wie Wachstum und Differenzierung abgestimmt. Die Regulation der Proteinsynthese über den mTOR Signalweg hat zum Beispiel direkte Auswirkungen auf die Funktion des 26S-Proteasoms. Da die Funktion des 26S-Proteasoms strikt von Energie in Form von ATP abhängig ist, sind auch die Mitochondrien - die Kraftwerke der Zelle - an der Regulation des Proteinabbaus durch das Proteasom beteiligt. Zusätzlich beeinflussen reaktive Sauerstoffspezies (ROS), die hauptsächlich von dysfunktionalen Mitochondrien produziert werden, den Aufbau und die Aktivität des 26S-Proteasoms negativ. Mitochondrien sind jedoch nicht nur die Hauptquelle von zellulärem ATP und ROS, sondern liefern auch wichtige Metaboliten und Vorläufermoleküle, die aus Zwischenprodukten des Citratzyklus gebildet werden und an zentralen zellulären Prozessen wie der Proliferation beteiligt sind.

Während eine Vielzahl von regulatorischen Mechanismen für Proteintranslation und 26S-Proteasom-vermittelten Proteinabbau bereits beschrieben wurde, konnte eine metabolische Regulation der zellulären Proteostase, die durch Mitochondrien vermittelt wird, bisher nicht nachgewiesen werden. Der Fokus der vorliegenden Studie lag daher auf der Aufklärung eines

möglichen Zusammenhangs zwischen mitochondrialem Metabolismus und zellulärer Proteostase. Dazu wurden drei verschiedene Modelle mitochondrialer Atmungskettendysfunktion verwendet: murine embryonale Fibroblasten (MEF), die aus dem so genannten mtDNA-Mutator-Mausmodell stammen, primäre menschliche Hautfibroblasten mit einer Mutation in der Untereinheit ND5 des Atmungskettenkomplexes I und primäre menschliche Haut- und Lungenfibroblasten, die mit dem Komplex-I-Inhibitor und Antidiabetikum Metformin behandelt wurden. Die verschiedenen Modelle sind alle durch ein Defizit an funktionalem Komplex I der Atmungskette gekennzeichnet, das nicht mit erhöhter ROS-Produktion verbunden ist. Die Zellen erhielten überlebenswichtige Prozesse aufrecht und zeigten keine Anzeichen von schwerem Stress trotz dysfunktionaler Atmungskette. Das mitochondriale Komplex-I Defizit in Mutator MEFs verursachte eine metabolische Umprogrammierung des TCA-Zyklus, was zu einer verminderten Aspartat-Biosynthese führte. Reduzierte Aspartatspiegel verursachten eine herunterregulierte Proteostase, da sowohl die Proteintranslation als auch die 26S-Proteasom-Assemblierung und -Aktivität in Respirations-defizienten Zellen vermindert war. Behandlung der Zellen mit Aspartat konnte die verminderte Proteostase jedoch reaktivieren. Darüber hinaus induzierte eine Supplementierung mit Aspartat mTORC1-vermittelte Proteinsynthese und mTORC1-abhängige transkriptionelle Aktivierung definierter Proteasom-Assemblierungsfaktoren, die in Zellen mit Komplex-I-Defizit an der Aktivierung der 26S-Proteasom-Assemblierung und -Aktivität beteiligt waren. Ähnliche Effekte wurden in ND5-mutierten Hautfibroblasten und bei der Behandlung von Wildtyp Zellen mit Metformin erzielt. Im Gegensatz zu einer verminderten Proteasomfunktion führte die chronische Beeinträchtigung der Atmungskette bei mutierten MEFs zu einer stark induzierten Expression und Aktivität des Immunproteasoms. Die Hochregulierung des Immunproteasoms ging während der chronischen mitochondrialen Dysfunktion mit einer erhöhten MHC I-Antigenpräsentation einher, was eine bisher unbekannte Stressantwort darstellt, die wahrscheinlich dazu dienen könnte, das Immunsystem zu alarmieren. Dieser Befund bedarf weiterer Analyse.

Aus diesen Ergebnissen kann also ein neuartiges Konzept abgeleitet werden, wie mitochondrialer Metabolismus Proteinsynthese und Proteinabbau durch das Proteasom adaptiv an den Stoffwechselzustand der Zelle anpasst. Diese Daten erweitern das Wissen über proteasomale Regulation in der Zelle und haben therapeutische Bedeutung für Pathologien und medikamentös gesteuerte mitochondriale Reprogrammierung.

1 Introduction

1.1 Protein homeostasis in the cell

Proteins or protein complexes exert the majority of vital cellular function such as provision of energy and proliferation. Therefore, the maintenance of protein turnover, which includes the correct synthesis and folding of proteins as well as their defined degradation in case of regulatory purposes or upon misfolding is essential for cellular viability (Figure 1.1) (Hipp et al., 2019; Klaips et al., 2018; Meiners and Ballweg, 2014; Powers and Balch, 2013). Disturbance of cellular protein homeostasis is associated with different diseases such as neurodegenerative diseases or fibrosis in the lung. In this context several stressors such as aging, environmental influences or genetic mutations have been identified to contribute to imbalanced protein homeostasis in the cell (Balch et al., 2014; Hipp et al., 2019; Klaips et al., 2018). Protein degradation in the cell is regulated by two proteolytic systems, which take over different functions during this process (Figure 1.1) (Hipp et al., 2019; Klaips et al., 2018; Meiners and Ballweg, 2014). The lysosome-autophagy pathway mainly removes hazardous protein aggregates or whole organelles whereas up to 80 % of the proteins synthesized in a cell are degraded by the ubiquitin-proteasome system. Thus, the proteasome is considered as a main component of cellular protein degradation (Collins and Goldberg, 2017; Wang et al., 2020). Besides its role in protein quality control and biosynthesis through the removal of misfolded proteins and the recycling of free amino acids the ubiquitin-proteasome system is also involved in important regulatory processes such as cell-cycle control during cellular growth, signal transduction, transcription, metabolic adaption or MHC class I antigen presentation in the context of an immune response (Ciechanover and Kwon, 2015; Collins and Goldberg, 2017; Wang et al., 2020).

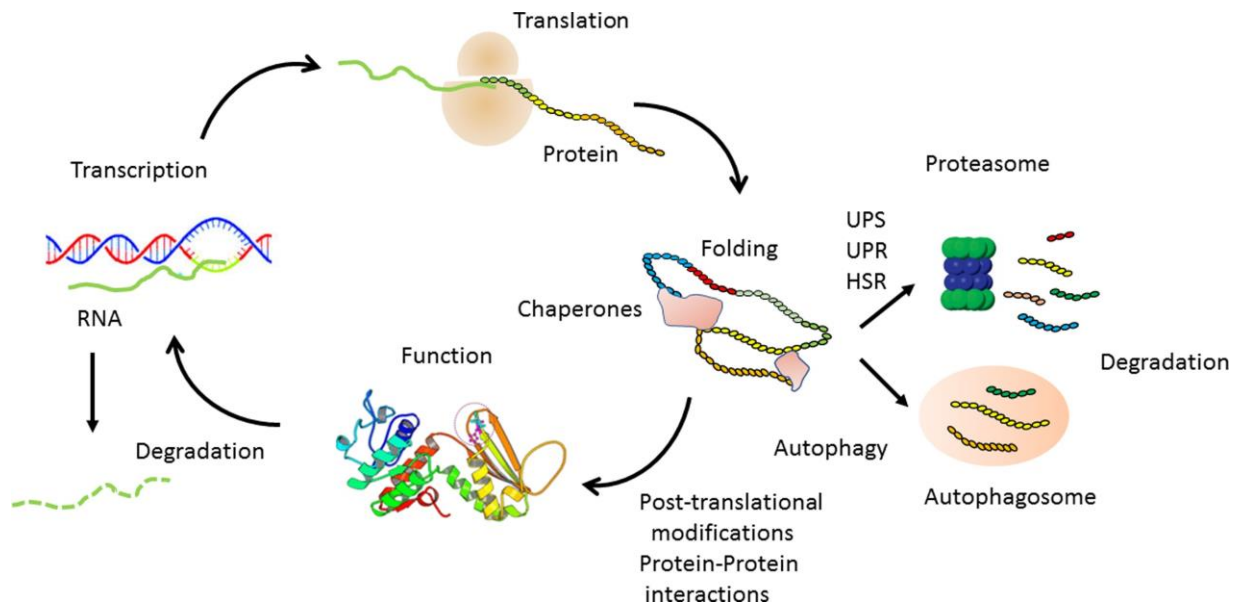


Figure 1.1: Cellular protein homeostasis. Cellular protein turnover defines the homeostasis between protein synthesis and degradation. This turnover involves the ribosomal synthesis of proteins as linear polypeptides, the folding into their native structure often assisted by chaperones and the degradation of regulatory, misfolded and damaged proteins or dysfunctional protein aggregates via the ubiquitin-proteasome system or the lysosome-autophagy pathway. Proteolysis both by the proteasome and the lysosome allows recycling of amino acids for new protein synthesis (taken from Grandi and Bantscheff, 2019).

To maintain protein homeostasis in the cell a tightly regulated interplay between protein synthesis and protein degradation is required. The mammalian target of rapamycin (mTOR) has been identified as a key player for the regulation of proteostasis. mTOR induced activation of protein synthesis leads to an activation of the ubiquitin-proteasome system by transcriptional activation of proteasomal gene expression to cope with the increased amounts of translated proteins (Zhang and Manning, 2015; Zhang et al., 2014). An acute block of protein translation via the inhibition of mTOR activates 26S proteasome assembly. However, in this case increased protein turnover is believed to support protein synthesis with the supply of amino acids (Rousseau and Bertolotti, 2016; Zhao et al., 2015).

1.2 The proteasome system

1.2.1 Proteasome structure and function

1.2.1.1 The standard proteasome

The proteasome is an evolutionary highly conserved self-compartmentalized protease complex with a molecular weight of 2.5 MDa, which is present in all eukaryotic cells and is localized both in the cytoplasm and the nucleus. It is formed by the so-called 20S core particle (CP) and different regulators, which mediate substrate recognition and gating into the 20S core particle where degradation of the linearized proteins into peptides is executed (Bard et al., 2018; Collins and Goldberg, 2017; Wang et al., 2020).

The core proteasome itself exhibits a barrel-like structure and consists of four stacked heptameric rings arranged in $\alpha\beta\alpha$ symmetry. Each of the two inner rings is built by seven β subunits (β 1-7) whereas each of the two outer rings is composed of seven α subunits (α 1-7), which seal the entry port of the core proteasome with their interlacing N-terminal regions to avoid unwanted protein degradation (Figure 1.3) (Groll et al., 1997, 2000).

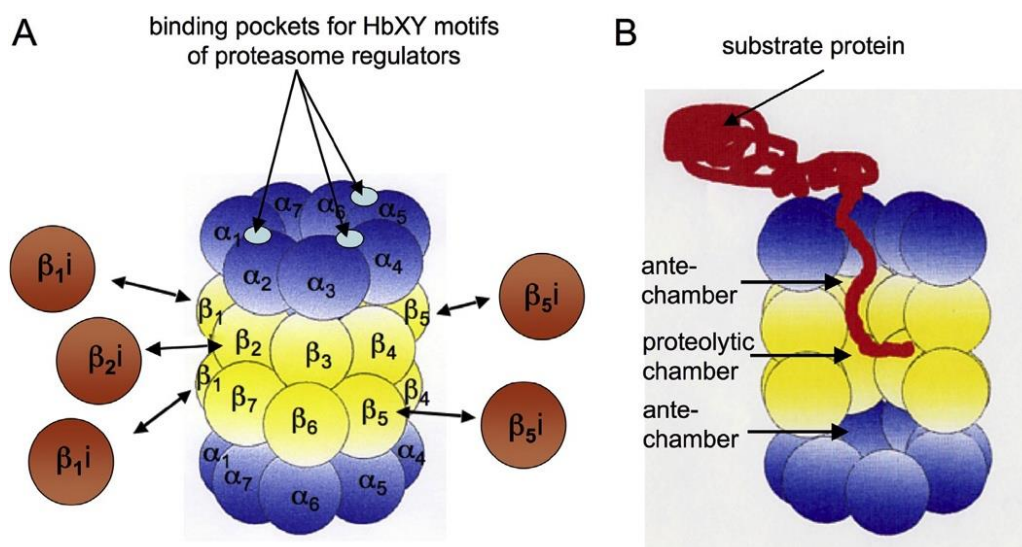


Figure 1.2: Structure and subunit composition of the 20S core particle. The 20S core particle exhibits a barrel-like architecture and is built up by 4 heptameric rings arranged as two outer α - and two inner β rings. The α rings are assembled of the subunits α 1-7 and the β rings are formed by the subunits β 1-7. Proteolysis is located inside the barrel and is performed by the three β -subunits β 1, β 2 and β 5. In the immunoproteasome the three active sites are replaced by the alternative β -subunits β 1i, β 2i and β 5i, which show different cleavage specificities than the standard β -subunits. The α -subunits seal the entry pores of the 20S core particle and provide binding pockets for different proteasome regulators, which are necessary for substrate recognition and opening of the entry pores for degradation by the 20S proteasome (Taken from Dahlmann, 2016).

The proteolytic activity of the proteasome resides inside the barrel and is mediated by the three β -subunits β 1, β 2 and β 5. These subunits are synthesized as inactive propetides to prevent premature proteolysis during the chaperone-assisted 20S assembly and have to be activated auto-proteolytically upon maturation of the 20S core particle. The assembly of the 20S core particle is mediated by the proteasome assembly chaperones (PACs) POMP1 and PAC1-4/PSMG1-4 (Wang et al., 2020). The three active sites extend into the cavity of the 20S proteasome and are therefore able to degrade incoming protein chains into smaller peptides according to their different cleavage specificities. Substrates are preferentially cleaved after acidic amino acids by the β 1-subunit (caspase-like (C-L) activity) and after basic residues by β 2 (trypsin-like (T-L) activity). The β 5-subunit mainly generates peptides with hydrophobic termini and is therefore also named chymotrypsin-like (CT-L) activity. Since the proteasome only generates peptides with a length from 3 to 22 residues cytoplasmic peptidases finish the recycling of proteins into single amino acids (Borissenko and Groll, 2007; Murata et al., 2009).

1.2.1.2 The immunoproteasome

While the described standard proteasome is constitutively expressed in all cell types, a second set of proteasomes containing distinct catalytic β -subunits has been identified in cells of hematopoietic origin. This so-called immunoproteasome is structurally identical to the standard proteasome except for the three catalytically active sites: Here, β 1, β 2, and β 5 are substituted by three alternative catalytic immunosubunits, that is, low molecular mass protein (LMP) 2 (β 1_i), multicatalytic endopeptidase complex-like 1 (MECL-1 or β 2_i), and LMP7 (β 5_i) (Groettrup et al., 2010) (Figure 1.2). These immunosubunits are incorporated during proteasome neosynthesis and are characterized by altered cleavage preferences compared to β 1, β 2, and β 5, which is caused by structural changes in the substrate binding pockets of the active sites (Huber et al., 2012). The replacement of β 1 by LMP2 leads, for example, to a strong reduction in post-acidic cleavage activity resulting in a pool of peptides with mainly hydrophobic C-termini, which match the binding requirements of MHC class I molecules much better than antigens generated by the standard proteasome (Groettrup et al., 2001). In contrast to immune cells, which exhibit high basal levels of immunoproteasomes, the expression of immunosubunits can be induced in non-immune cells by pro-inflammatory

cytokines such as interferon (IFN)- γ or tumor necrosis factor (TNF)- α secreted for example by activated cytotoxic CD8⁺ T cells during intracellular infection (Groettrup et al., 2001). The immunological benefit of immunoproteasomes in infected cells is to quantitatively and qualitatively improve MHC class I antigen presentation which facilitates the activation of pathogen-specific CD8⁺ T cells to eliminate infected cells and thus limit pathogen replication (Figure 1.3). This was experimentally shown by using proteasome inhibitors or knockout mice deficient in single or all immunosubunits (Basler et al., 2010; Kincaid et al., 2012; De Verteuil et al., 2010). IFN- γ - or TNF- α -induced expression of immunosubunits is accompanied by an upregulation of the proteasome activator PA28 α/β , which has been shown to be preferentially associated with immunoproteasomes than with standard proteasomes after stimulation with pro-inflammatory cytokines (Fabre et al., 2014) (Figure 1.3). Furthermore, the binding of this regulator to the immunoproteasome is supposed to have a strong impact on the quality and quantity of antigenic peptides generated resulting in a broader repertoire of MHC class I ligands. However, the mechanism which underlies the PA28 α/β -mediated change in the cleavage specificity of the immunoproteasome is not conclusively defined (Raule et al., 2014).

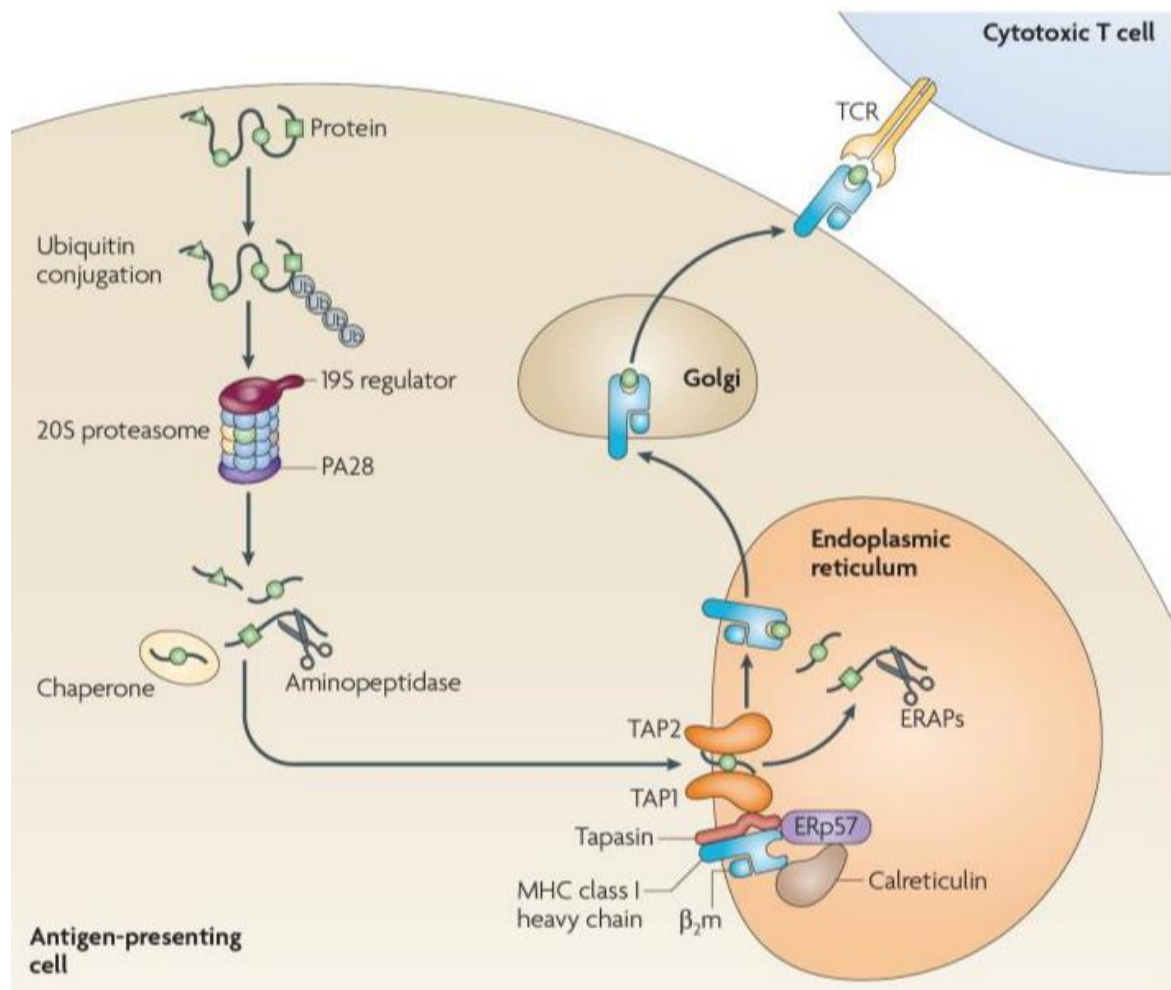


Figure 1.3: MHC I processing and presentation. Ubiquitinated proteins are degraded either by the standard- or the immunoproteasome to generate peptides, which fit the MHC I receptor. Immunoproteasomes have different cleavage preferences compared to standard proteasomes and produce peptides, which bind the MHC I receptor more efficiently. Proteasome derived peptides are trimmed by cytosolic peptidases and imported into the ER via the so-called TAP transporter. The MHC I complex is composed of different subunits and formed in the ER. The peptide is further trimmed by peptidases (ERAPs) and then binds to the MHC complex. The pre-made receptor is transported to the cell surface and presents the peptide to the immune system (taken from Groettrup et al., 2010).

1.2.2 Regulation of 20S activity

20S activity can be modulated on different levels such as the expression of proteasome subunits or the association of the 20S core particle with proteasome regulators. Expression of proteasomal subunits is mediated by at least two different transcription factors: nuclear factor erythroid-derived – related factor (NRF)1 and NRF2. These transcription factors activate the expression of proteasome subunits during starvation, oxidative stress or oncogenic proliferation to increase the proteolytic capacity of the cell (Digaleh et al., 2013; Koizumi et al., 2018; Walerych et al., 2016; Wang et al., 2020; Zhang et al., 2014). Stoichiometric requirements for the structure of 20S proteasomes lead to regulation of 20S assembly by the expression level of α and β subunits. For example, the 20S subunit α 4/PSMA7 has been shown to be rate-limiting for 20S core particle formation (Li et al., 2015). Furthermore, 20S assembly and activity can be suppressed by targeting the 20S assembly chaperone POMP1 (Zhang et al., 2015).

The 20S proteasome has only a low activity in its closed conformation and is unable to degrade large and folded proteins since the access to the 20S core particle is limited by the α ring subunits (Groll et al., 2000). However, there is increasing evidence that the 20S core particle is able to degrade partially or completely unfolded proteins (Aiken et al., 2011; Pickering and Davies, 2012; Wang et al., 2020). Additionally, native proteins with intrinsically disordered regions (IDRs) or substrates showing completely disordered regions have been found to be degraded by uncapped 20S proteasomes (Van Der Lee et al., 2014). Examples for intrinsically disordered proteins (IDPs) are signaling and regulatory factors, which are involved in growth control or oncogenesis (Dyson and Wright, 2005). Under oxidative conditions the 20S proteasome is able to maintain its activity in comparison to the more unstable 26S proteasome (Livnat-Levanon et al., 2014). Therefore, the majority of catalytic activity is provided by the 20S core particle under such conditions (Farout and Friguet, 2006; Wang et al., 2020). In total, about 20 % of the cellular protein content is assumed to be degraded by the 20S proteasome (Ben-Nissan and Sharon, 2014; Wang et al., 2020).

In addition to substrate degradation in its free conformation, the core particle is assisted by different proteasome activators that are recruited to and bind to the 20S proteasome at both sides of the barrel. Bound to the 20S core particle they determine the substrate specificity by

recognizing and binding the target proteins and modulate the turnover rate by controlling the opening of the 20S entry pores (Figure 1.4) (Stadtmueller and Hill, 2011). Currently, four different activators have been discovered, which can be grouped into ATP-dependent and -independent activators (Stadtmueller and Hill, 2011). The proteasome activator of 700 kD (PA700) or 19S regulatory particle is required for ATP-dependent degradation of folded and ubiquitinated proteins. It binds to either one or both sides of the 20S core particle forming singly and doubly capped 20S core particles, which are named 26S and 30S proteasomes (Finley, 2009).

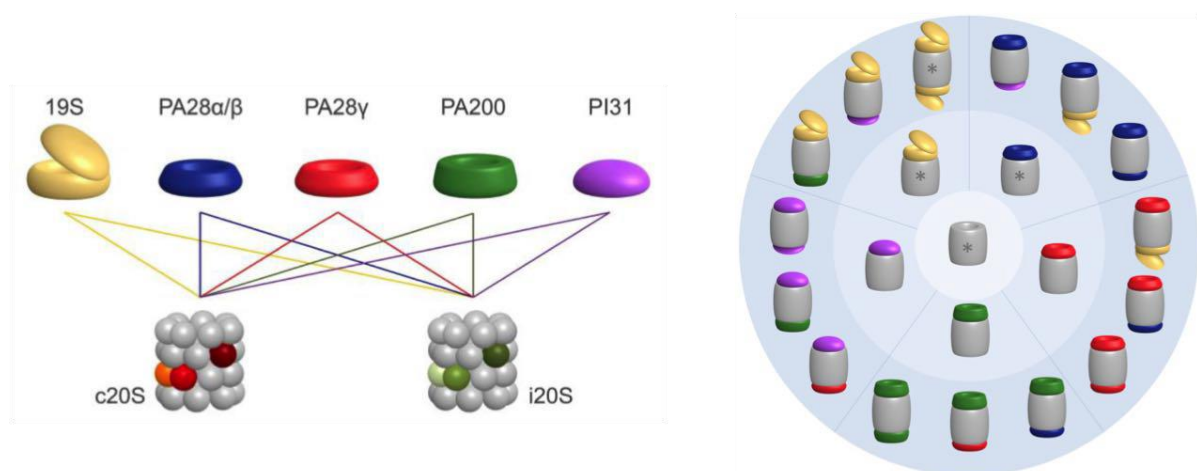


Figure 1.4: Regulators of 20S proteasome activity: Since the naked 20S core proteasome is unable to degrade large and folded proteins it is dependent on different regulators for the degradation of large and folded proteins. These regulators can bind to either one or both sides of the standard 20S core particle or the immunoproteasome and thereby determine proteasome substrate specificity and turnover. Until now four different types of proteasomal regulators have been identified. The 19S regulatory particle, the two 11S members PA28 $\alpha\beta$ and PA28 γ and PA200 have been shown to function as activators of proteasomal activity whereas PI31 shows an inhibitory influence on the proteasome (taken from Meiners et al., 2014, modified).

In addition to the 19S regulatory particle three further alternative activators have been identified until now. PA28 $\alpha\beta$, PA28 γ and PA200 can modify the activity of the 20S core particle independent of ubiquitin and ATP (Stadtmueller and Hill, 2011). The heteromeric interferon- γ or LPS induced PA28 $\alpha\beta$ complex is able to increase the generation of peptides in the proteasome appropriate for antigen presentation during the immune response whereas PA28 γ has been reported to promote the ubiquitin-independent degradation of distinct nuclear proteins involved in cell-cycle control and intracellular dynamics (Cascio, 2014; Li and Rechsteiner, 2001). PA200 is the most recently discovered proteasome activator and less is known about its specific cellular functions. Beside the described proteasome activators a further proteasome regulator has recently been discovered which is called PI31. In contrast

to the activators it is suggested to function as an inhibitor of proteasomal activity (Li et al., 2014).

The recruitment of different proteasomal activators and the binding to either one or both sides of the 20S core particle leads to the formation of a diverse set of alternative proteasome complexes including singly and doubly capped 20S proteasomes but also hybrid complexes consisting of different activators attached to the 26S proteasome (Figure 1.4). According to the so-called building block theory the cell is able to adapt the proteasome activity to different challenges by fast recruitment of preexisting activators to and assembly with the 20S core particle without the need for an increased expression of these activators. The newly formed complexes may then have diverse functions and substrate specificities appropriate for the temporary cellular needs (Lokireddy et al., 2015; Schmidt and Finley, 2013; Wang et al., 2020). This building block theory was recently supported by work from our lab: Welk et al. (2016) showed that the activators PA200 and PA28y are quickly recruited to the 20S proteasome from a preexisting pool after proteasome inhibition with catalytic proteasome inhibitors thereby possibly contributing to a protective cellular response upon proteasome inhibition (Welk et al., 2016).

1.2.3 Regulation of 26S proteasome activity and assembly

1.2.3.1 The 19S regulatory particle

The 19S regulatory particle is the most extensively studied proteasome regulator and has two important tasks during ATP-dependent protein degradation by the proteasome. On the one hand it is responsible for the recognition of polyubiquitinated substrates and on the other hand it is essential for ATP driven substrate unfolding, 20S gate opening and injection of the protein into the 20S catalytic chamber. In order to fulfill its functional requirements the 19S regulator is composed of two different structural parts. The 19S lid consists of 10 non-ATPase (Rpt) subunits and is responsible for the deubiquitination of target proteins. The 19S base is formed by 9 ATPase (Rpn) subunits and is bound to the α ring subunits shielding the 20S entry pore from the surrounding environment. It is arranged in an ATPase ring-like structure executing the substrate recognition and the ATP-dependent unfolding and translocation of the protein (Bard et al., 2018).

The assembly of the 19S regulatory particle occurs in two independent steps: base and lid assembly. While the lid is suggested to self-assemble via a helical bundle of C-terminal helices provided by the lid subunits, the base is built up with the assistance of five so-called 19S regulatory particle assembly chaperones in a complex multistep reaction (Estrin et al., 2013; Förster et al., 2009; Roelofs et al., 2009; Tomko et al., 2010). Finally, the 19S regulatory particle is formed by the assembly of 19S lid and base (Figure 1.5).

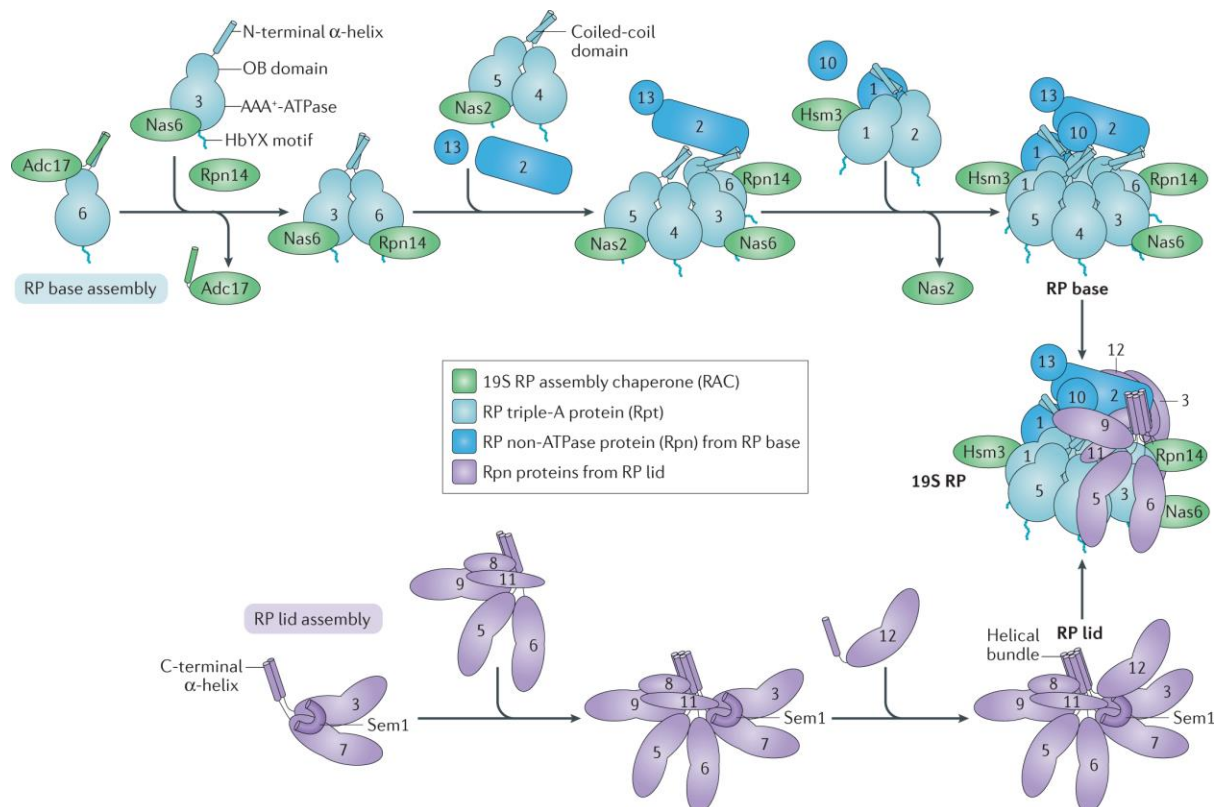


Figure 1.5: 19S regulatory particle assembly in yeast. The 19S regulatory particle is assembled in a complex multistep reaction. Base and lid are first built up independently and finally associate to form the mature 19S regulatory particle. While the assembly of the 19S base is assisted by five so-called assembly chaperones the formation of the lid occurs spontaneously by self-assembly (taken from Rousseau and Bertolotti, 2018).

The assembly chaperone Adc17 is only found in yeast whereas Nas6, Rpn14, Nas2 and Hsm3 have human homologues called p28/PSMD10, PAAF-1, p27/PSMD9 and S5b/PSMD5 (Rousseau and Bertolotti, 2018). None of the assembly chaperones is essential for the cell but a concerted downregulation of these 19S subunits leads to decreased 26S proteasome activity and assembly (Kaneko et al., 2009; Rousseau and Bertolotti, 2016). For some of these assembly chaperones additional cellular functions have been identified. For example, p28/PSMD10, which is also called gankyrin, has been shown to act as an oncoprotein by regulating cyclin-dependent kinase 4 and the degradation of the tumor suppressors Rb and

p53 (Wang et al., 2016). S5b/PSMD5 has been found to inhibit 26S proteasome activity and assembly when overexpressed in the cell. In intestinal tumors S5b levels were decreased leading to upregulated 26S proteasome activity. In contrast, when S5b was overexpressed in these cancer cells 26S proteasome activity was inhibited (Levin et al., 2018).

1.2.3.2 The 26S proteasome

The formation of assembled 26S or 30S proteasome complexes is mediated by the interaction of HbXY motifs located in the C-terminus of 19S Rpt proteins and the 20S α pockets (Figure 1.3). The insertion of HbXY motifs into the α pockets of the 20S core particle induces conformational changes in the α rings to open the gate for incoming substrates. 19S regulatory particle and 20S proteasome associate spontaneously *in vitro* (Liu et al., 2006; Livnat-Levanon et al., 2014). The whole assembly process of the 26S proteasome is fully reversible (Bajorek et al., 2003; Kleijnen et al., 2007). As the interaction between 19S regulatory particle and the 20S core particle is rather weak, the assembled 26S proteasome is stabilized by the essential 19S subunit Rpn6/Psm11, which functions as a molecular clamp between 19S Rpt and 20S α subunits (Pathare et al., 2012). The importance of Rpn6 for cell survival has been shown in knockdown experiments where silencing of this essential subunit caused massive cell death. Partial knockdown of Rpn6 levels already led to a diminished amount and activity of 26S proteasome complexes. Contrary, overexpression of this assembly factor induced 26S proteasome assembly (Semren et al., 2015; Vilchez et al., 2012). The correct structure of the assembled 26S proteasome might also be regulated by additional factors such as Ecm29, which represses protein degradation by the proteasome in case of dysfunctional assembly (Lee et al., 2011; Lehmann et al., 2010; Panasenko and Collart, 2011).

Stability and activity of the assembled 26S proteasome is influenced by a variety of different factors. Several signaling molecules can interact with the 26S proteasome contributing either to stability or disassembly of proteasome complexes. ATP is not only required for protein unfolding by the 19S regulatory particle but has also been shown to act as a stabilizer of assembled 26S proteasome complexes (Liu et al., 2006; Smith et al., 2005). When ATP is not available, NADH can take over its stabilizing role by binding to 19S subunits and thereby prevents disassembly of 26S proteasome complexes. Consequently, an increased

NADH/NAD⁺ ratio was found to activate 26S proteasome complexes (Tsvetkov et al., 2014). Oxidative stress in the form of reactive oxygen species (ROS) causes 26S proteasome disassembly and a decrease of proteolytic activity (Livnat-Levanon et al., 2014; Segref et al., 2014; Yu et al., 2019). Additionally, downregulated protein levels of single 19S subunits have been shown to increase the amount of free 20S and to reduce 26S proteasome activity (Acosta-Alvear et al., 2015; Shi et al., 2017; Tsvetkov et al., 2015, 2017). Posttranslational modifications of proteasome subunits also play a role for 26S proteasome assembly and activity. An increasing number of different activating or inhibiting modifications has been identified so far. Phosphorylation of proteins is a very dynamic and important way of regulation in the cell. The proteasome is also phosphorylated at different 19S or 20S subunits in order to regulate its activity and assembly (Guo et al., 2017). Protein kinase A (PKA) was shown to reversibly phosphorylate the assembly factor Rpn6/PSMD11, which leads to upregulated 26S proteasome activity and assembly (Lokireddy et al., 2015; VerPlank et al., 2019). Cell cycle progression is regulated by phosphorylation of the 19S subunit Rpt3/PSMC4. This modification increases substrate translocation and thereby induces 26S proteasome activity (Guo et al., 2016). The 19S subunits Rpn1 was recently found to be phosphorylated as well. This reversible modification also regulates 26S proteasome activity and assembly in the cell (Liu et al., 2020). In contrast, tyrosine phosphorylation of the 20S subunit $\alpha 4$ has been identified as an inhibitor of proteasome activity. Additionally, other posttranslational modifications such as acetylation, carbonylation, ubiquitination or N-acetylglucosamylation can influence 26S proteasome activity and assembly (Kors et al., 2019). To regulate 26S proteasome activity on expression level, the cell uses the two transcription factors NRF1 and NRF2. Both factors have been shown to upregulate expression of 19S and 20S subunits under conditions of oxidative or proteotoxic stress (Ben-Nissan and Sharon, 2014; Wang et al., 2020).

1.2.3.3 Ubiquitination of proteins assigned for proteasome degradation

In a healthy cell all kinds of proteins such as damaged, unfolded, mutant, short-lived or regulatory ones are recycled by the ubiquitin-proteasome pathway via selective ATP-dependent or -independent degradation (Rock et al., 1994). In general, substrates assigned for degradation are tagged with ubiquitin molecules, which are then recognized and are degraded in an ATP-dependent manner by the 26S proteasome (Figure 1.2, see below)

(Finley, 2009). These ubiquitin chains are synthesized via a cascade of the three ubiquitin ligases E1, E2 and E3. E1 activates the ubiquitin molecule at its C-terminus with the help of ATP for its linkage to the cysteine of the E1 active site forming a high-energy thioester bond between E1 and ubiquitin. In the next step the ubiquitin molecule is transferred to the ubiquitin-conjugating enzyme E2. Finally, the activated ubiquitin molecule is conjugated to a lysine residue of the target substrate with the help of the protein ligase E3 leading to a covalent isobond between substrate and ubiquitin (Ciechanover, 2015). The so-called ubiquitin code describes the type of ubiquitination meaning mono- or polyubiquitinations and defines the amino acid, which is linked to the ubiquitin modification. The type of ubiquitination and the linkage site define the effect of the modification on the target protein during different cellular processes. For proteasomal degradation a lysine-48 (K48) linked polyubiquitin chain serves as the main signal for substrate recognition. Contrary, a branched ubiquitin chain linked to lysine-63 (K63) is known to be involved in protein kinase activation and DNA damage response. Polyubiquitination of lysine 11 (K11) plays a role in cell cycle control and ER associated degradation (ERAD). In addition to the named modification a large number of other types of ubiquitinations has been discovered with mainly regulatory functions (Komander and Rape, 2012; Saeki, 2017; Suresh et al., 2016). Furthermore, there are also substrates that are recognized and degraded by the proteasome independent of ubiquitin (Finley, 2009; Komander and Rape, 2012).

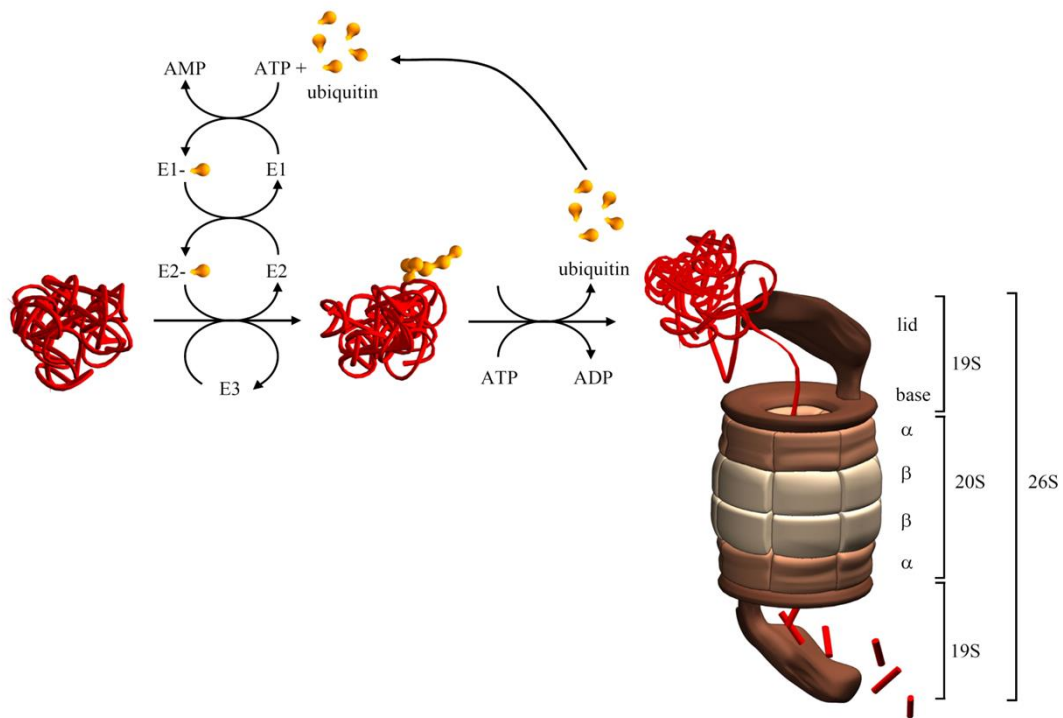


Figure 1.6: Proteolysis by the proteasome via ubiquitination of target proteins. Many proteins destined for proteasomal degradation are tagged with an ubiquitin chain, which is then recognized by the 26S proteasome. This ubiquitin chain is formed by an enzyme cascade composed of the ubiquitin ligases E1, E2 and E3 and removed before degradation of the protein in the proteasome (taken from Meiners et al., 2008).

1.3 Mitochondria – key metabolic organelles

1.3.1 Structure and function

Mitochondria are multifunctional organelles virtually present in every mammalian cell. These special organelles are evolutionary derived from α -proteobacteria, which have been consumed by early eukaryotes. The formed symbiosis enabled eukaryotes to use previously toxic oxygen for energy production in form of ATP (Gray et al., 1999; Herst et al., 2017). Therefore, one of the main tasks of mitochondria, which are also called “cellular powerhouses”, is provision of energy. However, so far a variety of additional functions essential for cellular viability have been identified (Figure 1.7). Beside energy production, mitochondria are complex signaling hubs, which mediate fundamental processes such as cellular apoptosis via cytochrome c release or anti-oxidant defense. Mitochondria also provide the cell with different biomolecules such as amino acids, lipids and nucleotide precursors produced via biosynthetic pathways. Important signaling pathways are regulated by mitochondrial reactive oxygen species (ROS) or Ca^{2+} molecules (Herst et al., 2017). Mitochondria are organized as comprehensive networks in the cell. The integrity of this network is ensured by a tightly regulated balance between mitochondrial fusion, fission, biogenesis and mitophagy (Herst et al., 2017; Nunnari and Suomalainen, 2012).

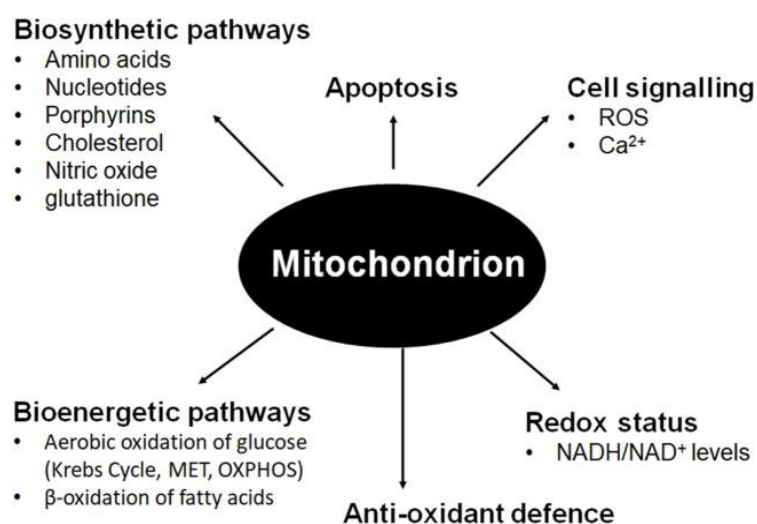


Figure 1.7: Mitochondria play an important role in fundamental cellular processes. Mitochondria are not only the main suppliers of energy by aerobic oxidation of glucose or β -oxidation of fatty acids but are also involved in processes critical for cellular viability such as regulation of apoptosis and anti-oxidant defense. Additionally, these organelles control important signaling pathways via release of ROS and Ca^{2+} and regulate the cellular redox status via NADH/NAD⁺ levels. The provision of a variety of essential biomolecules such as amino acids or nucleotides is another task of mitochondria, which contributes to normal cell function (taken from Herst et al., 2017).

As mitochondria developed from bacteria, they share structural similarities with them. Mitochondria and bacteria are enclosed by a double membrane. In mitochondria this membrane is separated into the outer membrane, the intermembrane space and the inner membrane (Figure 1.7). The so-called respirasome is composed of the different respiratory chain complexes and is located in the mitochondrial inner membrane. This membrane is folded into cristae to enlarge the surface for chemical reactions executed by the respiratory chain. Most of the chemical reactions in mitochondria except for respiration take place in the matrix. All enzymes involved in the tricarboxylic acid (TCA) cycle are for example located within the mitochondrial matrix (Herst et al., 2017; Nunnari and Suomalainen, 2012).

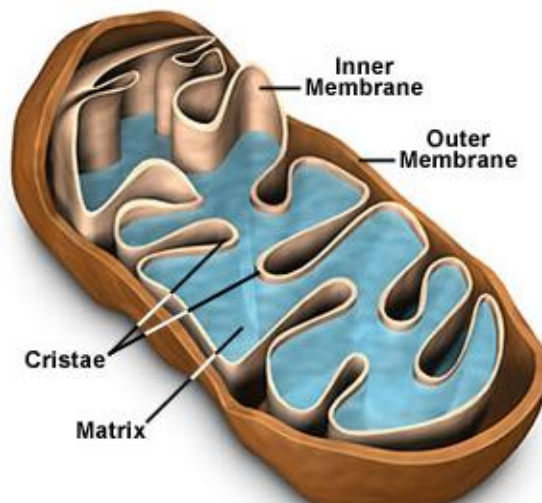


Figure 1.8: Mitochondrial structure. Mitochondria are enclosed by a double membrane, which is composed of an outer membrane and a heavily folded inner membrane with so-called cristae. Most of the chemical reactions catalyzed by a variety of enzymes are located in the mitochondrial matrix. The most prominent example is the TCA cycle (modified and taken from <https://micro.magnet.fsu.edu/cells/mitochondria/mitochondria.html>).

The fact that mitochondria have their own genome is another proof for the bacterial origin of these organelles. The mitochondrial genome consists of a double-stranded, closed-circular molecule. The 16.569 nucleotide pairs do not show intron regions in contrast to the nuclear genome. Mitochondrial genes encode for only 13 polypeptides, 22 transfer RNAs (tRNAs) and 12S and 16S rRNAs, which are needed for mitochondrial protein synthesis (Taanman, 1999). All proteins encoded by mitochondrial genes are subunits of the respiratory chain (7 of 45 subunits for respiratory chain complex I (RC-I), 1 of 11 subunits for RC-II, 3 of 13 subunits for RC-IV and 2 of 16 subunits for RC-V). Only 15 % of the respiratory chain subunits are produced by mitochondria themselves whereas the majority of subunits is encoded by the nucleus and needs to be imported. In total, 1500 so-called n-(nuclear)

mitoproteins are synthesized outside the mitochondria and need to be transported into them upon synthesis. The total mitochondrial proteome consists of enzymes involved in the TCA cycle, amino acid and lipid biosynthesis and components of transcription, translation and DNA repair (Hensen et al., 2014). In general, mitochondrial DNA is more prone to the occurrence of mutations than the nuclear genome due to its close vicinity to reactive oxygen species generated as by-products of the respiratory chain, the missing protection by histone molecules and reduced efficiency of DNA proofreading and repair processes. mtDNA mutations that affect the synthesis of one or the other of the 13 respiratory chain subunits lead to a loss of respiratory chain activity (van Gisbergen et al., 2015; Picard et al., 2016; Tuppen et al., 2010). Mutated mitochondrial DNA is associated with a variety of diseases such as neuromuscular and neurodegenerative mitochondrial pathologies. But mtDNA mutations are also found in diabetes, aging or cancer (Herst et al., 2017). mtDNA mutations associated with carcinogenesis are mainly located in the 22 mitochondrial tRNA genes. The single nucleotide polymorphism 3243A>G is the most frequently occurring mtDNA mutation and leads to defective leucine mt-tRNA. The faulty tRNA causes diminished translation of the 13 respiratory subunits and thereby affects overall mitochondrial respiration (Goto et al., 1990; Herst et al., 2017; Picard et al., 2014; Sasarman et al., 2008).

1.3.2 TCA cycle and oxidative phosphorylation

Cellular energy in form of ATP is mainly provided by glycolysis in the cytoplasm and mitochondrial respiration, which is also called oxidative phosphorylation (OXPHOS). While the oxidation of 1 glucose molecule to pyruvate during glycolysis produces only 2 ATP molecules, the mitochondrial TCA (Krebs) cycle together with oxidative phosphorylation of the respiratory chain generates in total around 32-34 ATP per glucose molecule. Even if glycolysis is a rather inefficient way of energy provision, cells use this pathway to compensate for missing ATP from OXPHOS caused by hypoxic conditions or a dysfunctional respiratory chain. This phenomenon is called metabolic shift or Warburg effect and is often observed in cancer cells, which have a high demand for fast energy (Sullivan et al., 2016). To keep glycolysis running NAD⁺ is regenerated from NADH by the reduction of pyruvate to lactate catalyzed by the lactate dehydrogenase (LDH) (Herst et al., 2017; Martínez-Reyes and Chandel, 2020; Spinelli and Haigis, 2018).

Under normal conditions when oxygen is available and the respiratory chain functional, pyruvate as the final product of glycolysis is transported into mitochondria to fuel the TCA cycle. As this multistep reaction loop drives mitochondrial energy production, it plays a central role for cellular metabolism. Briefly, acetyl-CoA, which is derived from different sources such as pyruvate oxidation, fatty or amino acids, and oxaloacetate (OAA) are used to finally generate NADH, FADH and 2 ATP molecules during a variety of chemical conversion reactions (Figure 1.9). While NADH fuels the respiratory chain via complex I, FADH interacts with complex II (Martínez-Reyes and Chandel, 2020; Spinelli and Haigis, 2018). The Krebs cycle is not only essential for energy provision via catabolism of glucose but also for cellular anabolism by providing important metabolites, which are transported to the cytoplasm where they serve as building blocks for macromolecule synthesis (De Berardinis and Chandel, 2016; Martínez-Reyes and Chandel, 2020; Spinelli and Haigis, 2018). Citrate, for example, is used for the generation of oxaloacetate and acetyl-CoA in the cytosol and thereby supports nucleotide and lipid synthesis (Mullen et al., 2012). Additionally, oxaloacetate derived from the TCA cycle is an important precursor for the nonessential amino acid aspartate. Sullivan et al. (2015) have shown that a dysfunctional respiratory chain impairs aspartate biosynthesis by blocking the Krebs cycle. As aspartate is an important precursor of purine nucleotides, the defective biosynthesis of this amino acid leads to impaired cellular proliferation *in vitro* and *in vivo* (Sullivan et al., 2015, 2018). Due to its importance for the cell as a key metabolic engine the TCA cycle needs to be tightly regulated. This is achieved by multiple positive and negative allosteric regulators, which monitor the metabolic flux of the TCA cycle (Martínez-Reyes and Chandel, 2020).

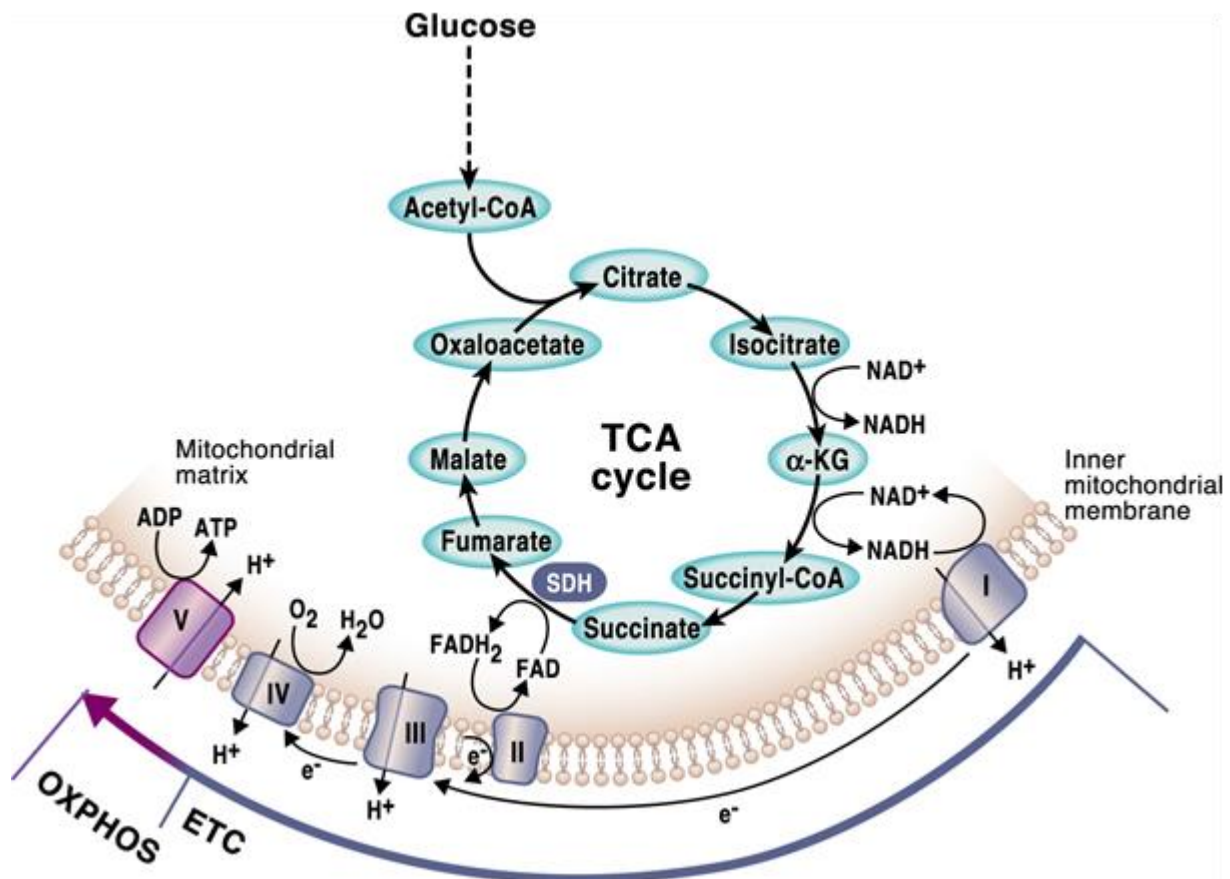


Figure 1.9: The TCA cycle is the metabolic engine of the cell. The TCA cycle is located in the mitochondrial matrix and provides not only important precursors such as oxaloacetate for the synthesis of different kinds of biomolecules but also generates the fuel for oxidative phosphorylation (OXPHOS) at the electron transport chain (ETC) in form of NADH and FADH₂. In a series of tightly regulated chemical reactions glucose derived acetyl-CoA and oxaloacetate are used to generate NADH and FADH₂, which serve as electron sources for the ETC. The entry points for electrons are respiratory chain complex I and II (taken from Martinez-Reyes and Chandel, 2020).

As already mentioned, TCA cycle and electron transport chain (ETC) are connected via respiratory chain complexes I and II. The process, in which the chemical energy of TCA cycle products is converted into an electrochemical gradient by the electron transport chain to produce ATP, is known as oxidative phosphorylation (OXPHOS). Electrons generated by the oxidation of the TCA cycle products NADH, FADH₂ or succinate are transferred to molecular oxygen via a series of respiratory chain complexes, which are also called the respirasome. During the electron transport over the respiratory chain the generated energy is stored in an electrochemical proton gradient ($\Delta\psi$). For this purpose, protons are pumped across the mitochondrial inner membrane into the intermembrane space, thereby building up the mitochondrial membrane potential. Protons flow back in the mitochondrial matrix along the gradient through proton channels in the F₁F₀ ATP synthase (respiratory chain complex V). This step catalyzes the final conversion of ADP to ATP. The respirasome, which is responsible

for electron transfer and generation of the proton gradient, is composed of the respiratory chain complexes I, II, III and IV (Figure 1.10). Protons are pumped into the intermembrane space only by complexes I, III and IV. Electron transfer between the complexes is mediated by liquid-soluble ubiquinone (Q) and water-soluble cytochrome c. Complex I or NADH dehydrogenase is the largest enzyme of the ETC and the first entry point for electrons from the TCA cycle. It catalyzes the oxidation of NADH. During this reaction, 2 electrons are transferred to ubiquinone and 4 protons are pumped across the mitochondrial inner membrane. Complex III (cytochrome c oxidoreductase) transfers electrons to the electron carrier cytochrome c and contributes 4 protons to the electrochemical gradient. Complex IV (cytochrome c oxidase) finally transfers electrons to molecular oxygen to generate water and pumps 2 protons in the intermembrane space. Complex II (succinate dehydrogenase) is not involved in the formation of the proton gradient but is the second entry point for electrons from the TCA cycle by oxidizing succinate and FADH_2 (Chaban et al., 2014; Letts and Sazanov, 2017; Martínez-Reyes and Chandel, 2020; Sousa et al., 2018).

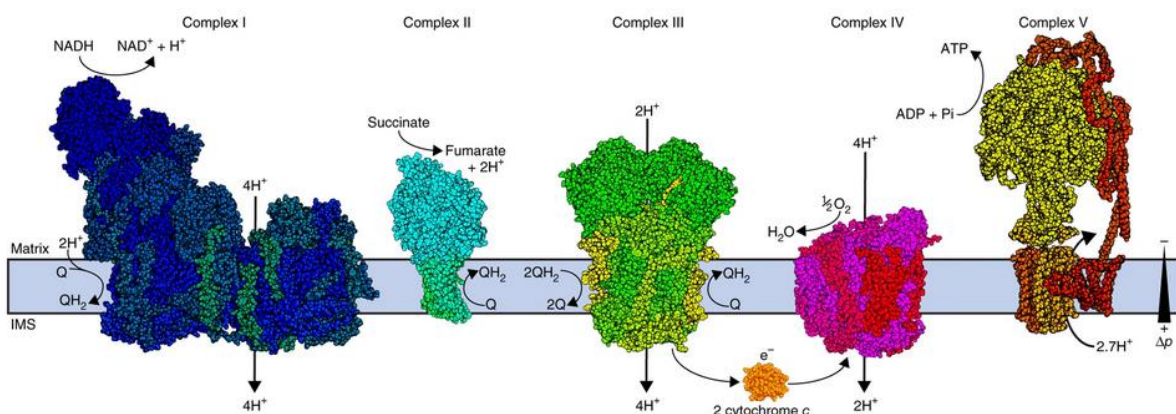


Figure 1.10: The electron transport chain (ETC). The electron transport chain or respiratory chain is located in the mitochondrial inner membrane and is composed of five large protein complexes with catalytic activity called respiratory chain complex I, II, III, IV and V. Its main task is the transport of electrons derived from the oxidation of NADH and FADH_2 at complex I and II. Electrons are finally transferred to molecular oxygen at complex IV to generate H_2O . During the electron transport protons are pumped over the inner membrane in the intermembrane space (IMS) to build up an electrochemical gradient (Δp). The proton flux along the gradient is used by complex V or ATP synthase to generate ATP from ADP (taken from Letts and Sazanov, 2017).

1.3.3 Mitostress signaling

Mitochondrial respiratory chain dysfunction causes activation of different conserved mitochondrial stress signaling pathways. As there are a vast number of different pathways, here only pathways, which are of interest for the following study, are mentioned. mtDNA mutations can cause faulty expression of respiratory chain complex subunits resulting in misshapen formation and function of the different ETC complexes. Premature electron leakage to oxygen can be a consequence of dysfunctional respiratory chain complexes I, II and III, which causes the generation of superoxide. Superoxide dismutase (Cu-ZnSOD: mitochondrial intermembrane space; MnSOD: matrix) then converts superoxide to hydrogen peroxide (H₂O₂). While H₂O₂ is neutralized to water and oxygen by glutathione peroxidase and peroxiredoxin under normal conditions, excess hydrogen peroxide produced during respiratory chain dysfunction can be converted into highly aggressive hydroxyl radicals. This oxidative stress then damages mitochondrial proteins, lipids and DNA and activates the Sirtuins Sirt1 and Sirt3, which are involved in the regulation of antioxidant responses and mitophagy (Herst et al., 2017; Quinlan et al., 2013; Zhao et al., 2019).

Impaired mitochondrial electron transfer is accompanied by decreased membrane potential. Under such conditions a variety of mitostress signaling pathways are activated, which induce specific nuclear transcriptional responses (Arnould et al., 2015; Herst et al., 2017; Picard et al., 2016). A dysfunctional respiratory chain causes diminished ATP synthesis and thereby leads to energy deprivation as indicated by high AMP/ATP ratio. As a consequence, AMP-activated protein kinase (AMPK) is activated, which in turn inhibits for example mTOR signaling to decelerate energy-demanding anabolic processes. This regulation is important for cellular viability as the TCA cycle is blocked by respiratory chain dysfunction and therefore does not produce enough metabolites for anabolic pathways anymore. Under conditions of high ATP demand the ADP/ATP ratio and AMP levels are elevated, which induces the catalytic activity of regulatory TCA cycle enzymes (Herzig and Shaw, 2018; Martínez-Reyes and Chandel, 2020). Respiratory chain dysfunction can also lead to an increased NADH/NAD⁺ ratio due to missing regeneration of NAD⁺ by complex I. This accumulation of NADH affects both membrane and cytosolic redox potential, which induce reductive stress. As NADH acts as an inhibitor for all regulatory enzymes of the TCA cycle, the accumulation of this molecule causes a shutdown of the cycle. ATP is known to block pyruvate dehydrogenase activity.

Consequently, high concentrations of ATP and NADH lead to a decelerated TCA cycle flux (Martínez-Reyes and Chandel, 2020). An altered NADH/NAD⁺ ratio also has an influence on the activity of NAD⁺-dependent poly [ADP-ribose] polymerase I (PARP-1), which plays a role for DNA damage repair. Mitochondrial proteotoxic stress can be induced by misfolded respiratory chain subunits or their altered expression. Such damaged respiratory chain subunits induce the so-called mitochondrial unfolded protein response (mtUPR) in the matrix. This stress response leads to accumulation of PINK1 in the mitochondrial intermembrane space and recruitment of PINK2 to the mitochondria, which results in the degradation of damaged mitochondria through mitophagy (Herst et al., 2017; Jin and Youle, 2013).

1.3.4 Mitochondrial models of respiratory chain dysfunction

1.3.4.1 ROS dependent models

There are different models for chronic mitochondrial dysfunction such as genetically or chemically induced deletion of central mitochondrial enzymes or whole DNA. Acute mitochondrial dysfunction can be induced by chemical inhibition of respiratory chain complexes. As mitochondria are the main source of reactive oxygen species (ROS) in the cell and mitochondrial respiratory chain dysfunction is usually accompanied by massive induction of ROS, which causes 26S proteasome disassembly, most of the models for mitochondrial respiratory chain dysfunction are not suitable for the investigation of ROS-independent effects of mitochondrial dysfunction on the proteasome. The TFAM knockout mouse model, which is a common model for loss of mitochondrial DNA and respiratory chain dysfunction, is known to have increased oxidative stress caused by elevated mitochondrial ROS production (Kaufman et al., 2007; Woo et al., 2012; Xie et al., 2016). The use of respiratory chain complex inhibitors is also difficult due to the massive release of ROS during the inhibition. ROS induction has been for example shown for rotenone (complex I inhibitor), antimycin A (complex III inhibitor) and oligomycin (complex V inhibitor) (Chou et al., 2010; Domingues et al., 2008; Huang et al., 2013). In contrast to this, KCN (complex IV inhibitor) and metformin (complex I inhibitor) have been demonstrated to block the activity of the respective complexes in the absence of ROS release (Chou et al., 2010; Vial et al., 2019).

1.3.4.2 ROS independent models – the mtDNA mutator mouse model

The mitochondrial DNA (mtDNA) mutator mouse model is a premature aging model, which is characterized by chronic respiratory chain dysfunction in the absence of increased mitochondrial and cytosolic ROS levels (Kujoth et al., 2005; Trifunovic et al., 2004, 2005). Due to the lack of ROS, this model of mitochondrial dysfunction is perfectly suited to analyze possible effects of respiratory chain dysfunction on the proteasome. The mitochondrial DNA polymerase subunit γ (PolG) of the mouse model is genetically modified by an amino acid substitution in the second exonuclease domain of PolG (D257A). The expression of alanine instead of aspartate leads to much lower 3'-5' exonucleolytic activity of the PolG catalytic subunit, which is equivalent to a proofreading deficient mtDNA polymerase. However, this defect does not impact DNA synthesis capacity of the polymerase but rather overall mtDNA integrity as the lack of proofreading strongly increases the mutation load in the mitochondrial genome. The massive, progressive and random accumulation of mtDNA mutations over time leads to a prominent respiratory chain dysfunction in mtDNA mutator mouse cells and organs (Trifunovic et al., 2004, 2005). Mice expressing a homozygous mtDNA mutator allele show the first signs of aging already after 25 weeks. The animals are characterized by a variety of aging hallmarks such as kyphosis, anemia, weight loss, alopecia and greying of hair (Trifunovic et al., 2004).

1.4 Mitochondria-to-proteasome signaling

As already described mitochondrial dysfunction leads to induction of several cellular stress responses. It has been shown that the proteasome is also affected by some of these stress signals. One of the best discovered mitochondria-to-proteasome signaling pathways is the effect of excessive ROS release on the proteasome in the course of respiratory chain dysfunction. In this context, inhibition of the respiratory chain in rat-derived cortical neurons led to decreased proteasome activity and protein ubiquitination (Huang et al., 2013). Similar observations were made in respiration-deficient yeast mutants ($\Delta f201$) characterized by induced ROS production. Here, ROS caused complete detachment of the 20S core particle and the 19S regulatory particle. In the same study, this 26S proteasome disassembly was confirmed in yeast and mammalian cells treated with hydrogen peroxide, the respiratory chain complex III inhibitor antimycin A or a cytochrome c reductase inhibitor. Oxidative

stress in form of ROS was proven to be causative for proteasome disassembly by reversing the effect using either antioxidants such as N-acetyl-cysteine (NAC) or dithiothreitol (DTT) as strong reducing agent (Livnat-Levanon et al., 2014). Segref et al. (2014) demonstrated similar inhibition of the proteasome by ROS in *C. elegans* using a reporter system with a short-lived ubiquitin fused protein that accumulated during proteasome impairment. In their screen they identified two mutants with defects in enzymes involved in mitochondrial leucine catabolism and fatty acid metabolism, which led to respiratory chain dysfunction and increased ROS production (Segref et al., 2014).

The proteasome is not only influenced by mitochondrial ROS but also by the availability of ATP produced by oxidative phosphorylation. ATP plays an important role during protein ubiquitination and 26S proteasome assembly and stability as summarized above. It has been shown that intracellular ATP concentrations have an effect on proteasome activity both in vitro and in cell culture (Huang et al., 2013). Low ATP levels negatively influence proteasome activity by blocking the binding of ubiquitin to ubiquitin-activating E1 enzyme (Huang et al., 2013).

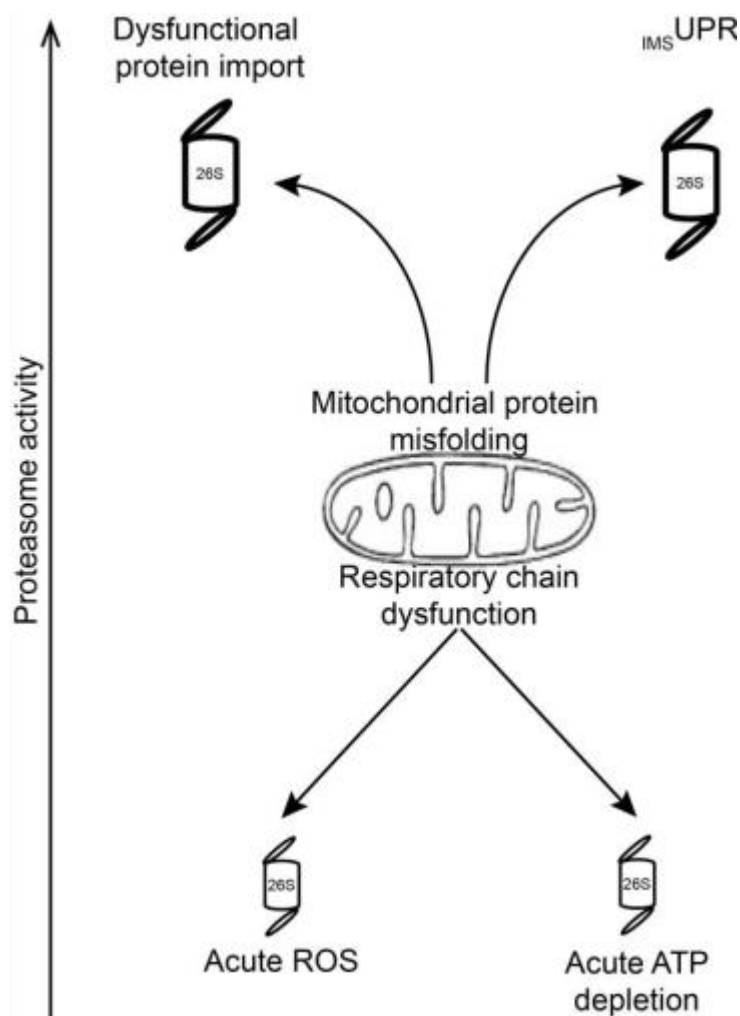


Figure 1.11: Mitochondrial dysfunction influences proteasome activity. Mitochondrial respiratory chain dysfunction is often accompanied by massive release of reactive oxygen species (ROS) and depletion of ATP. Both events can lead to 26S proteasome disassembly and decreased proteasome activity. In contrast to this, mitochondrial proteotoxic stress in form of an unfolded protein response (UPR) in the intermembrane space (IMS) or dysfunctional protein import into mitochondria results in an activation of the ubiquitin-proteasome system (taken from Berschneider (2016)).

Höglinger et al. (2003) demonstrated that inhibition of respiratory chain complex I decreased intercellular ATP levels, which in turn diminished proteasome activity in a model of Parkinson's disease. The effect could be reversed by increasing glucose concentrations (Höglinger et al., 2003). Additionally, the metabolic sensors AMPK and PKA play an important role in the context of cellular ATP availability and proteasome activity. As already described, mitostress in form of low ATP levels activates the central cellular energy sensor AMPK. The proteasome is inhibited when AMPK is induced whereas AMPK inhibition leads to increased proteasome activity (Ronnebaum et al., 2014; Viana et al., 2008; Xu et al., 2012). Although a direct connection between mitochondria mediated AMPK or PKA activity and the proteasome has not been described so far, there are two mechanisms of how AMPK could

modulate proteasome activity: via O-GlcNAc transferase mediated O-GlcNAcylation of the proteasome, which causes 26S proteasome disassembly (Xu et al., 2012) and direct interaction of AMPK with the proteasome and phosphorylation of Rpn6 (Moreno et al., 2009). The activating phosphorylation of proteasome subunits by PKA has already been described earlier in the introduction.

An increased need for protein quality control during mitochondrial dysfunction can also influence proteasome activity. Overexpression of an instable intermembrane space (IMS) protein, which activated the unfolded protein response of the IMS, for example, led to an elevated proteasome activity (Papa and Germain, 2011). Accumulation of mitochondrial proteins in the cytosol due to defective import of these proteins into mitochondria induced the ubiquitin-proteasome system as well (Boos et al., 2019; Ravanelli et al., 2020; Weidberg and Amon, 2018; Wrobel et al., 2015). Additionally, PINK1- and PARKIN-mediated autophagy has been shown to be accompanied by upregulated proteasome activity (Shiori Akabane et al., 2016)

2 Aims

As outlined above, the concept of mitochondria-to-proteasome signaling via ROS and ATP is already well established. Under conditions of respiratory chain dysfunction massive ROS release and/or reduced levels of ATP lead to proteasome disassembly and decreased proteolytic activity. However, the influence of mitochondrial anabolism on the proteasome system has not been investigated so far due to the lack of suitable models for respiratory chain dysfunction characterized by the absence of increased ROS production. We here used the above described mtDNA mutator mouse model as a model system for chronic respiratory chain dysfunction without induction of oxidative stress (Trifunovic et al., 2004, 2005) to investigate adaptive regulation of the proteasome by mitochondrial metabolism. Experiments were performed with immortalized mouse embryonic fibroblasts (MEFs) derived from either wildtype mice or mutator mice. The specific aims were defined as follows:

1. *Analyzing the proteasome system under conditions of chronic respiratory chain dysfunction in the absence of oxidative stress*

Both standard and immunoproteasome were analyzed in mouse embryonic fibroblasts (MEFs) derived from the mtDNA mutator mouse model with regard to composition and activity to dissect a possible influence of mitochondrial metabolism on the proteasome system.

2. *Dissecting the underlying mechanism of proteasomal regulation by mitochondrial metabolism*

Mitochondrial composition and function were characterized in WT and mutator MEFs to identify possible metabolic alterations caused by respiratory chain dysfunction. For this purpose, proteome and metabolome of isolated mitochondria were analyzed using mass spectrometry. The signaling pathway from dysfunctional mitochondria in mutator MEFs to the proteasome was investigated by different approaches such as rescue experiments, gene silencing or phosphoproteomics.

3. *Establishing adaptive mitochondrial regulation of the proteasome as a general model in murine and human cells*

To confirm the proposed mechanism for mitochondrial regulation of the proteasome in mutator MEFs, respiratory chain complex I was chemically inhibited without ROS induction in WT MEFs, primary human skin and lung fibroblasts and the proteasome was analyzed. Rescue experiments were performed with pyruvate and aspartate treatment.

3 Materials

3.1 Antibodies

3.1.1 Primary antibodies

Antigen	Product number	Host	Type	Application	Dilution	Provider
Akt (pan) (C67E7)	4691	Rabbit	Monoclonal	WB	1:1000	Cell Signaling, Danvers, USA
GAPDH (HRP-linked)	14C10	Rabbit	Monoclonal	WB	1:80 000	Cell Signaling, Danvers, USA
Lmp2 (Psmb8)	ab3328	Rabbit	Polyclonal	WB	1:1000	Abcam, Cambridge, United Kingdom
Lmp7 (Psmb9)	ab3329	Rabbit	Polyclonal	WB	1:1000	Abcam, Cambridge, United Kingdom
OXPPOS Rodent WB cocktail	45-8099	Rabbit	-	WB	1:1000	ThermoFisher, Waltham, USA
Pa28 α	ab155091	Rabbit	Monoclonal	WB	1:1000	Abcam, Cambridge, United Kingdom
Phospho-Akt (Ser473) (D9E)	4060	Rabbit	Monoclonal	WB	1:1000	Cell Signaling, Danvers, USA
Phospho-S6 kinase	9208	Rabbit	Polyclonal	WB	1:1000	Cell Signaling, Danvers, USA
Phospho-S6 ribosomal protein	4858	Rabbit	Monoclonal	WB	1:1000	Cell Signaling, Danvers, USA
p27 (Psmd9)	ab103408	Rabbit	Polyclonal	WB	1:1000	Abcam, Cambridge, United Kingdom
p28 (Psmd10)	ab182576	Rabbit	Monoclonal	WB	1:1000	Abcam, Cambridge, United Kingdom
Raptor	2280	Rabbit	Polyclonal	WB	1:1000	Cell Signaling, Danvers, USA
Rpn8 (Psmd7)	ab11436	Rabbit	Polyclonal	WB	1:1000	Abcam, Cambridge, United Kingdom
Rpn6 (Psmd11)	NBP1-46191	Rabbit	Polyclonal	WB	1:2000	Novus Biologicals, Littleton, USA
Stat1	9175	Rabbit	Polyclonal	WB	1:1000	Cell Signaling, Danvers, USA
S5b (Psmd5)	ab137733	Rabbit	Polyclonal	WB	1:1000	Abcam, Cambridge, United Kingdom
S6 kinase	2708	Rabbit	Polyclonal	WB	1:1000	Cell Signaling, Danvers, USA
S6 ribosomal protein	2317	Mouse	Polyclonal	WB	1:1000	Cell Signaling, Danvers, USA
Tbp1 (Rpt5)	A303-538A	Rabbit	Polyclonal	WB	1:1000	Bethyl Laboratories, Montgomery, USA
UBIK48	05-1307	Rabbit	Monoclonal	WB	1:1000	Merck Millipore, Billerica, USA
α 1-7 (MCP231)	ab22674	Mouse	Monoclonal	WB	1:1000	Abcam, Cambridge, United Kingdom
β 5	ab90867	Rabbit	Polyclonal	WB	1:1000	Abcam, Cambridge, United Kingdom
β -Actin (HRP-linked)	A3854	Mouse	Monoclonal	WB	1:80 000	Sigma Aldrich, St. Louis, USA

3.1.2 Secondary Antibodies

Antigen	Product number	Host	Application	Dilution	Provider
Anti-mouse IgG HRP-linked	7076	Horse	WB	1:40 000	Cell Signaling, Danvers, USA
Anti-rabbit IgG HRP-linked	7074	Horse	WB	1:40 000	Cell Signaling, Danvers, USA

3.2 Oligonucleotides

Primers for quantitative real time polymerase chain reaction (RT-PCR) were purchased from Eurofins, Germany.

3.2.1 Primers for quantitative RT-PCR

Gene	Species		Sequence 5'-3'
Psm3	mouse	FW	AGATGGTGTGCTTTGGGG
		REV	AACGAGCATCTGCCAACAA
Psm5	mouse	FW	TCAGTGATGGTCTGAGCCTG
		REV	CCATGGTGCCTAGCAGGTAT
Psm6	mouse	FW	CAGAACAACCACTGGGTCCT
		REV	CCCGGTATCGGTAACACATC
Psm7	mouse	FW	CCCGGTATCGGTAACACATC
		REV	TCCCAGCACCACAACAATAA
Psm8	mouse	FW	GCTATTCTGGAGGCGTTGTC
		REV	AGGCCTCTTCTCTCCTTGG
Psm9	mouse	FW	ATGCTGACTCGACAGCCTTT
		REV	GCAATAGCGTCTGTGGTGAA
Psm10	mouse	FW	AGC CCG TGA AGA GGT CTG G
		REV	CAT AGC CTG CAC AGT TTC CTC C
Psmc3	mouse	FW	GTGAAGGCCATGGAGGTAGA
		REV	GTTGGATCCCCAAGTTCTCA
Psm11	mouse	FW	GCTCAACACCCCAGAAGATGT
		REV	AGCCTGAGCCACGCATTTTA
Psm5	mouse	FW	TGTGAGCGCTACCCTGTTTT
		REV	TTCAGCTCCGTGGAAGCATT
Psm9	mouse	FW	TAGAAGCGCAGATCAAGGCC
		REV	TGTCACATTCAGGGGCTTCC
Psm10	mouse	FW	TTGAAGGAGCGCATTTTGGC
		REV	GAGACCAACCTGCGTCATCT
Rpl19	mouse	FW	TGTACCTGAAGGTGAAGGGG
		REV	GCGTGCTTCTTGGTCTTAG

3.2.2 siRNAs

Silencer® select siRNAs for RNA interference were obtained from Ambion, Thermo Fisher Scientific, Waltham, USA. siRNAs were dissolved in nuclease free water at a stock concentration of 20 μ M and stored in aliquots at -20 °C.

siRNA	siRNA ID	Product number	Species
Silencer Select Psdm5 siRNA 1	s84258		Mouse
Silencer Select Psmd5 siRNA 2	s84256		Mouse
Silencer Select Psmd9 siRNA 1	s84561		Mouse
Silencer Select Psmd9 siRNA 2	sS84652		Mouse
Silencer Select Psmd10 siRNA 1	sS203895		Mouse
Silencer Select Psmd10 siRNA 2	s79154		Mouse
Silencer Select Psmd11 siRNA 1	s87416		Mouse
Silencer Select Psmd11 siRNA 2	s87415		Mouse
Silencer Select Raptor siRNA	s92713		Mouse
Silencer Select Negative Control No.1	-	4390843	Mouse/Human
Silencer Select Negative Control No. 2	-	4390847	Mouse/Human

3.3 Cell culture

3.3.1 Cell lines

Immortalized wildtype (n=3) and mutator MEFs (n=4) were provided by Prof. Dr Aleksandra Trifunovic, University of Cologne, Institute for Mitochondrial Diseases and Ageing.

Cell line	Origin	Specification
mutator MEFs	mtDNA mutator mouse model	4 different cell lines
WT MEFs	wildtype mice	3 different cell lines

3.3.2 Primary human lung fibroblasts

Primary human lung fibroblasts were provided by Prof. Dr. Andreas Günther, Universities of Giessen and Marburg Lung Center (UGMLC), Giessen, Germany.

ID	Patient data
409Sp	Male, 51 years, peripheral normal lung tissue, organ donor

3.3.3 Primary human skin fibroblasts

Primary human skin fibroblasts were provided by Dr. Holger Prokisch, Technical University of Munich, Institute for Human Genetics.

ID	Description	Protein name	Molecular function	Location
67333	ND5 mutation	Mitochondrially encoded NADH dehydrogenase 5	Subunit of respiratory chain complex I	mtDNA

ID	Description	Protein name	Molecular function	Location
NHDF	healthy control	-	-	-

3.3.4 Cell culture media

Cell type	Cell culture medium	Product number	Provider
phLF	DMEM High Glucose without Glutamine/Pyruvate	11960085	Thermo Fisher Scientific, Waltham, USA
	10 % Fetal bovine serum (FBS) Superior	S 0615	Biochrom, Berlin, Germany
	100 U/mL Penicillin/Streptomycin	15140-122	Thermo Fisher Scientific, Waltham, USA
	2 mM L-glutamine	G7513	Sigma-Aldrich, St. Louis, USA
	2 ng/mL Basic-FGF	13256029	Thermo Fisher Scientific, Waltham, USA
	0.5 ng/mL EGF	E9644	Sigma-Aldrich, St. Louis, USA
	5 µg/mL Insulin	12585-O14	Thermo Fisher Scientific, Waltham, USA
phSF	DMEM High Glucose without Glutamine/Pyruvate	11960085	Thermo Fisher Scientific, Waltham, USA
	2 mM L-glutamine	G7513	Sigma-Aldrich, St. Louis, USA
	10 % FBS Superior	S 0615	Biochrom, Berlin, Germany
	100 U/mL Penicillin/Streptomycin	15140-122	Thermo Fisher Scientific, Waltham, USA
MEFs	DMEM High Glucose without Glutamine/Pyruvate	11960085	Thermo Fisher Scientific, Waltham, USA
	2 mM L-glutamine	G7513	Sigma-Aldrich, St. Louis, USA
	10 % FBS Superior	S 0615	Biochrom, Berlin, Germany
	100 U/mL Penicillin/Streptomycin	15140-122	Thermo Fisher Scientific, Waltham, USA

3.4 Drugs and treatments

Drug	Solvent	Stock concentration	Provider
Metformin	Water	1 M	Sigma Aldrich
Rapamycin		100 µM	Sigma Aldrich
Aspartate	Water	-	Sigma Aldrich
Pyruvate	Water	-	Sigma Aldrich
Cycloheximide	DMSO	-	Sigma Aldrich

3.5 Enzymes

Product	Provider
DNase 2 U/µL	Peqlab, Erlangen, Germany
M-MLV Reverse Transcriptase	Sigma-Aldrich, St. Louis, USA

3.6 Kits

Product	Provider
LightCycler 480 SYBR Green I Master	Roche Diagnostics, Mannheim, Germany
Pierce BCA Protein Assay Kit	Thermo Fisher Scientific, Waltham, USA
Proteasome-Glo™ Assay	Promega, Fitchburg, USA
Roti-Quick RNA Extraction Kit	Carl Roth, Karlsruhe, Germany
WT PLUS Reagent Kit	Affymetrix, Santa Clara, US

Product	Provider
NAD/NADH GloTM assay	Promega, Fitchburg, USA
Click-iT Plus OPP Protein Synthesis Assay Kit	Life Technologies, Carlsbad, USA

3.7 Markers

Product	Provider
Protein Marker IV (10-245 kDa)	AppliChem, Darmstadt, Germany

3.8 Buffer formulations

All buffers were prepared with Milli-Q® water.

Buffer	Reagent	Concentration
5x Native loading buffer	Tris	250 mM
	Glycerol	50 % (v/v)
	Bromophenol blue	0.01% (w/v)
6x Laemmli buffer	Tris	300 mM
	Glycerol	50 % (v/v)
	SDS	6% (w/v)
	Bromophenol blue	0.01 % (w/v)
	DTT	600 mM
Native gel running buffer	Tris	89 mM
	Boric acid	89 mM
	EDTA	2 mM
	MgCl ₂	5 mM
	ATP	2 mM
	DTT	1 mM
PBST washing buffer	NaCl	137 mM
	KCl	2.7 mM
	Na ₂ HPO ₄	10 mM
	KH ₂ PO ₄	2 mM
	Tween-20	1 % (v/v)
Phosphate buffered saline (PBS) pH 7.4	NaCl	137 mM
	KCl	2.7 mM
	Na ₂ HPO ₄	10 mM
	K ₂ HPO ₄	2 mM
Proteasome activity overlay assay reaction buffer	Tris pH 7.5	50 mM
	ATP	1 mM
	MgCl ₂	10 mM
	DTT	1 mM
	Suc-LLVY-AMC	0.05 mM
RIPA lysis buffer pH 7.5	Tris/HCl pH 7.5	50 mM
	NaCl	150 mM
	IGEPAL	1 % (v/v)
	Sodium deoxycholate	0.5 % (w/v)
	SDS	0.1 % (w/v)
	cComplete® protease inhibitor	1x
SDS PAGE running buffer	Tris	25 mM
	Glycin	192 mM
	SDS	0.1 % (w/v)

Buffer	Reagent	Concentration
Solubilization buffer	Na ₂ CO ₃	66 mM
	SDS	2 % (w/v)
	β-mercaptoethanol	1.5 % (v/v)
TSDG buffer pH 7.0	Tris pH 7.0	10 mM
	NaCl	10 mM
	MgCl ₂	1.1 mM
	EDTA	0.1 mM
	DTT	1 mM
	NaN ₃	1 mM
	Glycerol	10 % (v/v)
Western blot transfer buffer	Tris	25 mM
	Glycine	192 mM
	Methanol	10 % (v/v)

3.9 Reagents

Product	Solvent	Stock concentration	Provider
Activity based probe LW124	DMSO	2.5 μM	Prof. Dr. H. Overkleeft, University of Leiden, Netherlands
Activity based probe MV151	DMSO	50 μM	Prof. Dr. H. Overkleeft, University of Leiden, Netherlands
Activity based probe MVB127	DMSO	25 μM	Prof. Dr. H. Overkleeft, University of Leiden, Netherlands
Adenosine triphosphate (ATP)	-	-	Roche Diagnostics, Mannheim, Germany
Bz-valine-glycine-arginine-aminomethylcoumarine (Bz-Val- Gly-Arg-AMC)	DMSO	2 mM	Bachem, Bubendorf, Switzerland
cOmplete™ protease inhibitor cocktail	H ₂ O	25x	Roche, Basel, Switzerland
Dithiothreitol (DTT)	H ₂ O	1 M	Life Technologies, Carlsbad, USA
ECL prime Western blotting reagent	-	-	GE Healthcare, Cölbe, Germany
Lipofectamine® RNAiMAX	-	-	Thermo Fisher Scientific, Waltham, USA
Luminata™ Classico Western HRP Substrate	-	-	Merck Millipore, Darmstadt, Germany
Luminata™ Forte Western HRP Substrate	-	-	Merck Millipore, Darmstadt, Germany
Nuclease-Free Water	-	-	Ambion, Thermo Fisher Scientific, Waltham, USA
Nucleotide Mix	-	10 mM	Promega, Fitchburg, USA
Opti-MEM Reduced Serum Medium	-	-	Thermo Fisher Scientific, Waltham, USA
Penicillin/Streptomycin	-	-	Thermo Fisher Scientific, Waltham, USA
Random Hexamers	-	250 μM	Promega, Fitchburg, USA
RNASin RNase Inhibitor	-	40 U/μL	Promega, Fitchburg, USA
Roti-Block	-	10x	Carl Roth, Karlsruhe, Germany

Product	Solvent	Stock concentration	Provider
Succinyl-leucine-leucine-valine-tyrosine-aminomethylcoumarine (Suc-LLVY-AMC)	DMSO	2 mM	Bachem, Bubendorf, Switzerland
SuperSignal West FEMTO	-	-	Thermo Fisher Scientific, Waltham, USA
Trypsin (0.25 % EDTA)	-	-	Thermo Fisher Scientific, Waltham, USA
Z-norleucine-proline-norleucine-aspartate-aminomethylcoumarine (Z-nLPnLD-AMC)	DMSO	2 mM	Bachem, Bubendorf, Switzerland

3.10 Chemicals

Product	Provider
Boric acid	AppliChem, Darmstadt, Germany
Bromophenol blue	AppliChem, Darmstadt, Germany
Dithiotreitol (DTT)	Life Technologies, Carlsbad, USA
DMSO	Carl Roth, Karlsruhe, Germany
EDTA	AppliChem, Darmstadt, Germany
EGTA	AppliChem, Darmstadt, Germany
Ethanol	AppliChem, Darmstadt, Germany
Glycerol	AppliChem, Darmstadt, Germany
Isopropanol (p. A.)	AppliChem, Darmstadt, Germany
Magnesium acetate	Sigma-Aldrich, St. Louis, USA
Magnesium chloride	AppliChem, Darmstadt, Germany
Methanol (p. A.)	AppliChem, Darmstadt, Germany
Potassium chloride	AppliChem, Darmstadt, Germany
Potassium phosphate monobasic	AppliChem, Darmstadt, Germany
Sodium azide	AppliChem, Darmstadt, Germany
Sodium chloride	AppliChem, Darmstadt, Germany
Sodium citrate tribasic dihydrate	AppliChem, Darmstadt, Germany
Sodium deoxycholate	AppliChem, Darmstadt, Germany
Sodium phosphate dibasic	AppliChem, Darmstadt, Germany
Sodiumdodecylsulfate (SDS)	AppliChem, Darmstadt, Germany
Tris	AppliChem, Darmstadt, Germany
Triton X-100	Life Technologies, Carlsbad, USA
Tween-20	AppliChem, Darmstadt, Germany
β -Mercaptoethanol	AppliChem, Darmstadt, Germany

3.11 Consumables

Product	Provider
6/24/96 well plates	TPP, Trasadingen, Switzerland
96 well plates, white, for luminescence detection	Berthold Technologies, Bad Wildbad, Germany
Cell culture dishes (6 cm, 10 cm 15 cm)	Nunc, Wiesbaden, Germany
Cell culture flasks (75 cm ² , 175 cm ²)	Nunc, Wiesbaden, Germany
Cryovials 1.5 ml	Greiner Bio-One, Frickenhausen, Germany
D-Tube™ Dialyzer Midi, MWCO 3.5 kDa	Merck Millipore, Darmstadt, Germany
Falcon tubes (15 mL, 50 mL)	BD Bioscience, Heidelberg, Germany
Glass pasteur pipettes	VWR International, Darmstadt, Germany
Microplate 96-well, PS, flat bottom (for BCA assay)	Greiner Bio-One, Frickenhausen, Germany
NuPAGE Novex 3-8 % Tris-Acetate Gel 1.5 mm (10 & 15 well)	Thermo Fisher Scientific, Waltham, USA
PCR plates, white, 96 well	Biozym Scientific, Hessisch Oldendorf, Germany
Pipet tips	Biozym Scientific, Hessisch Oldendorf, Germany
PVDF membrane	Bio-Rad, Hercules, USA
SafeSeal reaction tubes (0.5 mL, 1.5 mL, 2.0 mL)	Sarstedt, Nümbrecht, Germany
Sealing foil for qPCR plate	Kisker Biotech, Steinfurt, Germany
Serological pipettes Cellstar 2, 5, 10, 25 and 50 mL	Greiner Bio-One, Frickenhausen, Germany
Super RX Fuji medical X-ray film	Fujifilm Corporation, Tokyo, Japan
Syringes (10 mL, 20 mL, 50 mL)	Neolab, Heidelberg, Germany
Whatman blotting paper 3 mm	GE Healthcare, Freiburg, Germany

3.12 Technical devices and further equipment

Technical device	Provider
-20 °C freezer MediLine LGex 410	Liebherr, Biberach, Germany
-80 °C freezer	Eppendorf, Hamburg, Germany
-80 °C freezer U570 HEF	New Brunswick, Hamburg, Germany
Analytical scale XS20S Dual Range	Mettler-Toledo, Gießen, Germany
Autoclave DX-45	Systec, Wettenberg, Germany
Autoclave VX-120	Systec, Wettenberg, Germany
Cell culture work bench Herasafe KS180	Thermo Fisher Scientific, Waltham, USA
Centrifuge MiniSpin plus	Eppendorf, Hamburg, Germany
Centrifuge Rotina 420R	Hettich, Tuttlingen, Germany
Centrifuge with cooling, Micro220R	Hettich, Tuttlingen, Germany
CO ₂ cell incubator BBD6620	Thermo Fisher Scientific, Waltham, USA
Dry ice container Forma 8600 Series, 8701	Thermo Fisher Scientific, Waltham, USA
Film developer Curix 60	AGFA, Morsel, Belgium
Fluorescent scanner Typhoon TRIO+	Amersahm Biosciences, Amersham, UK
Gel imaging system ChemiDoc XRS+	Bio-Rad, Hercules, USA
Ice machine ZBE 110-35	Ziegra, Hannover, Germany
Light Cycler LC480II	Roche Diagnostics, Mannheim, Germany
Liquid nitrogen cell tank BioSafe 420SC	Cryotherm, Kirchen/Sieg, Germany
Liquid nitrogen tank Apollo 200	Cryotherm, Kirchen/Sieg, Germany
Magnetic stirrer KMO 2 basic	IKA, Staufen, Germany
Milli-Q® Advantage A10 Ultrapure Water Purification System	Merck Millipore, Darmstadt, Germany
Milli-Q® Integral Water Purification System for Ultrapure Water	Merck Millipore, Darmstadt, Germany
Mini Centrifuge MCF-2360	Schubert & Weiss Omnilab, Munich, Germany
Nalgene Freezing Container (Mister Frosty)	Omnilab, Munich, Germany
pH meter InoLab pH 720	WTW, Weilheim, Germany

Technical device	Provider
Plate centrifuge 5430	Eppendorf, Hamburg, Germany
Plate reader Sunrise	Tecan, Crailsheim, Germany
Plate reader TriStar LB941	Berthold Technologies, Bad Wildbach, Germany
Power Supply Power Pac HC	Bio-Rad, Hercules, USA
Refrigerator Profi Line	Liebherr, Biberach, Germany
Research plus pipettes	Eppendorf, Hamburg, Germany
Roll mixer	VWR International, Darmstadt, Germany
Scale XS400 2S	Mettler-Toledo, Giessen, Germany
Shaker Duomax 1030	Heidolph, Schwabach, Germany
Thermomixer compact	Eppendorf, Hamburg, Germany
Vacuum pump NO22AN.18 with switch 2410	KNF, Freiburg, Germany
Vortex mixer	IKA, Staufen, Germany
Water bath Aqua Line AL 12	Lauda, Lauda-Königshofen, Germany

3.13 Software

Software	Provider
Adobe Illustrator	Adobe Systems, San Jose, USA
GraphPad Prism 5 and 7	GraphPad Software, La Jolla, USA
Image Lab	Bio-Rad, Hercules, USA
Imaris Software	Oxford Instruments; USA
ImageJ	National Institutes of Health, Bethesda, USA
LightCycler® 480 SW 1.5	Roche Diagnostics, Mannheim, Germany
Magellan Software	Tecan, Crailsheim, Germany
Microsoft Office Professional Plus 2010	Microsoft, Redmond, USA
Tristar MicroWin 2000	Berthold Technologies, Bad Wildbach, Germany

4 Methods

Parts of this chapter were recently published as preprint:

Thomas Meul, Korbinian Berschneider, Sabine Schmitt, Christoph H. Mayr, Laura F. Mattner, Herbert B. Schiller, Ayse Yazgili, Xinyuan Wang, Christina Lukas, Cornelia Prehn, Jerzy Adamski, Elisabeth Graf, Thomas Schwarzmayr, Fabiana Perocchi, Alexandra Kukat, Aleksandra Trifunovic, Laura Kremer, Holger Prokisch, Bastian Popper, Christine von Toerne, Stefanie M. Hauck, Hans Zischka, Silke Meiners (2020) Adaptive mitochondrial regulation of the proteasome *bioRxiv* 2020.04.07.026161; doi: <https://doi.org/10.1101/2020.04.07.026161>

4.1 Cell culture

4.1.1 Cultivation of mammalian cells

The different cell types were cultured in cell culture flasks (Thermo Fisher Scientific) of different sizes (75 cm² or 175 cm²) in a humidified environment with 5 % CO₂ at 37 °C. Mouse embryonic fibroblasts (MEFs) were cultured in DMEM High Glucose (4.5 g/L) medium without L-glutamine and sodium pyruvate (Thermo Fisher Scientific) supplemented with 10 % (v/v) fetal bovine serum (FBS) (Biochrome), 100 U/mL penicillin/streptomycin (Gibco, Thermo Fisher Scientific) and 4 mM L-glutamine (Thermo Fisher Scientific). The same medium was used for primary human lung and skin fibroblasts. Medium for lung fibroblasts was additionally supplemented with 5 µg/mL insulin (Thermo Fisher Scientific), 2 ng/mL basic-FGF (Thermo Fisher Scientific) and 0.5 ng/mL human EGF (Sigma-Aldrich). The different cell lines were grown until 80 – 90 % confluency and then splitted in new cell culture flasks twice a week.

4.1.2 Cell harvest

Following the respective treatment time, cells were first washed with PBS and then detached using trypsin (5 min at 37 °C). Trypsin was stopped with normal cell culture medium containing FCS. Cells were then collected and centrifuged for 5 min at 1000 rpm (Room temperature). For further analysis the cell pellet was washed once with PBS and centrifuged again to collect the cell pellet, which was stored at -80 °C until usage. Cells destined for RNA

extraction were directly collected in 500 µl RotiQuick 1 solution (Carl Roth) and stored at -20 °C until continuing the RNA extraction.

4.1.3 Treatment of cells

4.1.3.1 Aspartate and pyruvate treatment

Aspartate and pyruvate were freshly dissolved in high glucose medium without FCS. Concentrations are indicated in the specific experiments of the results section. As aspartate changed the pH to acidic, medium supplemented with aspartate was incubated at 37 °C until pH was alkaline again through gas exchange with room air. Both aspartate and pyruvate medium was sterile filtered with sterile, non-pyrogenic, hydrophilic filters (VWR) and supplemented with 10 % (v/v) FCS. 20.000 cells of the different cell types were seeded in 6 wells the day before the treatment. On the following day, cells were washed with PBS and treated with 4 ml aspartate or pyruvate medium for up to 72 h.

4.1.3.2 Metformin and Rapamycin treatment

Metformin (respiratory chain complex I inhibitor) or rapamycin (mTORC1 inhibitor) treatment was performed in combination with aspartate/pyruvate supplementation. First, non-toxic concentrations for metformin and rapamycin were determined in dose curve experiments. For metformin the influence on cellular proliferation served as read-out to find the optimal treatment concentration in the different cell types. The applied concentrations are indicated in the experiment description of the results section. Rapamycin concentrations for specific inhibition of mTORC1 were determined by assaying phosphorylation of p70S6 kinase. 0.5 nM rapamycin led to almost complete loss of p70S6 kinase phosphorylation whereas phosphorylation of the mTORC2 target Akt was not decreased. For cell treatments, the respective amount of metformin or rapamycin was mixed with aspartate/pyruvate medium and cells were incubated for up to 72 h.

4.1.4 Cell proliferation assay

The proliferation rate per day in different cell types was determined according to the protocol published by Sullivan et al. (2015). 20.000 cells were seeded in 6 well plates the day before the starting point of the assay. On the following day control wells were counted to determine the initial cell number per cell line on day 1. Cells were then grown for additional 3 days and counted again on day 4 to define the final cell number. Doublings per day were calculated using the following formula:

$$\text{Proliferation Rate (Doublings per day)} = \log_2(\text{Final cell count (day 5)}/\text{Initial cell count (day 1)})/4 \text{ (days)}$$

4.1.5 Measurement of nascent protein synthesis

Protein synthesis in aspartate treated mutator MEFs was measured using the EZClick™ Global Protein Synthesis Assay Kit (Biovision). Cells were seeded on cover slips. After overnight recovery cells were treated with 10 mM aspartate for 48 h. To proof assay specificity, cells were then treated for 4 h either with normal medium or medium containing 100 μM cycloheximide, which served as protein synthesis inhibitor. Following, cycloheximide medium was removed and substituted by medium containing EZClick™ O-propargyl-puromycin (OPP) reagent. Cells were incubated with EZClick™ O-propargyl-puromycin (OPP) reagent for another 30 minutes. Afterwards, cells were washed with PBS and fixed with 4 % PFA for 15 min. Next, cells were permeabilized in PBS containing 0.5 % TritonX-100 for 15 min, washed twice with PBS and stained by adding 500 μl EZClick™ fluorescence azide reaction cocktail for 30 min. Nuclei staining was performed with 4'-6-Diamidin-2-phenylindol (DAPI) (Sigma-Aldrich) in PBS for 30 min. After a final washing step with PBS, cells were mounted on object slides using DAKO mounting medium (DAKO). Fluorescence intensity in single cells was determined by LSM710 fluorescence microscope (Zeiss). For quantification of protein synthesis in the different mutator cell lines, the mean fluorescence intensity of 3000 – 5000 cells was calculated.

4.1.6 siRNA mediated gene silencing

Gene silencing using small interfering RNA (siRNA) was performed by reverse transfection of the cells with one or two different siRNAs targeted against the respective mRNAs of Psmd5, Psmd9, Psmd10, Psmd11 and Raptor. Control cells were transfected with scrambled (non-targeted) siRNAs. The applied siRNA concentrations are indicated in the respective experiments of the results section. For a transient gene knockdown in WT and mutator MEFs 20.000 cells per well were seeded in 6 well plates and cultured in transfection medium (DMEM High Glucose, 10 % FCS without penicillin/streptomycin). The respective targeting or scrambled siRNAs were incubated in 500 μ l Opti-MEM for 5 min at room temperature. Subsequently, 5 μ l lipofectamine RNAiMAX (10 μ l/ml) per sample was added to the diluted siRNAs and the mixture was incubated for 20 min at room temperature to enable the formation of siRNA-liposome complexes. Finally, the respective transfection mixes were added to the cells and after 16 h the transfection medium was exchanged with DMEM High Glucose medium supplemented with 10 % FCS and 1 % penicillin/streptomycin. Gene silencing was performed for 72 h and knockdown efficiency was checked by Western blot analysis.

4.2 Protein biochemistry

4.2.1 Protein extraction from cells

4.2.1.1 Native protein extracts

To prepare native cell extracts, frozen cell pellets were dissolved in TSDG buffer containing 1x cOmpleteTM protease inhibitor cocktail (Roche) and 1x PhosSTOP phosphatase inhibitor cocktail (Roche Diagnostics). Lysis buffer volume was adjusted to the cell pellet size. Cell lysis was performed by disrupting the cell membrane in 7 freezing-thawing steps using liquid nitrogen. Following, cell extracts were centrifuged for 20 min at 14.000 rpm and 4 °C to get rid of cellular debris. Cleared cell lysates were stored at minus 80 °C until further usage.

4.2.1.2 Denatured protein extracts

RIPA lysis buffer was used to prepare denatured protein extracts. Here, frozen cell pellets were dissolved in a cell pellet size dependent volume of RIPA buffer, which contained 1x cOmplete™ protease inhibitor cocktail (Roche) and 1x PhosSTOP phosphatase inhibitor cocktail (Roche Diagnostics). Cell lysis was performed on ice for 20 min followed by centrifugation of the crude cell lysates for 20 min at 14.000 rpm and 4 °C. Cleared cell lysates were stored at minus 80 °C until further usage.

4.2.2 Bicinchoninic acid (BCA) assay

In order to determine protein concentrations in cell lysates the Pierce BCA protein assay kit (Thermo Fisher Scientific) was used. Here, the respective samples were diluted 1:10 in PBS to a total volume of 20 µl were mixed with 200 µl BCA working solution in a 96 well plate. A standard curve of bovine serum albumin in different known concentrations served for the final quantification of the unknown protein concentrations in the samples. After 30 min at 37 °C the absorbance of each sample and the standard curve was measured in triplicates on the same 96 well plate at a wavelength of 562 nm using the Sunrise Plate Reader.

4.2.3 Western blot analysis

15 µg of protein per sample (RIPA or TSDG lysates) was diluted to equal volumes in water and mixed with 6x Laemmli loading buffer. Each sample was incubated for 5 min at 95 °C. Equal volumes were then loaded on 12 % or 15 % SDS-PAGE gels depending on the size of the target protein. Electrophoresis was performed at 130 V in running buffer. Subsequently proteins were blotted onto a polyvinylidenedifluoride (PVDF) membrane in transfer buffer at 250 mA for 90 min at 4 °C. Membranes were incubated in Roti®-Block for at least 1 hour to block unspecific binding sites and incubated with primary antibodies diluted according to the data sheet overnight at 4 °C. After washing in PBST secondary HRP-linked antibodies diluted in PBST were applied for 1 h at room temperature. After repeated washing of the membranes ECL (GE Healthcare) or Luminata™ Classico or Forte reagent (Merck Millipore) was applied to generate chemiluminescent signals that were detected on Super RX Fuji medical X-ray films using a Curix 60 developer (Agfa, Mortsels, Belgium).

Densitometric analysis of the detected bands was performed in a linear range using ImageLab Software (Biorad, Hercules, CA).

4.2.4 Native gel electrophoresis

To analyze native and assembled proteasome complexes, native cell extracts from the TSDG lysis (Paragraph 4.2.1.1) were used. 15 µg of protein were diluted with water to a final volume of 16 – 20 µl. According to the volume 5x native loading buffer was diluted to a 1 x concentration in the final sample volume. All sample preparation steps were performed on ice. Samples were loaded on a commercially available 3-8 % gradient NuPAGE Novex Tris-acetate gel (Life Technologies). Native gels were run in a freshly prepared native gel running buffer (see Methods section) at 150 V and 4 °C for 4 h. Determination of CT-L activity of the different separated proteasome complexes was performed with an in-gel activity assay. Gels were incubated in a freshly prepared activity assay buffer (see Methods section) at 37 °C for 30 min. Proteasomal cleavage of the Suc-LLVY-AMC peptide substrate generates fluorescence, which can be detected at an excitation wavelength of 380 nm and emission wavelength of 460 nm using the ChemiDoc XRS+ system (BioRad). For immunoblotting native gels were incubated in a solubilization buffer (see Methods section) at RT for 15 min to facilitate the transfer of assembled proteasome complexes on a PVDF membrane. The same transfer conditions were used as for Western blot analysis. Finally, the membrane was blocked with Roti®-Block for 1 h and then incubated with the respective primary antibody overnight.

4.2.5 Proteasome activity assay with luminescent substrates

Activity of the three different proteasomal cleavage sites (chymotrypsin-like (CT-L) and caspase-like (C-L) and trypsin-like (T-L)) was determined using the Proteasome-Glo™ Assay (Promega, Fitchburg), which is based on the measurement of chemiluminescence. 1 µg of protein per active site diluted in a final volume of 20 µl TSDG buffer was used from native TSDG lysis extracts. Each active site was measured in triplicates. Samples were pipetted in white flat bottom 96-well plates. Afterwards, 20 µl of the respective active site substrate (Succinyl-leucine-leucine-valine-tyrosine-aminoluciferin (CT-L), Z-leucine-arginine-arginine-aminoluciferin (C-L) and Z-norleucine-proline-norleucine-aspartate-aminoluciferin (T-L)) was

added to each well of the prepared 96-well plate. Water mixed with substrate served as background control. By cleaving the respective substrate proteasomes released aminoluciferin, which was then used by luciferase to generate a luminescent signal. The generated signal was measured by a Tristar LB 941 plate reader. Chemiluminescence was measured every 5 min for 1 h and values, which reached the plateau of the signal were used for quantification.

4.2.6 Labeling of active proteasome complexes with activity-based probes (ABPs)

In addition to the proteasome activity assay with luminescent substrates, the so-called activity-based probes (ABPs) were used to determine the catalytic activity of the different 20S active sites in native 20S and assembled 26S proteasome complexes. ABPs are proteasome inhibitors, which bind irreversibly to the respective 20S active sites. The different ABPs (MV151 binds to all 20S active sites, MVB127 is specific for $\beta 5/\beta 5i$ and LW127 for $\beta 1/\beta 1i$) are fluorescently labeled and can be therefore detected in a gel-based assay (Verdoes et al., 2006). 7.5 μg protein per sample (TSDG lysate) were diluted in TSDG buffer to obtain comparable TSDG buffer volumes in each sample. Samples were incubated with 5 μM MV151, 1 μM MVB127 or 0.25 μM LW124 on a shaker at 600 rpm for 1 h at 37 °C. Subsequently 6x Laemmli loading buffer was added and samples were loaded onto a 15 % SDS-PAGE gel. Electrophoresis was performed at 80 V for 15 min until samples reached the resolving gel and then continued at 130 V for 2 h. Active sites in the proteasome visualized by the site specific binding of the fluorescent activity based probes were detected by a Typhoon TRIO+ scanner (GE Healthcare). Quantification of the obtained signal was performed using ImageJ software. Pahe Blue staining (Thermo Fisher Scientific) of the gels served as loading control.

4.3 Mass spectrometry analysis

4.3.1 Proteomics screen

4.3.1.1 Sample preparation and measurement

WT and mutator MEFs were cultured for 48 h, harvested and lysed in RIPA buffer. Protein concentration was determined using the BCA assay. 10 µg protein per cell line was diluted in water. The same amount of protein was used for mass spectrometry analysis of isolated mitochondria. Samples were further processed and measured by Dr. Christine von Törne, Research Unit Protein Science (HMGU).

4.3.1.2 Bioinformatic MS data analysis

Analysis of mass spectrometry data was performed in collaboration with Christoph Mayr using the Perseus software suite (version 1.5.8.7) (Tyanova et al., 2016). Briefly, log₂ transformed mass spectrometry intensity values were filtered to have at least three out of four quantified values in either the WT or the mutator group. Zero values were imputed with a normal distribution of artificial values generated at 1.6 standard deviations, subtracted from the mean, of the total intensity distribution and a width of 0.3 standard deviations. This places the imputed values at the lower limit of the intensity scale, which represents detection limit of the used instrumentation. For gene annotation enrichment analysis of the data from isolated mitochondria, we used 710 proteins that were confirmed to be true mitochondrial proteins based on the Mitominer software .

Gene annotation enrichment analysis was performed with the 1D annotation enrichment algorithm as previously described (Schiller et al., 2015). As gene annotations for significance tests, we used the Uniprot Keyword annotation as well as Gene Ontology terms Biological process (GO:BP), Molecular function (GO:MF) and Cellular Component (GO:CC) (Cox and Mann, 2012). In brief, it is tested for every annotation term whether the corresponding numerical values have a preference to be systematically larger or smaller than the global distribution of the values for all proteins, which is reported as normalized enrichment score. Additional pathway analysis was performed with the DAVID Bioinformatic Resources 6.8. MS data for protein translation from WT and mutator MEF lysates were analyzed as follows: Pathway analysis (DAVID Bioinformatic Resources 6.8) was performed on significant proteins

(625 of 3058) with a p -value $>5\%$. Unsupervised hierarchical clustering using Pearson correlation of z-scored log₂ label-free mass spectrometry intensity values of proteins that correspond to the term "Translation" resulted in the heat map (Meul et al., 2020)

4.3.2 Phosphoproteomics screen

4.3.2.1 Sample preparation

300.000 cells of one representative mutator cell line were seeded in 6 well plates. Cells for 4 technical replicates were plated. After overnight recovery, cells were treated either with control medium or with 10 mM aspartate for 4 h. Cells were washed with TBS-T and scrapped off using pre-chilled (4 °C) sodium deoxycholate (SDC) lysis buffer. Following, cell lysates were heated up to 95 °C for 5 min to inactivate endogenous proteases and phosphatase. The Bioruptor device (Diagenode) was applied to homogenize the lysates at 4 °C with 2 cycles at maximum output power. Protein concentration of the different samples was determined using the BCA assay. Caramidomethylate cysteine residues and disulfide bonds were reduced by adding 30 µL of reduction/alkylation buffer. Protein digestion was performed by lys-C (Wako) and trypsin (Sigma) overnight at 37 °C on a shaker (1500 rpm).

4.3.2.2 Phosphopeptide enrichment

Phosphopeptide enrichment (EasyPhos) was performed according to the protocol published by (Humphrey et al., 2018). Briefly, samples were diluted with EP enrichment buffer and isopropanol. TiO₂ beads for phosphopeptide capturing were resuspended in EP loading buffer at a concentration of 1 mg/µl. Each sample was mixed with one aliquot of TiO₂ beads. Binding of phosphopeptides to the beads was performed at 40 °C for 5 min on a shaker (2000 rpm). After several washing steps, phosphopeptides were eluted from the beads using EP elution buffer and centrifugation at 1500 g and RT for 4 min. Eluted phosphopeptides were further processed and measured by mass spectrometry. Sample preparation, measurement and bioinformatic analysis was performed in collaboration with Laura Mattner and Christoph Mayr.

4.3.3 Metabolomics screen

1 Mio cells were seeded per WT (n=3) and mutator (n=4) cell line per well in 6 well plates. One 6 well plate per cell line was used for metabolomics analysis and another plate for determination of the exact cell number, which was later used to normalize the obtained mass spectrometry intensities. Cells destined for mass spectrometry analysis were washed twice with PBS and overlaid with 300 μ l dry ice cold methanol. Next, cells were scrapped off the plates and collected in a 0.5 ml PP-Sarstedt Micro tube (Sarstedt). Samples were immediately frozen on dry ice and then stored at -80 °C until measurement. Targeted metabolomics analysis was performed by Dr. Cornelia Prehn at the Helmholtz Zentrum München, Institute of Experimental Genetics, Genome Analysis Center in Neuherberg, Germany. Metabolites were quantified using the Absolute/DQ™ Kit p180 (BIOCRATES Life Sciences AG, Innsbruck, Austria) and LC-ESI-MS/MS and FIA-ESI-MS/MS measurements as described previously (Zukunft et al., 2013).

4.4 Nucleic acid biochemistry

4.4.1 Quantitative real-time RT-PCR

To extract total RNA from WT and mutator MEFs, the Roti®-Quick-Kit (Carl Roth) was used. After cell lysis in 500 μ L Roti®-Quick 1 solution, phenol/chloroform was added to the cells to separate RNA from other cell components. RNA was then precipitated in 500 μ L Roti®-Quick 3 at -80 °C for 40 min. Concentration of washed and water dissolved RNA was determined using the NanoDrop 1000 (Thermo Fisher Scientific). Following, 1 μ g of RNA was transcribed into cDNA by M-MLV reverse transcriptase using the following master mix: 1x First Strand Buffer, 10 mM DTT, 0.5 mM dNTPs, 1 U/ μ L RNAsin RNase Inhibitor, 10 U/ μ L M-MLV transcriptase. Reaction ran with annealing for 5 min at 25 °C and elongation for 60 min at 37 °C using a Mastercycler Nexus (Eppendorf). Genomic DNA was digested with 1 U DNase at 37 °C for 15 min. DNase was heat inactivated at 75 °C for 10 min. To quantify mRNA level, a SYBR Green LC480 system (Roche) was used. 2.5 μ L cDNA and 5 μ L LC480 SYBR Green I Master mix (Roche) were mixed and transferred in a 96-well plate. 2.5 μ L forward and reverse primer dilution was added (final concentration of 0.5 μ M). Prepared 96-well plates were analyzed with the standard program of the Light Cycler 480II (Roche). Ribosomal protein L 19

(*RPL19*) and hypoxanthine-guanine phosphoribosyltransferase (*HPRT*) served as housekeeping genes. The $\Delta\Delta C_T$ method was applied to calculate relative gene expression in the respective samples.

4.4.2 Bulk mRNA sequencing

300.000 cells from one representative WT and mutator MEF cell line were seeded in 6 well plates. Cells for 5 technical replicates per cell line were plated. After 48 h cells were harvested and total RNA was isolated using the Total RNA kit (Peqlab, VWR). RNA integrity was confirmed by determining the RNA integrity number (RIN) with the Agilent 2100 BioAnalyzer (RNA 6000 Nano Kit, Agilent). 1 μ g of RNA from each sample was sent to the Core Facility Next-Generation Sequencing at the Helmholtz Center Munich for strand specific, polyA-enriched RNA sequencing according to (Haack et al., 2013). Further sample preparation, sequencing and first data processing was performed by Dr. Elisabeth Graf and Dr. Thomas Schwarzmayr. FPKM (Fragments Per Kilobase of transcript per Million fragments mapped) was used as normalization method. Normalized data set was analyzed in collaboration with Christoph Mayr using the Perseus Software as described in the proteomics section.

4.5 Characterization of mitochondria

4.5.1 Isolation of functional mitochondria

Cells from one representative WT and mutator cell line were seeded in 150 cm² cell culture flasks to obtain a final cell number of around 40×10^6 cells per isolation experiment. Cells were harvested, counted and resuspended in isolation buffer. The final concentration was $5-7 \times 10^6$ per ml isolation buffer. Mitochondria from WT and mutator cells were then isolated as previously described (Schmitt et al., 2015). Briefly, cells diluted in isolation buffer are pumped by a high precision pump via gastight syringes with a constant rate through the "Balch-homogenizer". Cells are broken up while passaging through tungsten carbide balls of different diameters. This defined clearance (square) was first adjusted for WT and mutator MEFs. Cells were pumped 4 times through a clearance of 6 μ m (flow rate 700 μ l/min). Homogenized cells were collected in 2 ml Eppendorf tubes followed by differential centrifugation. First, nuclei and cellular debris was removed at 800 x g and 4 °C.

Mitochondria were then pelleted at 10000 x g to generate a mitochondria and endoplasmic reticulum rich fraction. The ER rich fraction was directly used for detection of MHC I antigen presentation components via mass spectrometry analysis. For further purification, mitochondria loaded on a Nycodenz[®] (Axis Shield PoC AS) density gradient (24 %/18 %). Centrifugation at 30.000 rpm for 15 min at 4 °C in a Beckman ultracentrifuge (rotor SW 55.Ti) collected purified mitochondria at the 24 %/18 % interphase. The purified mitochondria were then used for further analysis. For mass spectrometry 10 µg purified mitochondria or ER-rich fraction was lysed with RIPA buffer and further processed and measured by Dr. Christine von Törne.

4.5.2 Electron microscopy

For electron microscopy of whole cells, WT and mutator MEFs were seeded, cultured for 48 h, harvested and the pellets were collected. Cell pellets were fixed in 2.5 % glutaraldehyde in 0.1 M sodium cacodylate buffer, pH 7.4 (Electron Microscopy Science) for longer than 24 h. The further sample preparation for whole cells and isolated mitochondria was done by Dr. Sabine Schmitt (Institute of Toxicology and Environmental Hygiene, TU Munich) as previously described (Zischka et al., 2008). Electron microscopy was performed by Dr. Bastian Popper (Biomedical Center, Core facility animal models, Ludwig-Maximilian-University Munich).

4.5.3 Quantification of mitochondrial volume

Proportion of mitochondrial volume was quantified as described by Lucocq and Hacker (2013) (Lucocq and Hacker, 2013). Quantification was performed by Dr. Sabine Schmitt (Institute of Toxicology and Environmental Hygiene, TU Munich). Briefly, the area of the whole cell served as reference space. Analysis was done with ImageJ, using a grid lattice size of 20 µm² (cytoplasm and nucleus) or 2µm² (mitochondria), respectively. In total, 30 electron micrographs (1000 x magnification) from three wildtype clones (two technical replicates, each) and 43 electron micrographs (1000 x magnification) from four mutator clones (two technical each) were used for quantification.

4.6 Statistical analysis

Figure legends for the different experiments of the results section indicate the statistical analysis, which was used to determine significance of the generated data. To test whether differences between WT and mutator MEFs were significant, the student's unpaired t-test with Welch correction was applied. Aspartate and pyruvate treatment of different mutator MEFs was analyzed using the student's paired t-test due to strong differences between the single mutator cell lines. When single cell lines were used in technical replicates for experiments the one-sample t-test was chosen. The one-sample t-test was especially used to determine significance when native gel immunoblotting was performed with one single cell line or different mutator cell lines to eliminate signal intensity differences between replicates or individual mutator cell lines. Significance was indicated in the figures as *: $p < 0.05$, **: $p < 0.01$ or ***: $p < 0.001$. Data are shown in the figures as mean \pm SEM. Statistical analysis was performed with GraphPad Prism software (version 5.00 and 7.00) (Meul et al., 2020).

5 Results

Parts of this chapter were recently published as preprint:

Thomas Meul, Korbinian Berschneider, Sabine Schmitt, Christoph H. Mayr, Laura F. Mattner, Herbert B. Schiller, Ayse Yazgili, Xinyuan Wang, Christina Lukas, Cornelia Prehn, Jerzy Adamski, Elisabeth Graf, Thomas Schwarzmayr, Fabiana Perocchi, Alexandra Kukat, Aleksandra Trifunovic, Laura Kremer, Holger Prokisch, Bastian Popper, Christine von Toerne, Stefanie M. Hauck, Hans Zischka, Silke Meiners (2020) Adaptive mitochondrial regulation of the proteasome *bioRxiv* 2020.04.07.026161; doi: <https://doi.org/10.1101/2020.04.07.026161>

5.1 Mutator MEFs with chronic mitochondrial dysfunction maintain functions required for cellular viability

Experiments of the present study were performed with murine embryonic fibroblasts (MEFs) derived from the earlier described mtDNA mutator mouse model. Four different mutator MEF clones (from four different mice) and three distinct WT MEF cell lines were used to minimize clonal differences in the accumulation of mitochondrial DNA mutations (Trifunovic et al, 2005). Chronic respiratory chain dysfunction in mutator MEFs, which has been already shown by Berschneider (Berschneider, 2016), was confirmed in isolated mitochondria using the Oroboros™ device. Oxygen consumption of isolated mitochondria from one WT and one mutator cell line was analyzed in three independent experiments over a specific time period using the respective metabolites and inhibitors relevant for respiratory chain activity (Figure 1.1). The left axis shows the O₂ concentration in the chamber whereas the right axis indicates the drop of oxygen in pmol/(s*ml) during the measurement. The blue/cyan lines represent the changing oxygen concentration over time. Oxygen consumption of mitochondria is presented by purple/red lines. For optimal respiratory chain function substrates for different complexes of the respiratory chain were added at certain time points as shown by vertical lines. Glutamate and malate are complex I substrates whereas succinate is used up by complex II. By adding the combination of these substrates the respiratory chain consumes a specific amount of oxygen to maintain the membrane potential without producing ATP. When ADP was added together with the substrates oxygen consumption increased because ATP is produced in addition to the maintenance of the membrane potential. FCCP was used as a decoupler of the electron transport chain to induce maximal respiratory chain activity.

Antimycin A acts as complex III inhibitor and thereby blocks electron transport. This inhibitor was used to determine the “background”, i.e. oxygen consumption, independent of respiratory chain activity. The purple line (lower panel) indicates much lower oxygen consumption in mutator mitochondria compared to WT mitochondria (red line, upper panel). As oxygen consumption is directly connected to the activity of the mitochondrial respiratory chain, this measurement confirmed the chronic respiratory chain dysfunction in mutator MEFs.

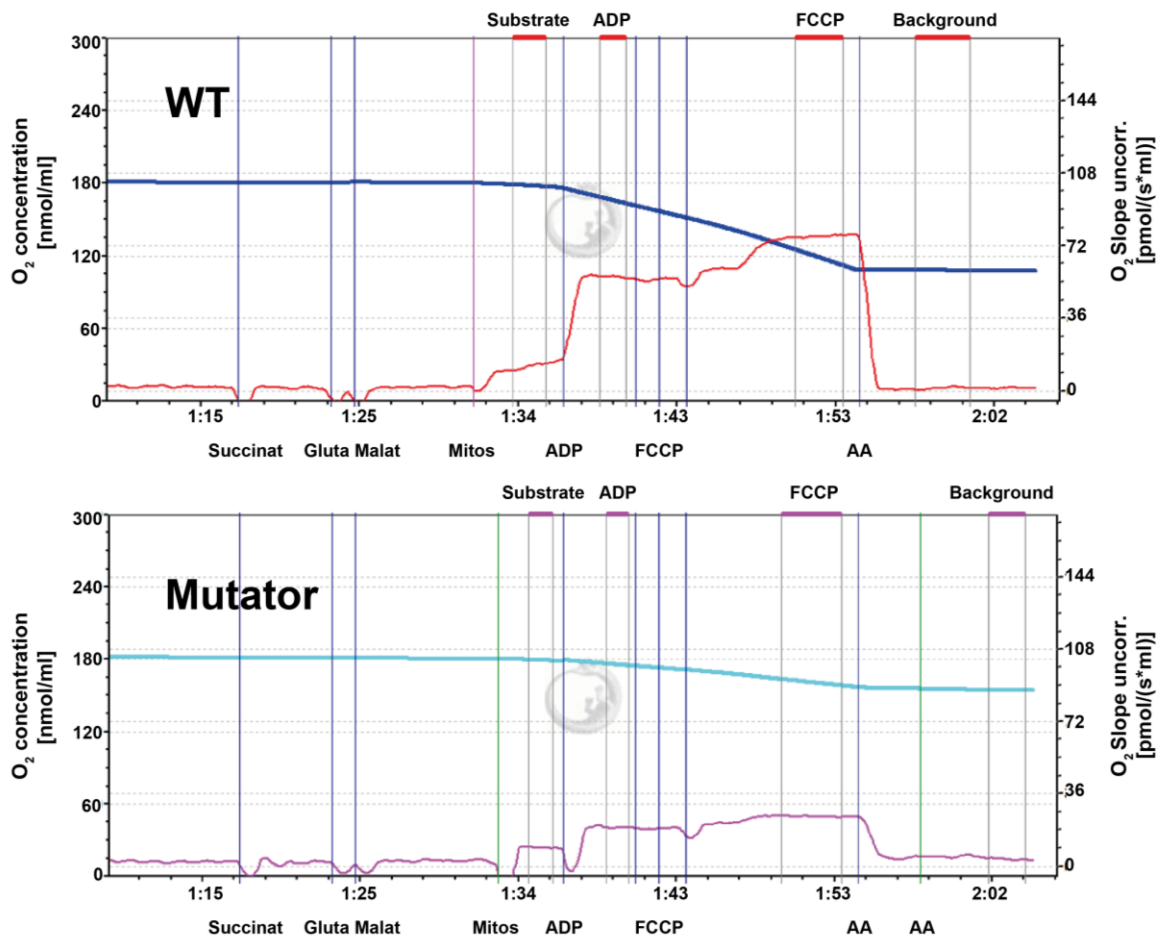


Figure 1.1 Measurement of oxygen consumption in mitochondria isolated from WT and mutator MEFs confirmed dysfunctional respiratory chain in mutator MEFs. Determination of mitochondrial respiratory chain activity in mitochondria isolated from one WT and one mutator cell line. Measurement was performed in an Oroboros™ oxygen chamber. Blue and cyan lines indicate the oxygen concentration in the chamber during the measurement. Red and pink lines represent the oxygen consumption of isolated mitochondria. Vertical purple lines label the time point when the respective reagents are added to the chamber. Succinate, glutamate and malate are added to induce mitochondrial respiratory chain activity, which is required to maintain the membrane potential in the absence of ATP production. ADP together with the other substrates leads to oxygen consumption by the respiratory chain to maintain the membrane potential and simultaneously produce ATP. FCCP is used as a decoupler to induce maximal respiratory chain activity. Antimycin A (AA) works as an inhibitor of respiratory chain function.

To further characterize the cellular state of mutator MEFs, the doubling rate per day was determined in WT and mutator MEFs using the proliferation assay according to Sullivan et al., 2015. Mutator MEFs grew significantly slower than WT MEFs (Figure 1.2A). However, this reduced doubling rate was not accompanied by any change in cellular morphology in mutator MEFs (Figure 1.2B). These data indicate that chronic respiratory chain dysfunction does not induce massive stress responses in mutator MEFs. This is in line with data from Trifunovic et al., 2005, which show that there is, for example, no increased oxidative stress in mtDNA mutator MEFs (Trifunovic et al., 2005). Furthermore, stress-related signaling pathways were not upregulated as demonstrated by proteomic analysis of WT and mutator MEFs (data not shown).

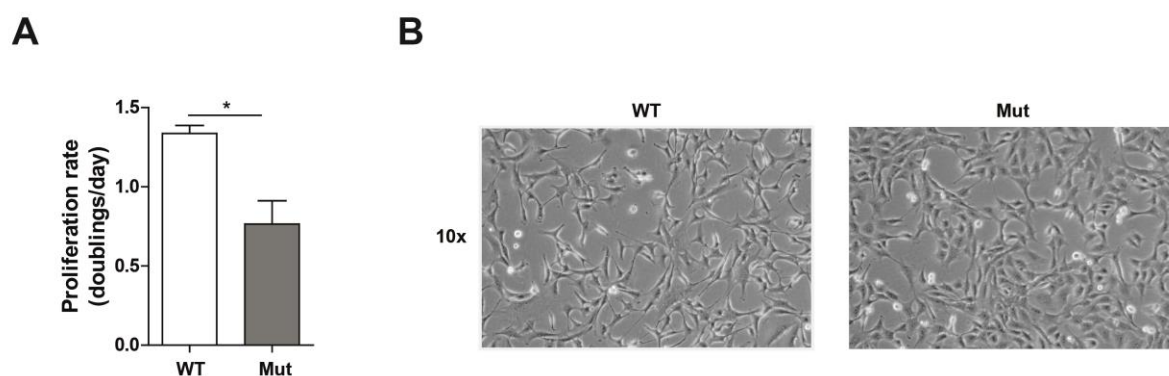


Figure 1.2 Mutator MEFs with impaired mitochondrial respiratory chain show reduced proliferation but normal cell morphology. (A) Proliferation rates of WT (n=3) and mutator (n=4) cell lines were determined by counting cells at day 1 and day 5 after seeding of the cells. Doublings per day were then calculated as explained in the methods part. Bar graphs show mean \pm SEM. Significance was determined using student's unpaired t-test. (B) Representative images show cellular morphology of WT and mutator MEFs. Magnification: 10x.

5.2 Proteasome activity and assembly is impaired in mutator MEFs with chronic mitochondrial dysfunction

To assess whether chronic mitochondrial respiratory chain dysfunction has an effect on the ubiquitin-proteasome system, proteasome activity was analyzed in WT and mutator MEFs. Enzymatic activity was determined by measuring cleavage of model peptides specific for the three 20S catalytically active sites CT-L, C-L and T-L via emitted chemiluminescence. The activity of all three proteolytic sites was significantly decreased in mutator compared to WT MEFs (Figure 2.1A). Of note, loss of proteasome activity by almost 50 % did not result in an accumulation of ubiquitinated proteins in mutator MEFs as shown by immunoblotting for UbiK48 (Figure 2.1B). This observation is remarkable and points to an adaptation of protein

turnover to the altered conditions in mutator MEFs where chronically reduced proteasome activity is balanced by diminished protein biosynthesis. In contrast, acutely reduced proteasome activity as for example induced by proteasome inhibition impairs degradation of ubiquitinated proteins and thereby results in a massive accumulation of such substrates in the cell (Heinemeyer et al., 1991; Hipp et al., 2012; Meiners et al., 2006).

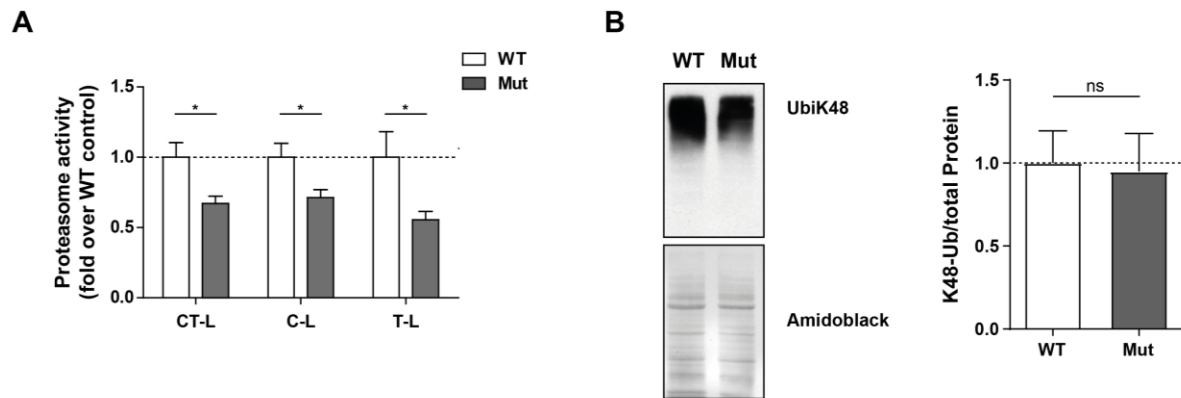


Figure 2.1 Proteasome activity is reduced in mutator MEFs without having an effect on levels of ubiquitinated proteins. (A) Activity of the three different proteasomal cleavage sites chymotrypsin-like (CT-L), caspase-like (C-L), or trypsin-like (T-L) in WT (n=3) and mutator (n=4) MEFs was determined by measuring chemiluminescence generated by proteasomal cleavage of luminogenic substrates specific for the respective active sites. Two-way ANOVA with Bonferroni multiple comparison test was applied to determine statistical significance between WT and mutator MEFs. Bar graphs show mean±SEM. All values were normalized to the mean of WT MEFs. (B) Levels of ubiquitinated proteins in WT (n=3) and mutator (n=4) MEFs were determined using Western blot analysis followed by immunostaining with an antibody specific for UbiK48-linked proteins. A representative Western blot is shown. Amido black staining was used as loading control. Bar graphs show levels of ubiquitinated proteins normalized to the mean of WT MEFs (mean±SEM). Significance was determined using student's unpaired t-test. Data were generated together with Korbinian Berschneider.

As the observed downregulation of proteasome activity in mutator MEFs could be a consequence of altered expression of proteasome subunits, levels of 20S proteasome and 19S regulatory particle subunits were analyzed using mass spectrometry and bulk mRNA sequencing in WT and mutator MEFs. However, differences between WT and mutator MEFs were neither found on protein nor on mRNA level. Proteomics data were generated from cell lysates of WT (n=3) and mutator (n=4) MEFs. The heatmap in Figure 2.2A shows a selection of identified proteasome subunits, which were all not significantly regulated between WT and mutator MEFs (p value < 0.05). Differences in the color code of the heat map indicate that levels of only single 20S and 19S subunits are slightly altered in WT and mutator MEFs. Bulk mRNA sequencing was performed in one WT and one mutator cell line. Five technical replicates were measured per cell line. The volcano plot in Figure 2.2B shows all genes, which were identified in the screen. The red dots indicate all identified proteasome subunits. The

majority of these subunits are located in the middle of the plot meaning that there is no difference in the expression between WT and mutator MEFs.

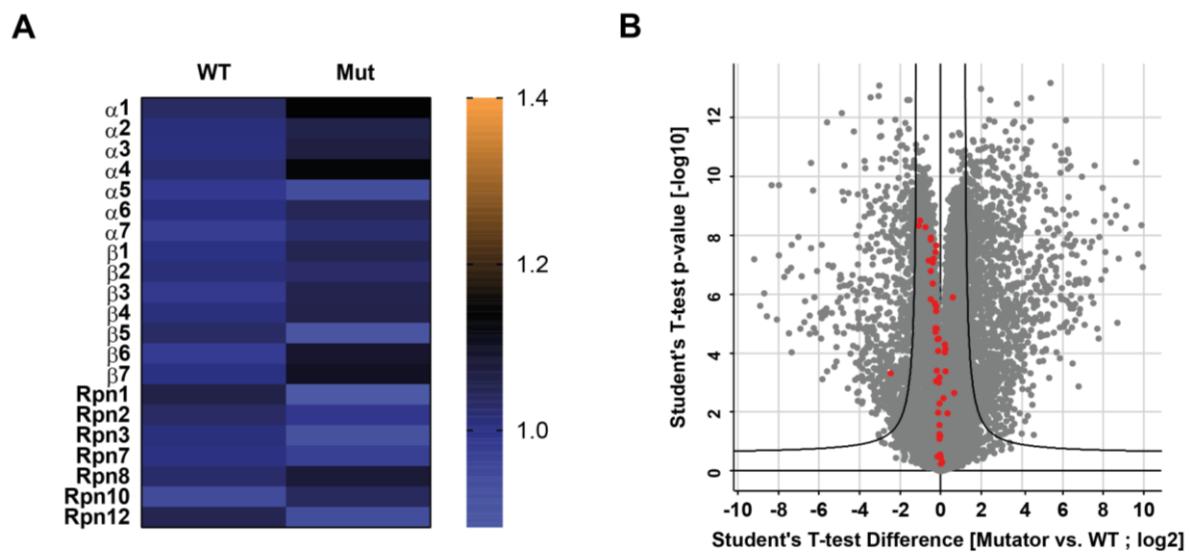


Figure 2.2 Expression of proteasome subunits is not affected by chronic mitochondrial dysfunction in mutator MEFs. (A) Heat map shows averaged protein levels of proteasome subunits between WT (n=3) and mutator (n=4) MEFs. Values obtained from mass spectrometry measurement were normalized to mean expression of all WT MEFs. (B) mRNA expression levels in one representative mutator MEF (n=5 technical replicates) and one representative WT MEF (n=4 technical replicates) cell line generated by mRNA bulk sequencing. Volcano plot shows all identified genes and proteasome subunits are highlighted in red. A 1% FDR was used to define statistical significance (values within the black line).

To check whether the general loss of proteasome activity in mutator MEFs is caused by a decreased assembly of active 26S and 30S proteasome complexes, native gel analysis was performed. Native gel electrophoresis allows for the separation of active proteasome complexes. CT-L activity of the different complexes was determined via an in-gel activity assay using fluorogenic peptides. The amount of active proteasome complexes was quantified by immunoblotting of the native gel and staining for 20S proteasomes using an α 1-7 antibody (Figure 1.5A). The in-gel activity assay clearly shows that the decreased proteasome activity in mutator MEFs is caused by lower activity of assembled 26S and 30S proteasome complexes compared to WT MEFs (Figure 2.3A, left panel). Immunoblotting revealed that not only activity but also the amount of assembled 26S and 30S proteasome complexes is reduced in mutator MEFs (Figure 2.3A, right panel). The levels of free 20S proteasomes were slightly however not significantly increased in mutator MEFs (Figure 1.5, quantification). To investigate whether assembly 20S proteasomes in mutator MEFs is altered, the total amount of 20S proteasomes was quantified from native gel blots and

mRNA level of the main 20S assembly factor Pomp were analyzed using qPCR. Total 20S was rather decreased in mutator MEFs (Figure 2.3B) and Pomp levels were significantly lower in mutator MEFs compared to WT MEFs (Figure 2.3C). These data indicate reduced assembly of active 26S and 30S proteasome complexes in mutator MEFs, which is adapted to altered cellular needs caused by chronic mitochondrial dysfunction.

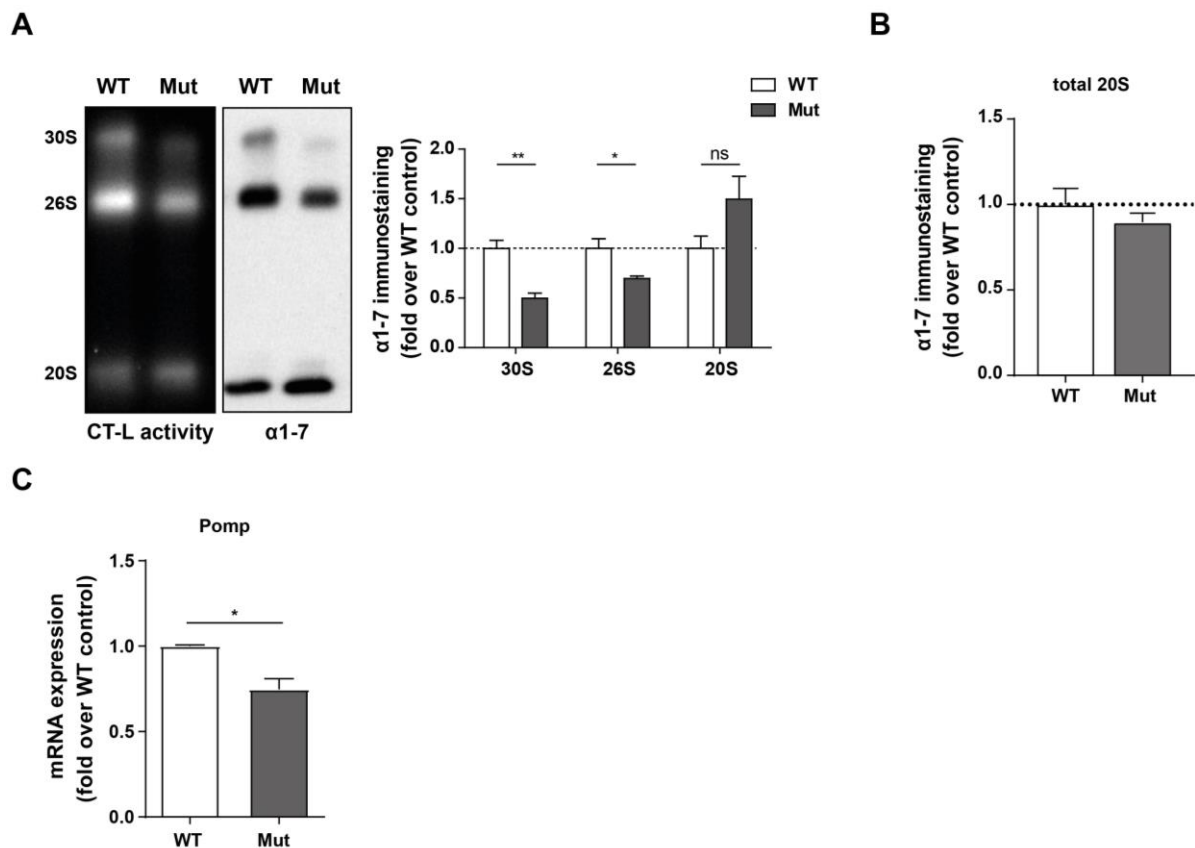


Figure 2.3 General loss of proteasome activity is caused by impaired assembly of 26S and 30S proteasome complexes. (A) Representative native in-gel activity assay of native cell lysates from WT (n=3) and mutator (n=4) MEFs for CT-L activity of separated 30S, 26S and 20S proteasome complexes (left panel) followed by α 1-7 immunostaining of the blotted native gel (right panel). Quantification shows mean \pm SEM relative to WT controls. Significance was determined using student's unpaired t-test. (B) Quantification of amounts of total 20S complexes in WT and mutator cells as resolved by blotting of native gels and immunostaining for the 20S subunits α 1-7. Bar graph shows combined signals for 30S, 26S and 20S related to WT controls. Significance was determined using student's unpaired t-test. (C) RT-qPCR analysis of Pomp mRNA expression in WT (n=3) and mutator (n=4) cells. Data represent mean \pm SEM relative to WT control. Statistical test: unpaired t-test.

5.3 Respiratory chain complex I deficiency leads to diminished aspartate biosynthesis in mutator MEFs

It has been shown before that mitochondrial dysfunction can influence the ubiquitin-proteasome system for example by increased ROS production or ATP deprivation (Paragraph 1.4). Berschneider, 2016 demonstrated that neither ROS nor ATP is responsible for the

decreased proteasome activity in mutator MEFs (Berschneider, 2016). Therefore, mitochondria from mutator and WT MEFs were characterized in detail to identify possible metabolic alterations, which could have an effect on proteasome activity and assembly. First, mitochondrial morphology was analyzed in WT and mutator MEFs using cytochrome C staining and electron microscopy. Cytochrome C staining, which visualizes the mitochondrial network, did not reveal any differences between WT and mutator MEFs (Figure 3.1A, upper panel). To identify alterations of the mitochondrial membrane or the inner structures electron microscopy images were taken of WT and mutator MEFs. These images show that the mitochondrial membrane is structurally intact in mutator MEFs but the inner cristae structure is slightly altered compared to WT MEFs (Figure 3.1A, lower panel). Additionally, quantification of mitochondrial volume related to whole cell space confirmed that the number of mitochondria is comparable between WT and mutator MEFs (Figure 3.1B).

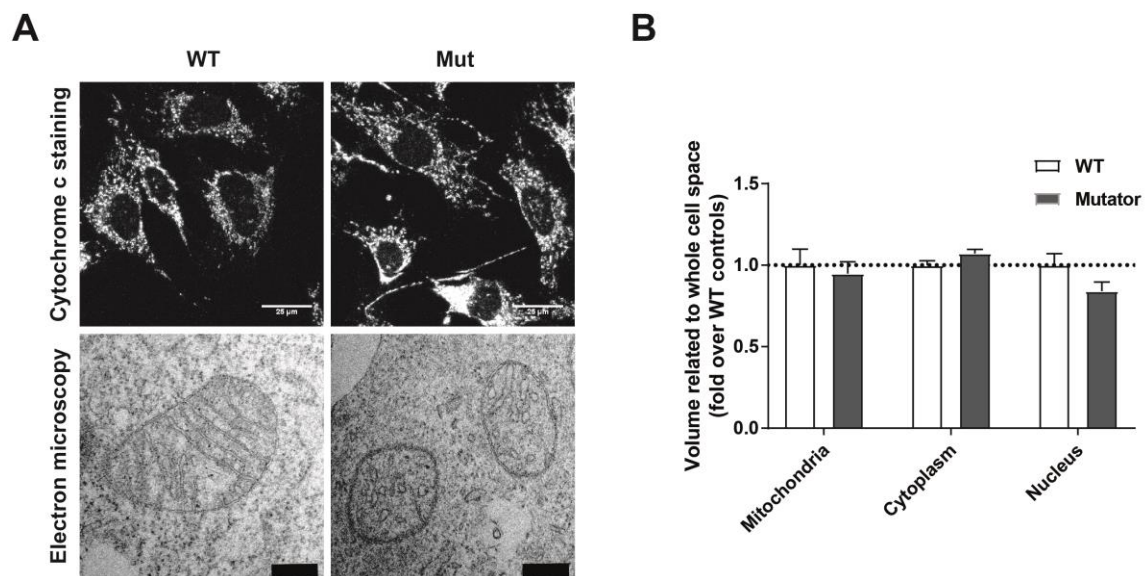


Figure 3.1 Mutator MEFs have structurally intact mitochondria and amount of mitochondria is not altered between WT and mutator MEFs. (A) Mitochondrial network in WT (n=3) and mutator (n=4) cells was analyzed by cytochrome c staining using an antibody specific for cytochrome c (upper panel). Scale bar: 25 μ m. Data were generated by Korbinian Berschneider. In the lower panel mitochondria in WT (n=3) and mutator (n=4) MEFs were visualized by electron microscopy. Scale bar: 1 μ m. (B) Mitochondrial volume was quantified in relation to cytoplasm and nucleus as described before (Hacker and Lucocq, 2013). In total, 30 electron micrographs (1000x magnification) from three wildtype clones (two technical replicates, each) and 43 electron micrographs (1000x magnification) from four mutator clones (two technical each) were used for quantification. Data represent mean \pm SEM relative to WT controls. Statistical test: student's unpaired t-test. Electron microscopy was done by Sabine Schmitt and Bastian Popper.

In a next step, intact mitochondria of WT and mutator MEFs were isolated. The isolation of structurally intact and functional mitochondria is a difficult procedure and requires an optimized protocol. To fulfill these requirements, the unique protocol from Schmitt et al., 2015 was used for isolation of WT and mutator mitochondria. In Figure 3.2A the procedure and the self-built device is schematically illustrated. Briefly, cells are homogenized with an automated high precision pump and mitochondria are separated from other cellular components by differential centrifugation. Finally, mitochondria are purified using a density gradient. Electron microscopy images as shown in Figure 3.2B confirmed the successful isolation of intact mitochondria both from WT and mutator cells. Higher magnification of isolated mitochondria (Figure 3.2B, lower panel) showed that mitochondrial membranes were structurally intact whereas the cristae were slightly altered in mitochondria isolated from mutator MEFs similar to the observations made with intact WT and mutator cells. Especially images with smaller magnification (Figure 3.2B, upper panel) revealed that comparable amounts of mitochondria could be isolated from WT and mutator MEFs. This impression was confirmed by comparable amounts of protein obtained from isolated WT and mutator mitochondria. Protein concentration was measured using the Bradford assay.

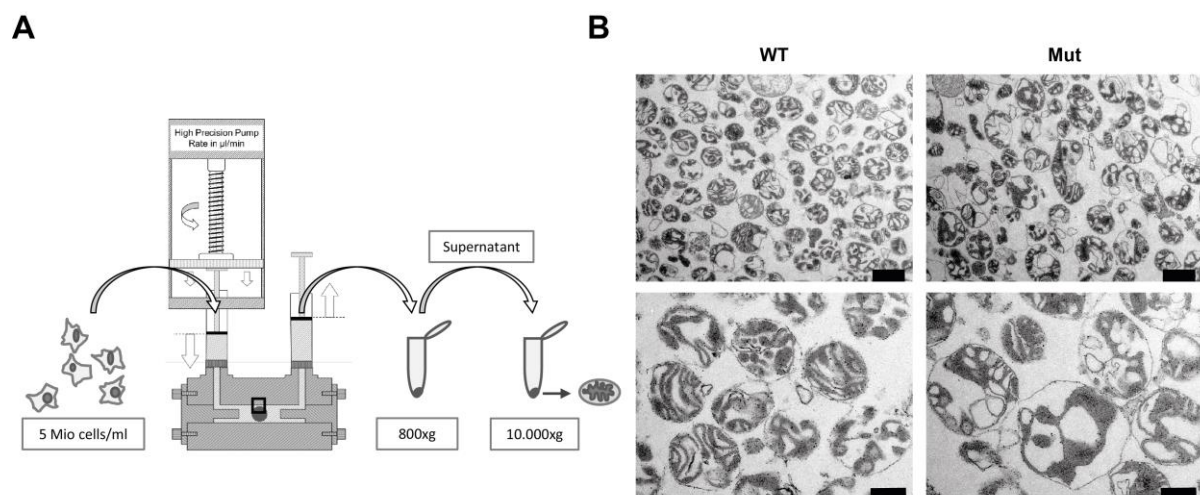


Figure 3.2 Isolation of structurally intact and functional mitochondria from WT and mutator MEFs.

(A) Scheme of the mitochondrial isolation procedure (B) Representative electron microscopy images of mitochondria isolated from one WT and one mutator cell line. Scale bar: upper panel 1 μm , lower panel 500 nm. Electron microscopy images were generated by Sabine Schmitt and Bastian Popper.

To analyze the composition of the respiratory chain, fractions of purified mitochondria isolated from WT and mutator MEFs were used for a proteome analysis via mass spectrometry. Evaluation of obtained proteomics data resulted in the identification of 714

mitochondrial proteins according to MitoCarta 2.0 (Calvo et al., 2016). More than 90 % of these mitochondrial proteins were not regulated more than twofold. To identify the main protein categories regulated in mutator cell mitochondria a so-called 1D annotation enrichment was performed on the whole data set. This analysis revealed an upregulation of glycolysis related proteins and a strong decrease in proteins linked to respiratory chain and here especially of proteins constituting respiratory complex I and IV (Figure 3.3A). The mitochondrial DNA encodes 13 subunits of the different respiratory chain complexes. All other components are expressed in the nucleus and imported into mitochondria (Herst et al., 2017). Most of the mtDNA encoded subunits are part of complex I (7 subunits). The other 6 subunits are distributed over the other complexes. As mutations are accumulating in the mitochondrial DNA of mutator MEFs, this leads to defective expression products and thereby to disrupted formation of the different complexes (Edgar et al., 2009; Trifunovic et al., 2005). The heatmap in Figure 3.3B clearly shows the reduced levels of complex I and IV components in mutator mitochondria. For this illustration only proteins were used, which were significantly different between WT and mutator mitochondria meaning that subunits of other complexes were either not detected or not significantly altered. Downregulation of complex I and IV proteins was confirmed by immunodetection of complex I (Ndufb8, nuclear) and complex IV (Mtco1, mitochondrial) subunits and points towards a drastic impairment of complex I and IV formation in mutator mitochondria. In contrast, protein levels of the complex III subunit Uqcrc2 (nuclear) were only slightly reduced and no difference was observed for complex II (Sdhb, nuclear) and IV (Atp5a, nuclear) (Figure 3.3C). For the immunodetection the Anti-OxPhos Rodent WB Antibody Cocktail (ThermoFisher) was used. In comparison to the heatmap in Figure 3.3B only single subunits of the different complexes are detected by the specific antibodies.

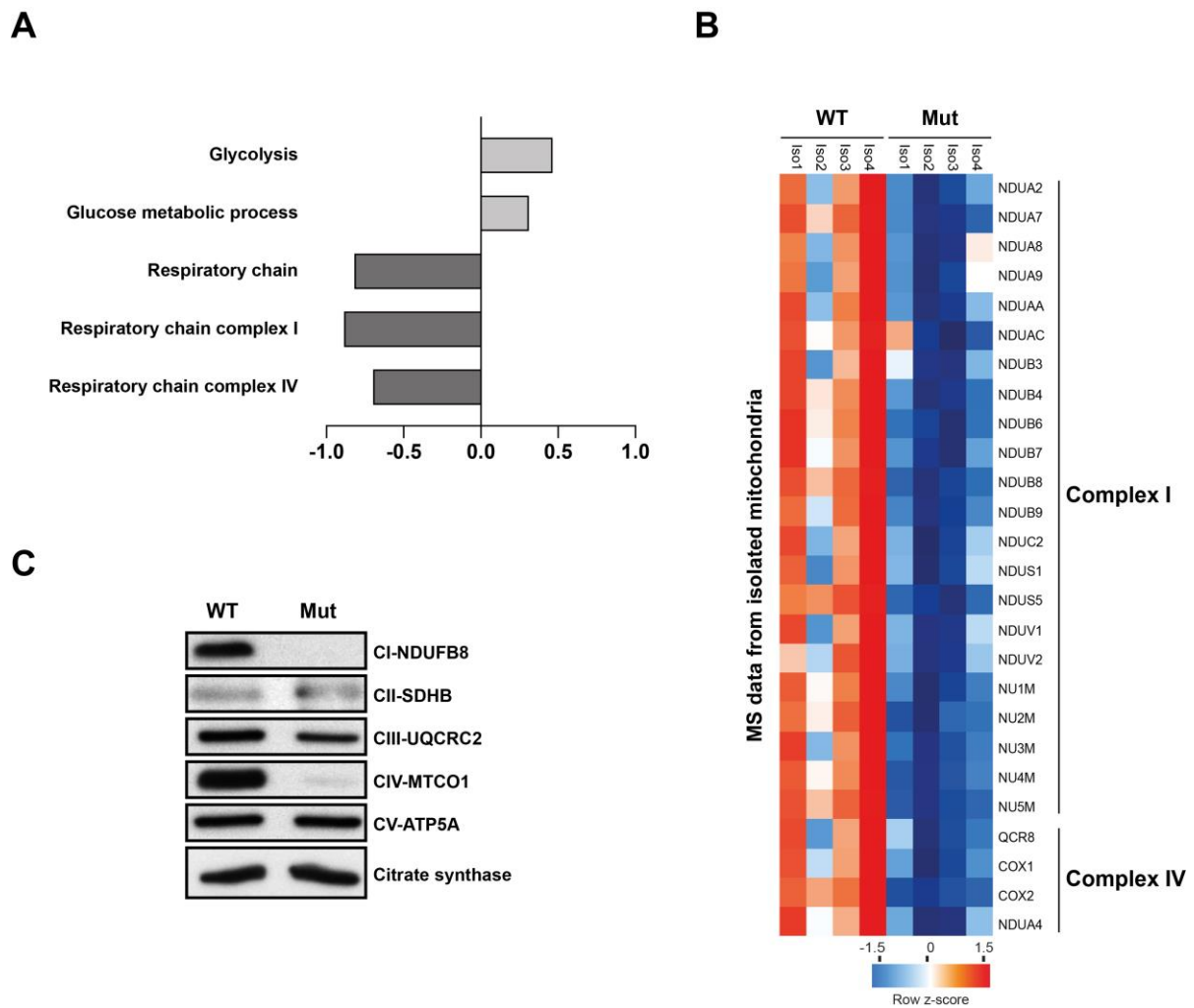


Figure 3.3 Mitochondria isolated from mutator MEFs show severe complex I and IV deficiency. (A) The bar graph shows the normalized annotation enrichment score of UniProt keyword and Gene Ontology (GO) annotations for a selection of mitochondrial metabolism related processes that were significantly regulated (FDR < 5%) between mitochondria isolated from one WT and one mutator cell line in the respective proteomics data set. For each cell line, 5 technical replicates were measured. The technical replicates were generated in independent isolation experiments. Due to experimental complexity only one representative WT and mutator cell line was chosen for the isolation procedure. (B) Heatmap representing z-scored relative protein mass-spectrometric intensities of significantly regulated respiratory chain complex subunits of mitochondria isolated from one mutator (4 technical replicates) and one WT (4 technical replicates) cell line. (C) Representative Western blot analysis of single respiratory chain complex subunits in mitochondria isolated from one WT and mutator cell line. Four independent isolations were used for Western blots. Citrate synthase served as a loading control (Meul et al., 2020).

Mitochondrial complexes I and IV are both essential parts of a functional respiratory chain. The loss of these complexes in mutator mitochondria explains the severe respiratory chain dysfunction in mutator MEFs. However, complex I plays a special role for the transfer of electrons over the respiratory chain because it is the entry point for electrons. Moreover, it is responsible for the regeneration of NAD^+ from NADH , which is generated in the TCA cycle. Loss of complex I would not only block the mitochondrial electron transfer but also the

regeneration of NAD^+ . These events would finally result in an accumulation of NADH (Figure 3.4A). To confirm these assumptions, NADH levels were determined in WT and mutator MEFs using the NAD/NADH-Glo assay kit (Promega). Indeed, an increase of NADH levels by almost 10 fold was observed in mutator MEFs compared to WT cells (Figure 3.4B).

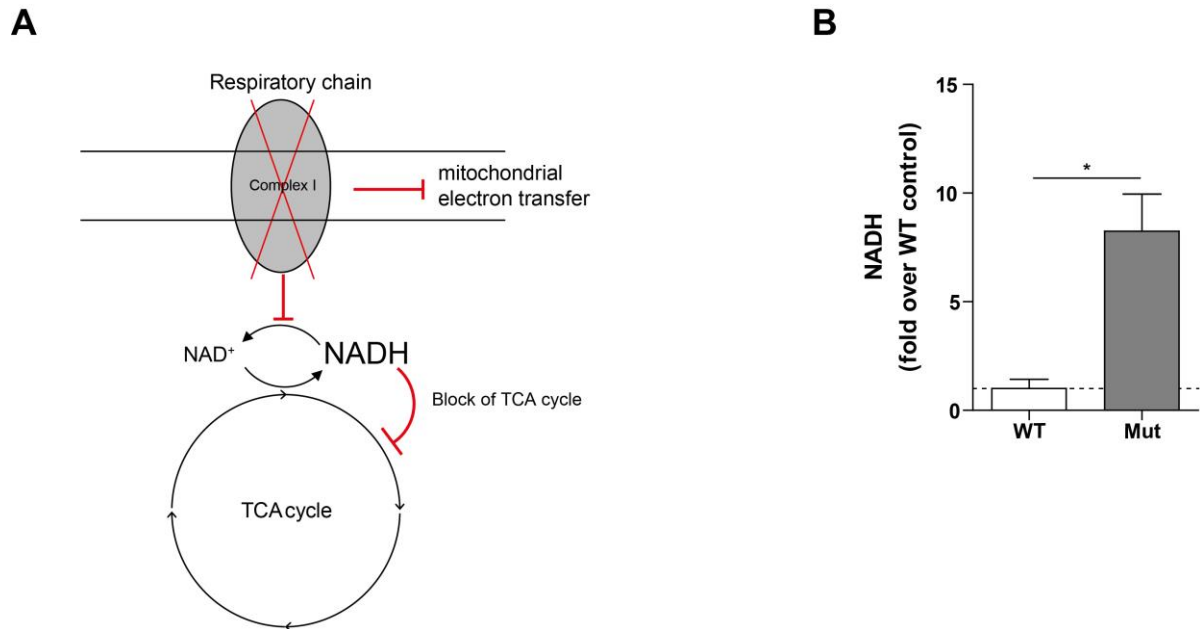


Figure 3.4 Loss of complex I in the respiratory chain leads to an accumulation of NADH in mutator MEFs.

(A) Schematic illustration showing effects of respiratory chain complex I deficiency on NAD^+ regeneration and mitochondrial electron transfer. (B) Cellular NADH levels in WT ($n=3$) and mutator ($n=4$) MEFs were measured using the NAD/NADH-Glo assay kit (Promega). Bar graphs illustrate values (mean \pm SEM), which were normalized to WT MEFs. Statistical significance between WT and mutator MEFs was determined using the student's unpaired t-test. Data were generated together with Korbinian Berschneider.

The concept of blocking the TCA cycle by increased NADH levels is well established (Martínez-Reyes and Chandel, 2020). In Figure 3.5A the TCA cycle is schematically illustrated and the steps of the cycle, which are inhibited by NADH, are indicated. As the biosynthesis of the two nonessential amino acids aspartate and glutamate depends on the activity of the TCA cycle its inhibition by NADH could lead to a disturbed production of these amino acids. To test this hypothesis a metabolomics screen for all 21 amino acids was performed in WT and mutator MEFs. The overall amino acid levels were not altered between WT and mutator MEFs, which indicates that amino acid uptake and overall biosynthesis of amino acids is not affected in mutator cells (Figure 3.5B, left panel). Glutamate can be also converted from glutamine that is supplemented in the cell culture medium used for MEF cultivation. Accordingly, levels of glutamate were found to be similar between WT and mutator MEFs

(Figure 3.5B, middle panel). Contrary, a significant reduction of aspartate levels was observed in mutator MEFs (Figure 3.5B, right panel). This finding is reasonable because aspartate is not supplemented in the medium and needs to be synthesized by the cells themselves. These data revealed an impaired biosynthesis of aspartate possibly due to impaired TCA cycle activity in mutator MEFs.

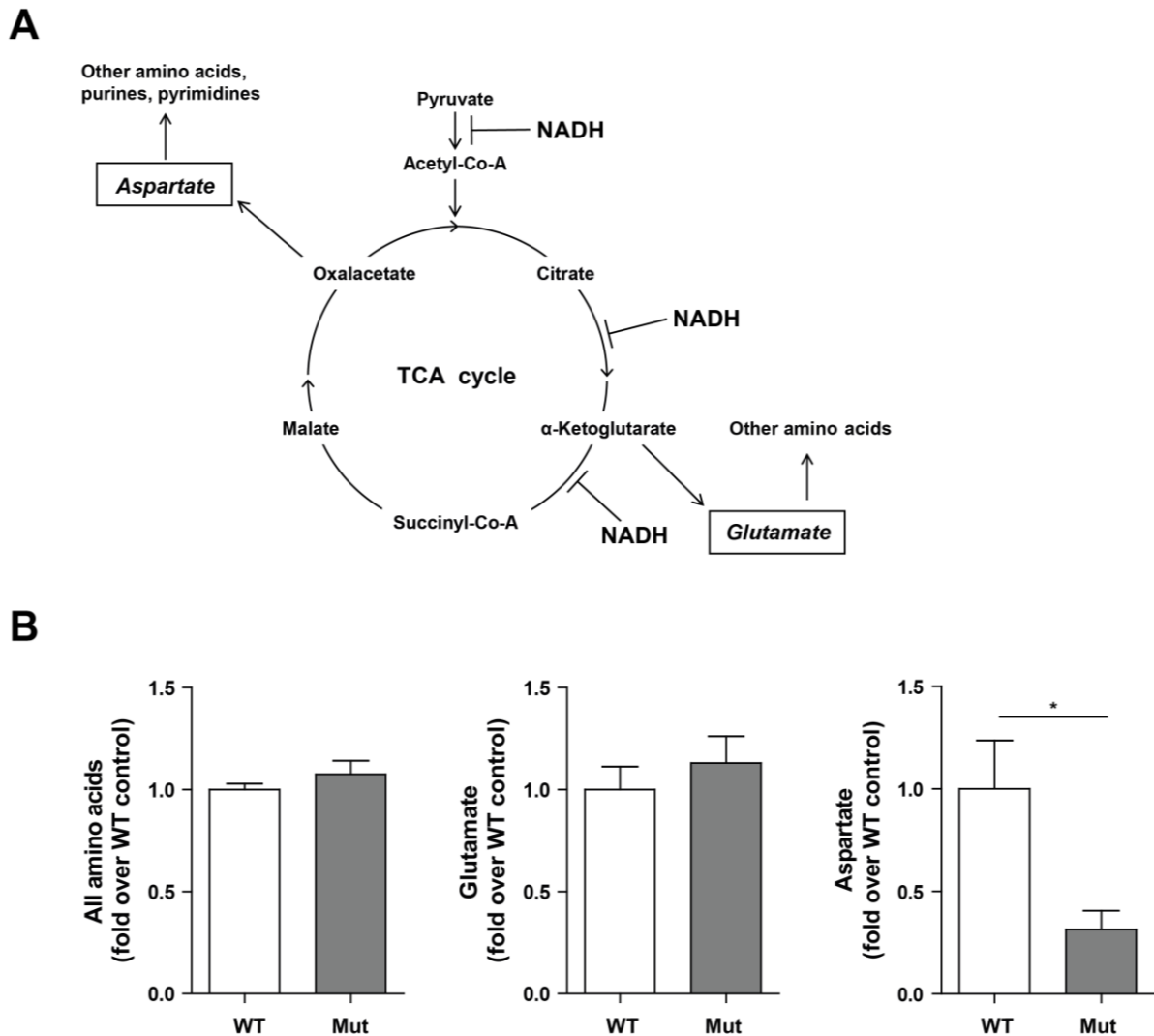


Figure 3.5 Aspartate biosynthesis is impaired in mutator MEFs with disturbed TCA cycle. (A) Schematic representation of the TCA cycle showing its involvement in the provision of amino acids. Increased NADH levels can inhibit the TCA cycle at the indicated stages. Aspartate and glutamate are especially important for the synthesis of other amino acids or purines and pyrimidines. (B) Quantification of amino acids in WT (n=3) and mutator (n=4) MEFs using targeted metabolomics (mass spectrometry based). 6 replicates were measured for each cell line and the respective values were normalized to the cell number of each cell line. Bar graphs show mean±SEM relative to WT controls. Significance was determined using student's unpaired t-test.

5.4 Aspartate deficiency causes global cellular alterations in mutator MEFs including protein synthesis

To further analyze effects of aspartate deficiency on global cellular processes in mutator MEFs, a proteomics analysis of WT and mutator cell lysates was performed. The earlier described 1D enrichment analysis was used again to identify significantly regulated pathways in mutator MEFs. In addition to mitosis related pathways the entire protein synthesis machinery was found to be downregulated (Figure 4.1). It has been demonstrated before that mitochondrial dysfunction can lead to aspartate deficiency (Birsoy et al., 2015; Sullivan et al., 2015). In this context, aspartate has been identified as an essential precursor of nucleotide synthesis. Consequently, aspartate deficiency has been found to cause decelerated proliferation in cells (Birsoy et al., 2015; Sullivan et al., 2015, 2018). This finding is in line with the decreased doubling rate in mutator MEFs. In contrast, impaired protein synthesis as a consequence of aspartate deficiency is a novel observation.

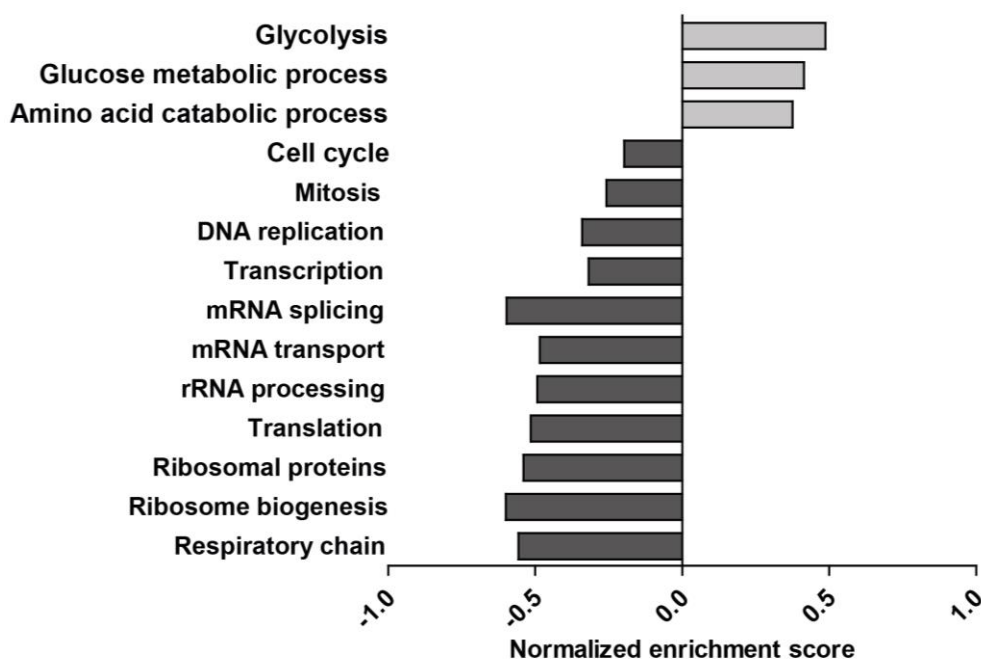


Figure 4.1 Aspartate deficiency causes global cellular alterations in mutator MEFs. Bar graph shows the normalized annotation enrichment score of UniProt keyword and Gene Ontology (GO) annotations for a selection of central cellular processes that were significantly regulated (FDR < 5%) between WT (n=3) and mutator (n=4) cells in the respective proteomics data sets.

To confirm the observed downregulation of protein synthesis in mutator MEFs, protein translation rates were determined using the Click-iT Plus OPP Protein Synthesis Assay Kit (Life Technologies, Carlsbad, CA, USA). To proof specificity of the generated fluorescence signal, cycloheximide (CHX) was used as an inhibitor of translation. Control cells were treated with 100 μ M of the inhibitor for 4 h and then the Click-iT Plus OPP Protein Synthesis Assay Kit was applied. Quantification of the signal in the CHX treated cells, which is almost completely gone, confirmed the specificity of the assay (Figure 4.2A). The obtained fluorescence signal, which is generated by native protein translation in the cell, was significantly lower in mutator compared to WT MEFs (Figure 4.2A). Hierarchical clustering of all significantly altered proteins between WT and mutator MEFs, which are related to protein biosynthesis, showed that not only the rate of translation is downregulated in mutator MEFs but also the protein levels of the entire protein synthesis machinery (Figure 4.2B). Downregulation of protein synthesis together with decreased proteasome activity indicates an adaptation of proteostasis to chronic mitochondrial dysfunction in mutator MEFs.

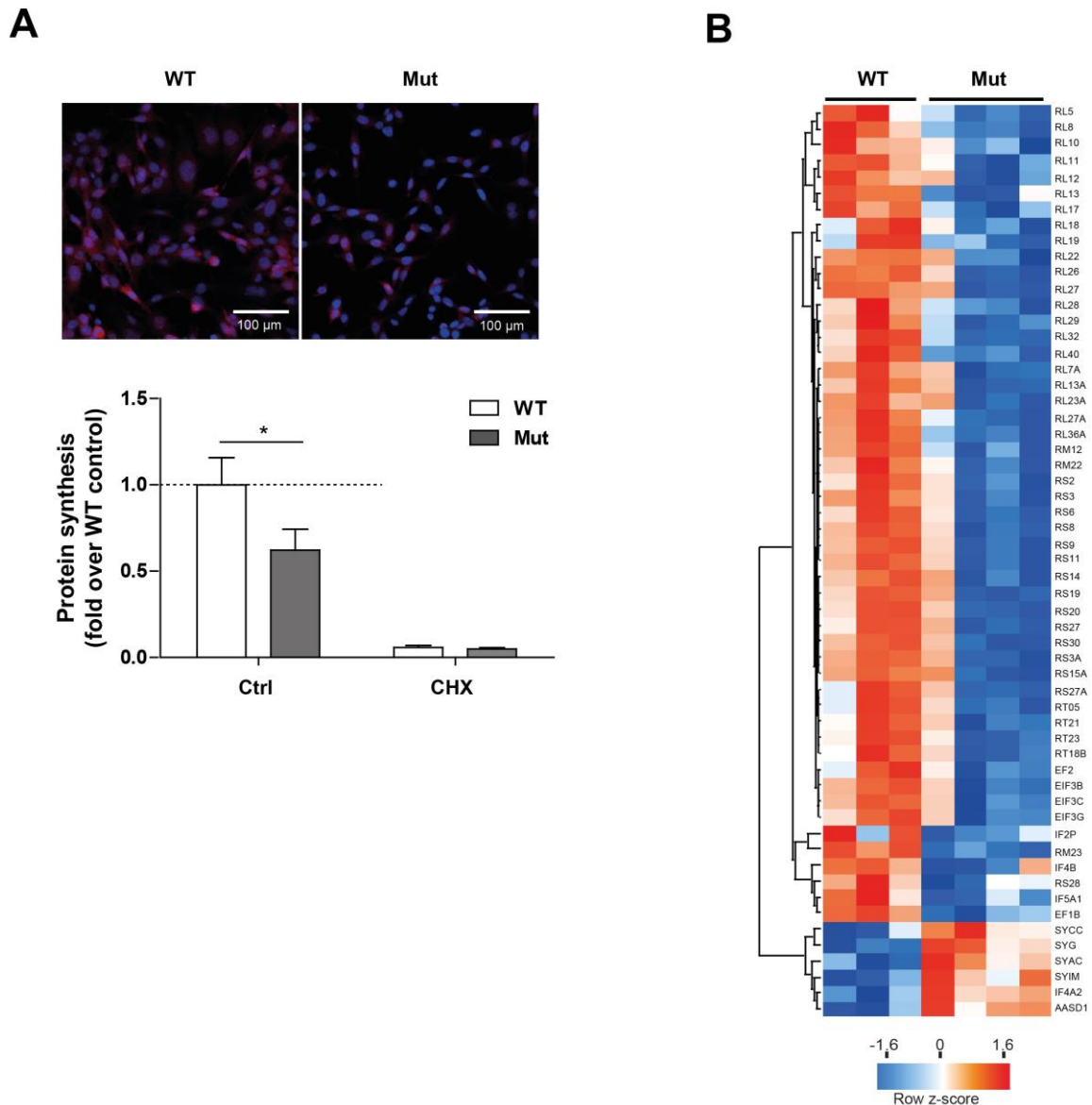


Figure 4.2 Protein synthesis is downregulated in mutator MEFs. (A) Determination of cellular protein translation rate using the puromycin analog OPP. Representative fluorescence images showing nascent protein synthesis (red signal) and cell nuclei (blue signal) in WT ($n=3$) and mutator ($n=4$) cells. Specificity of the assay was confirmed by treating cells with 100 μM protein synthesis inhibitor cycloheximide (CHX) for 4 h. Scale bar: 100 μm . Bar graph shows quantification of red signal (Mean fluorescence intensity). Data are represented as $\text{mean} \pm \text{SEM}$ relative to WT for Ctrl and CHX treated samples. Statistical test: Two-way ANOVA with Bonferroni multiple comparison test. Data were generated by Korbinian Berschneider. (B) Z-score of relative protein mass spectrometric intensities was used for unsupervised hierarchical clustering (using pearson correlation of rows) of significantly regulated proteins involved in translation. WT ($n=3$) and mutator ($n=4$) cells.

5.5 Aspartate supplementation activates proteasome activity and protein synthesis in mutator MEFs

To investigate whether the supplementation of the single amino acid aspartate can reverse the observed effects on proliferation and proteostasis in mutator MEFs, cells were treated with 10 mM aspartate for 72 h. As it has already been shown that aspartate supplementation can rescue proliferation in a different model of mitochondrial dysfunction (Birsoy et al., 2015; Sullivan et al., 2015), first, the doubling rate of mutator MEFs treated with aspartate was assessed. For that, cells of the four different mutator MEF lines were seeded the day before aspartate treatment. Cells were counted before and after aspartate treatment. The doubling rate per day was then calculated as described in the methods section. Aspartate significantly increased proliferation in all four mutator MEF cell lines after 72 h (Figure 5.1).

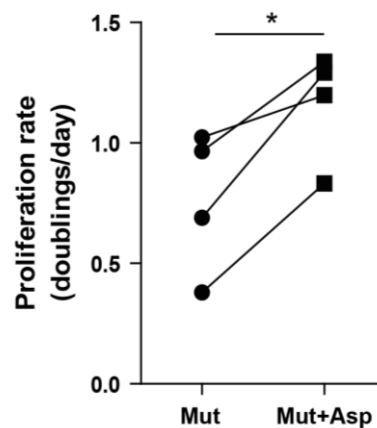


Figure 5.1 Proliferation is induced in mutator MEFs after aspartate supplementation. Proliferation rates of mutator (n=4) cell lines treated with 10 mM aspartate were determined by counting cells at day 1 and day 4 after seeding of the cells. Doublings per day were then calculated as explained in the methods part. Graph shows increase for each mutator cell line after aspartate supplementation. Significance was determined using student's paired t-test.

Next, the effects of aspartate on proteasome activity were analyzed. Here, the degradation of model peptides specific for the CT-L active site was significantly increased in mutator MEFs after aspartate supplementation (Figure 5.2A). To confirm this finding and to analyze the activity of the other two active sites of the proteasome, i.e. the C-L and T-L active sites, an activity based probe (ABP) was used (Verdoes et al., 2006, 2010). ABPs are fluorescently labeled optimized peptide substrates and bind specifically and irreversibly to the active sites in the native and assembled proteasome complexes. After SDS gel electrophoresis, proteasome complexes are broken apart, the active subunits are resolved by molecular weight and fluorescently labeled subunits indicate the number of different active sites.

Quantification of the obtained ABP bands revealed that aspartate mainly induced CT-L and T-L activity within the 20S core particle (Figure 5.2B).

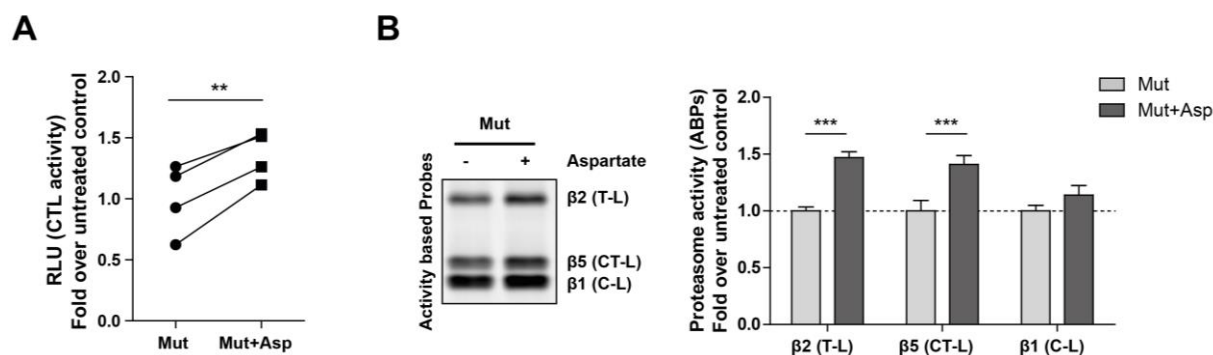


Figure 5.2 Aspartate supplementation leads to increased proteasome activity in mutator MEFs.

(A) Activity of the proteasomal cleavage site chymotrypsin-like (CT-L) was determined in mutator MEFs ($n=4$) treated with 10 mM aspartate for 72 h by measuring chemiluminescence generated by proteasomal cleavage of a luminogenic substrate specific for the respective active site. Graph shows control and aspartate treatment for each individual cell line (connected with a line). All values are normalized to the mean of untreated control MEFs. Statistical test: student's paired t-test. (B) Representative labeling of active proteasomal cleavage sites with Activity Based Probes (ABPs) in mutator cells ($n=4$) upon aspartate treatment for 72 h. Densitometric analysis shows activity of the three catalytically active sites (mean \pm SEM) between untreated control cells and aspartate treated mutator cells. Significance was determined using student's paired t-test.

Analysis of proteasome complexes by native gel electrophoresis followed by Western blotting in native protein extracts showed that aspartate supplementation in mutator MEFs for 72 h did not only induce proteasome activity but also assembly of 26S and 30S proteasome complexes. In-gel overlay with a substrate specific for CT-L activity revealed a much stronger signal for 26S and 30S proteasome complexes in aspartate treated cells compared to control cells indicating an increased activity of these complexes after aspartate supplementation (Figure 5.3A, left panel). Additionally, immunostaining and quantification of the blotted native gel with an antibody specific for the 20S subunits $\alpha 1-7$ confirmed a significantly higher amount of assembled 26S and 30S proteasome complexes in mutator MEFs treated with aspartate (Figure 5.3A, right panel + quantification). To determine the time point of aspartate induced proteasome activation in mutator MEFs a time course experiment with aspartate treatment for 6 h, 24 h and 48 h was performed. Therefore, proteasome complexes in native extracts isolated from aspartate treated mutator MEFs were separated using native gel electrophoresis followed by in-gel substrate overlay activity assay for CT-L activity and immunoblotting and staining for 20S $\alpha 1-7$ subunits. The first induction of 26S and 30S proteasome activity (Figure 5.3B, left panel) and amount

(Figure 5.3B, right panel) in aspartate treated cells could be observed after 24 h while the 6 h time point showed no differences between aspartate treated and nontreated mutator MEFs. Both activity and amount of 26S and 30S proteasome complexes were further increased after 48 h compared to 24 h of aspartate treatment. These data indicate that aspartate has no direct effect on the proteasome but rather activates it indirectly. Sullivan et al., (2015) have previously demonstrated that pyruvate can serve as an electron acceptor and helps to regenerate NAD^+ from NADH in a model of respiratory chain dysfunction. In their study pyruvate had the same effects on the rescue of proliferation as aspartate (Sullivan et al., 2015). Based on these findings mutator cells were treated with 1 mM pyruvate for 72 h to analyze whether proteasome activity and assembly could be induced by pyruvate comparable to aspartate. Native gel analysis showed that activity and amount of 26S and 30S proteasome complexes was indeed significantly higher in mutator MEFs after pyruvate treatment.

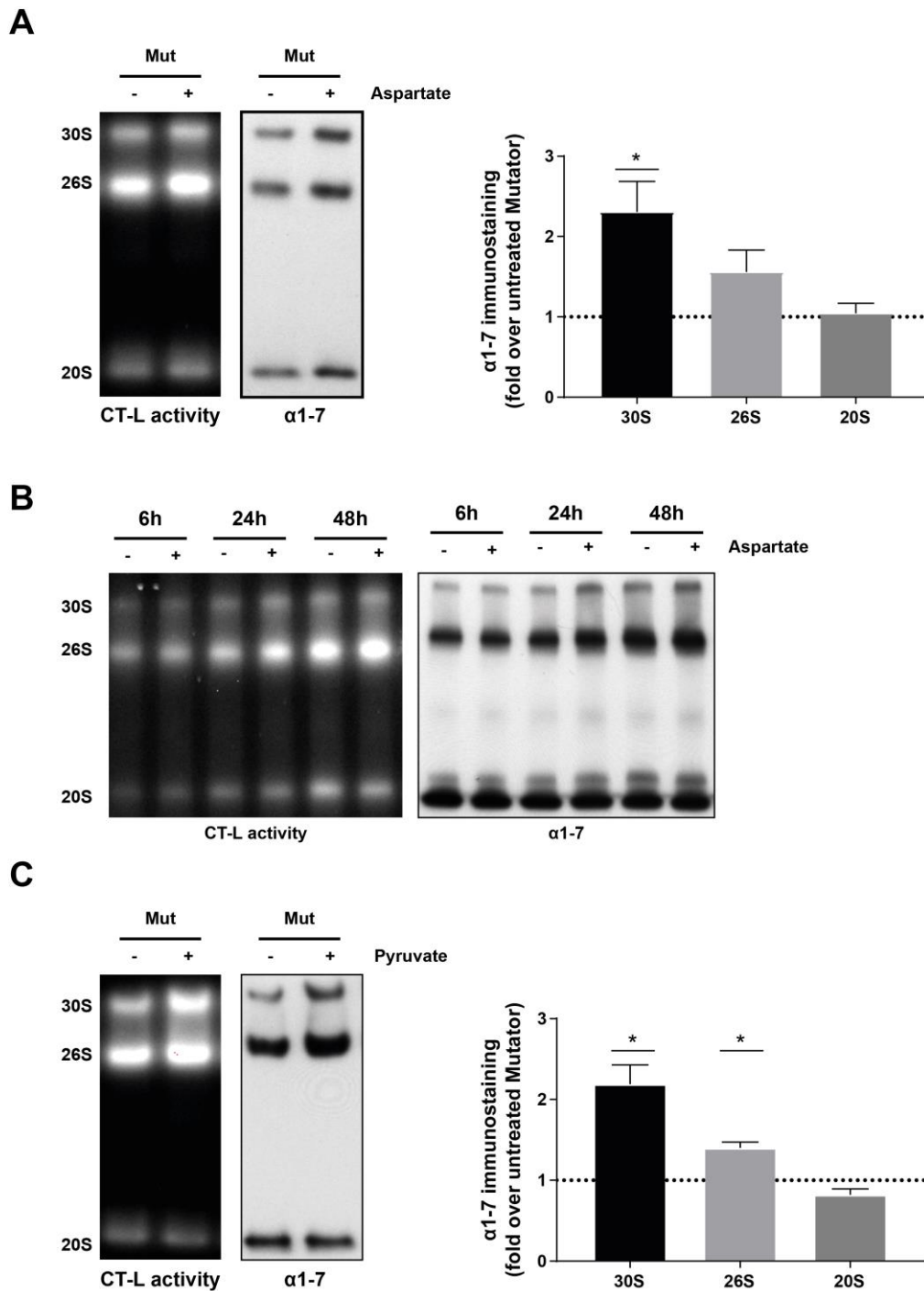


Figure 5.3 Aspartate or pyruvate supplementation activates proteasome assembly in mutator MEFs.

(A) Representative native in-gel activity assay (CT-L activity) of 30S, 26S and 20S proteasome complexes separated by native gel electrophoresis from mutator MEFs ($n=4$) treated with 10 mM aspartate for 72 (left panel) followed by $\alpha 1-7$ immunostaining of the blotted native gel (right panel). Quantification shows mean \pm SEM of the different aspartate treated mutator MEFs related to the respective control. Significance was determined using the one-sample t-test. (B) Representative native gel analysis of active proteasome complexes in cell lysates from one mutator cell line treated with 10 mM aspartate for 6 h, 24 h and 48 h. Chymotrypsin-like (CT-L) substrate overlay assay and immunoblotting for 20S $\alpha 1-7$ subunits is shown. (C) Representative native in-gel activity assay (CT-L activity) of 30S, 26S and 20S proteasome complexes separated by native gel electrophoresis from mutator MEFs ($n=3$) treated with 1 mM pyruvate for 72 (left panel) followed by $\alpha 1-7$ immunostaining of the blotted native gel (right panel). Quantification shows mean \pm SEM of the different pyruvate treated mutator MEFs related to the respective control. Significance was determined using the one-sample t-test.

To confirm that the observed effects of aspartate and pyruvate on proteasome activity and assembly were specific for the respiratory defect, mutant cells WT MEFs were treated with aspartate or pyruvate for 72 h. Cells of the three different WT MEF lines were seeded and treated the next day with 10 mM aspartate for 72 h. The doubling rate per day was assessed according to the formula in the methods part. Figure 5.4A shows that there is no difference in the proliferation rate between aspartate treated WT and control cells. Activity and amount of proteasome complexes in native extracts from aspartate (10 mM) or pyruvate (1 mM) treated WT MEFs were analyzed using native gel electrophoresis followed by in-gel overlay with a CT-L specific substrate and immunostaining for 20S α 1-7 subunits. Neither aspartate nor pyruvate induced activity or assembly of 26S and 30S proteasome complexes in WT MEFs after 72 h of treatment (Figure 5.4B+C). Analysis of proliferation and proteasome activity showed that these metabolites have no influence on MEFs with functional mitochondria (Figure 5.4).

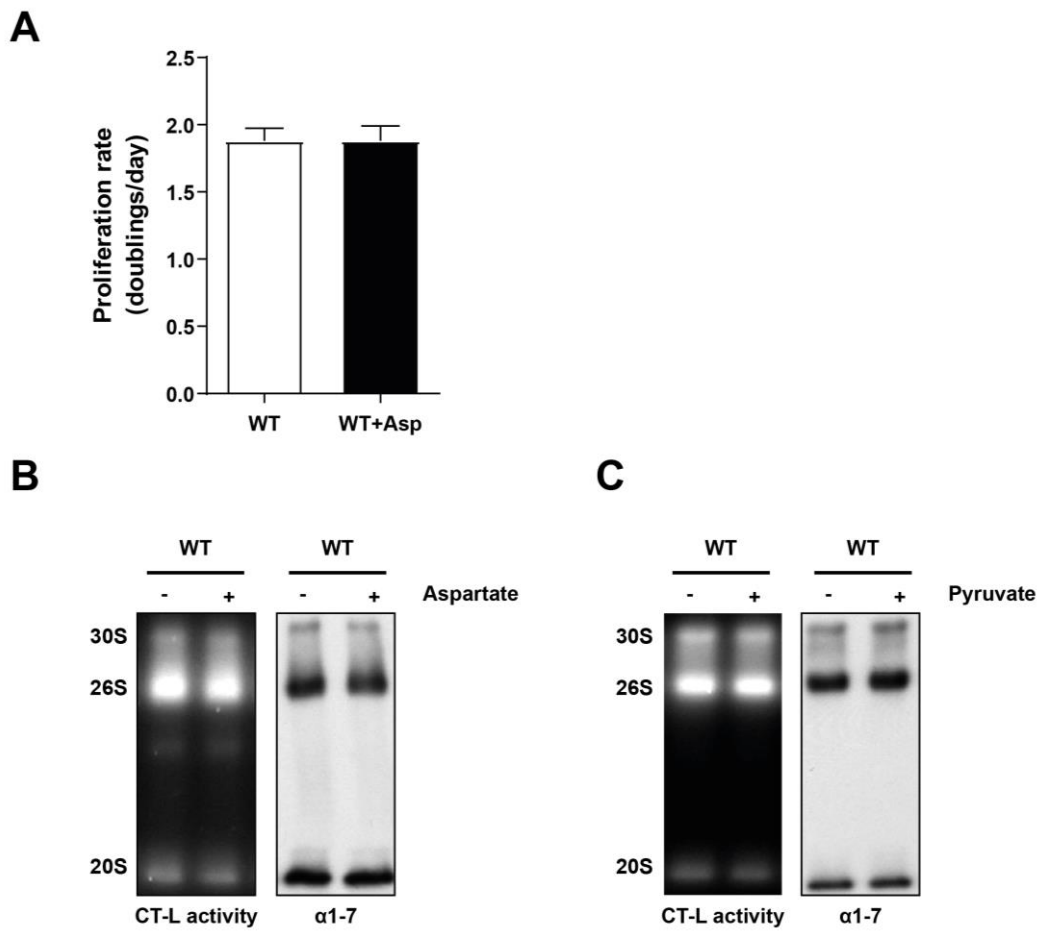


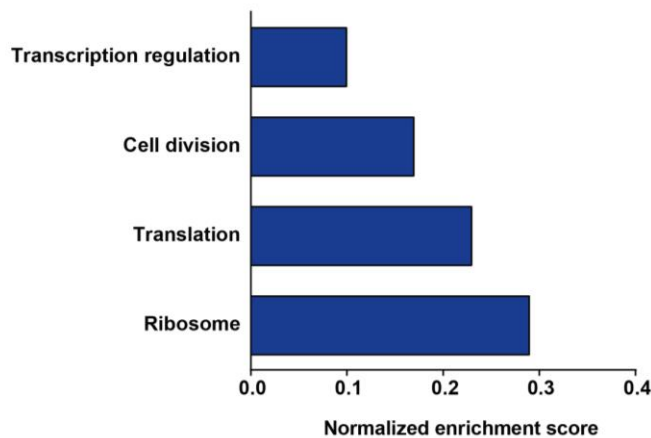
Figure 5.4 Aspartate or pyruvate supplementation has no effect on WT MEFs. (A) Proliferation rates of WT MEFs (n=3) treated with 10 mM aspartate for 72 h were determined by counting cells at day 1 and day 4 after seeding of the cells. Bar graph doubling rate per day for aspartate treated WT MEFs and untreated MEF controls. Significance was determined using student's paired t-test. (B+C) Native gel analysis of proteasome complexes in native extracts isolated from one WT MEF cell line (n=3 independent experiments) treated with 10 mM aspartate or 1 mM pyruvate for 72 h. CT-L activity and amount of proteasome complexes were determined by an in-gel substrate overlay assay followed by Western blotting and immunostaining with an antibody specific for the 20S subunits α 1-7.

Next, it was investigated whether aspartate treatment was also able to reactivate protein synthesis in mutator MEFs. First, mass spectrometry was used to determine differences in the proteome of the four mutator MEF cell lines in the absence and presence of 10 mM aspartate for 72 h. 1D annotation enrichment analysis of the whole proteomics data set showed that protein synthesis related pathways were upregulated in mutator MEFs supplemented with aspartate (Figure 5.5A). 1D enrichment also confirmed the already shown induction of proliferation in mutator MEFs after aspartate treatment (Figure 5.5A). To further assess effects of aspartate on protein synthesis, mutator MEFs (n=4) were treated with 10 mM aspartate for 48 h and translation rates were determined using the EZClick™ O-propargyl-puromycin (OPP) reagent. Control cells were treated with

100 μ M cycloheximide for 4 h to confirm specificity of the assay by inhibiting cellular translation. Native protein synthesis was found to be significantly upregulated in all four mutator cell lines after aspartate treatment (Figure 5.5B). The obtained data point to an adaptive regulation of proteostasis by mitochondrial metabolism in mutator cells with chronic respiratory chain dysfunction.

A

Aspartate treatment vs Control cells Uniprot GOBP & Keyword category enrichment



B

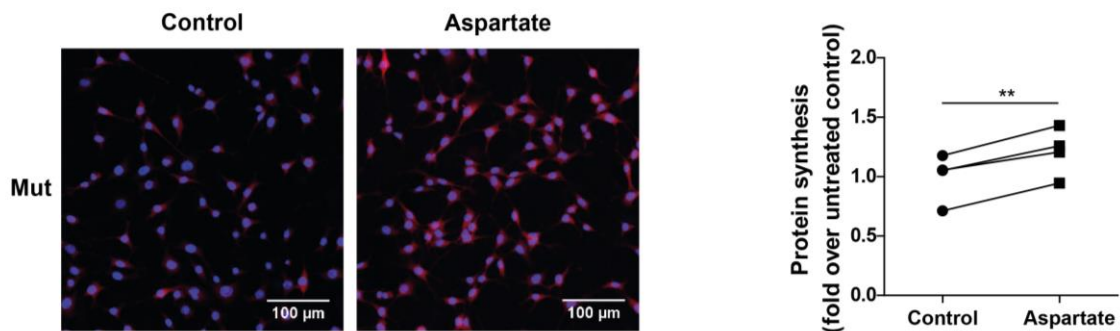


Figure 5.5 Aspartate supplementation reactivates protein translation in mutator MEFs. (A) Bar graph shows the normalized annotation enrichment score of UniProt keyword and Gene Ontology (GO) annotations for a selection of translation related processes that were significantly regulated (FDR < 5%) between aspartate treated mutator MEFs and untreated controls in the respective proteomics data set. (B) Protein translation in aspartate treated mutator MEFs (n=4) was analyzed using EZClick™ Global Protein Synthesis Assay Kit (Biovision), which is based on the puromycin analog OPP. Representative fluorescence images show protein synthesis rate in untreated controls and mutator MEFs treated with aspartate for 48 h. Cells were identified via DAPI staining (blue signal) and protein synthesis rate was quantified by measuring the mean fluorescence intensity (MFI) of the red signal. Graph shows control and aspartate treatment for each individual cell line (connected with a line). All values are normalized to the mean of untreated control MEFs. Scale bar: 100 μ m. Statistical test: student's paired t-test.

5.6 Aspartate supplementation induces 26S proteasome complex assembly by the expression of specific proteasome assembly factors

To analyze the mechanistic details that mediate aspartate induced activation of proteasome activation in mutator MEFs, expression levels of proteasome subunits and factors involved in the assembly of 26S and 30S proteasome complexes were determined upon aspartate treatment using Western blot analysis and quantitative RT-PCR. Western blot analysis revealed that protein levels of 20S subunits α 1-7 and β 5 were not changed in mutator MEFs after 72 h of aspartate treatment while the levels of the assembly factors Rpn6 (Psm11), p27 (Psm9) and p28 (Psm10) were significantly increased (Figure 6.1A). Table 1 shows corresponding protein and gene names for the different assembly factors. S5b, p27 and p28 are members of the 19S assembly chaperone family whereas Rpn6 is an essential 19S subunit responsible for the assembly of 19S and 20S (Pathare et al., 2012; Rousseau and Bertolotti, 2016). Of note, S5b was the only assembly chaperone, which was not induced by aspartate (Figure 6.1A). Proteomics analysis of aspartate treated mutator MEFs (n=4) and untreated controls (n=4) confirmed that the majority of proteasome subunits is not regulated by aspartate (Figure 6.1B). Volcano plot shows all proteins identified in the proteomics screen of aspartate treated mutator MEFs. Proteasome subunits are indicated as red dots. Quantitative RT-PCR confirmed the specific upregulation of assembly factors after aspartate treatment. However, on mRNA level the effect was already detectable after 6 h of aspartate supplementation indicating an early transcriptional activation of specific assembly factors as a response to aspartate (Figure 6.1C). Moreover, comparison of assembly factor levels between WT and mutator MEFs showed that these subunits are significantly downregulated in mutator MEFs (Figure 6.1D). This observation points to a regulation of proteasome activity via expression of specific assembly factors in order to adopt protein turnover to the current cellular needs. The assembly chaperone S5b was neither regulated on protein nor on mRNA level after aspartate supplementation. However, its protein levels were significantly upregulated in mutator MEFs compared to WT MEFs (Figure 6.1D).

Protein name	Gene name
Rpn6	Psm11
S5b	Psm5
p27	Psm9
p28	Psm10

Table 1 Nomenclature for specific assembly factors

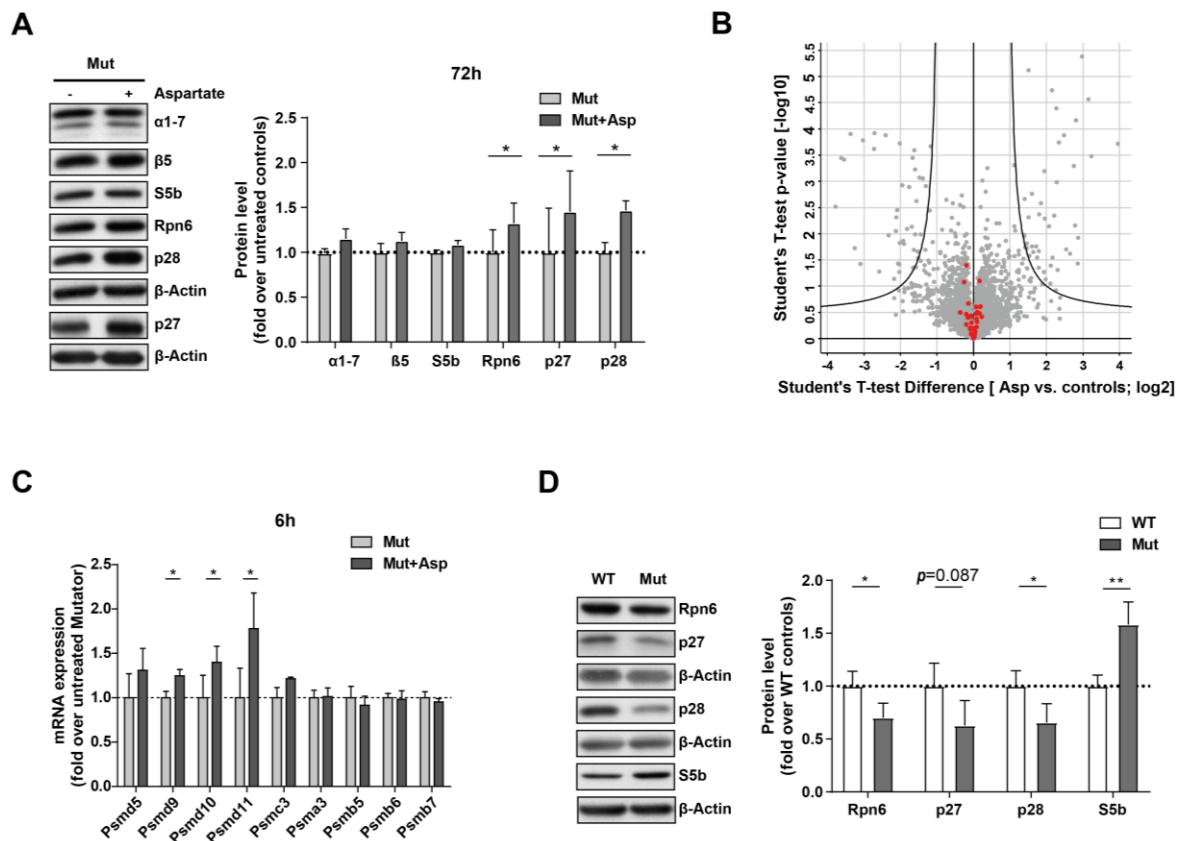


Figure 6.1 Aspartate supplementation induces the expression of specific proteasome assembly factors in mutator MEFs. (A) Protein levels of 20S (α 1-7, β 5) and 19S (Rpn6, p27, p28, S5b) subunits were analyzed by Western blot analysis in mutator MEFs ($n=4$) treated with 10 mM aspartate for 72 h. Western blot images show one representative treated and nontreated mutator MEF cell line. β -Actin was used as a loading control. Bar graph shows the corresponding quantification of the signals obtained for the individual subunits. Values are normalized to the mean of the untreated controls and illustrated as mean \pm SEM. Student's paired t-test was applied to determine statistical significance. (B) Protein levels in mutator MEFs ($n=4$) treated with aspartate for 72 h were measured by mass spectrometry. Volcano plot shows all identified proteins in aspartate treated mutator MEFs vs untreated controls. Proteasome subunits are highlighted in red. A 10 % FDR was used to define statistical significance (values within the black line). (C) mRNA expression of 20S subunits (Psm3, Psm5, Psmb6, Psmb7) and 19S subunits (Psm5, Psm9, Psm10, Psmc3) was determined by RT-qPCR in mutator MEFs ($n=3$) treated with aspartate for 6 h. Bar graphs show mean \pm SEM of the individual treated and nontreated mutator MEFs. Significance was determined using student's paired t-test. (D) Protein levels of the assembly factors Rpn6, p27, p28 and S5b were analyzed by Western blot analysis in WT ($n=3$) and mutator ($n=4$) MEFs. Western blot images show one representative WT and mutator MEF cell line. β -Actin was used as a loading control. Bar graph shows the corresponding quantification of the signals obtained for the individual subunits. Values are normalized to the mean of the WT controls and illustrated as mean \pm SEM. Student's unpaired t-test was applied to determine statistical significance.

To confirm the involvement of the assembly factors S5b, p27, p28 and Rpn6 in aspartate induced proteasome assembly, silencing experiments were performed in the absence and presence of aspartate. To reduce complexity, one representative mutator cell line was chosen for all silencing experiments. Technical replicates were generated in at least four independent silencing experiments. Cells were reverse transfected either with two different target siRNAs for S5b, p27, p28 and Rpn6 or with a mixture of two scrambled control siRNAs on the seeding day. The next day, cells were treated with fresh medium containing 10 mM aspartate for 72 h. As the assembly chaperones S5b, p27, p28 are not essential for the cell, silencing was performed with 10 nM of siRNA mixture. In contrast, Rpn6 is essential for cell viability and therefore only a partial knockdown of this subunit with 0.5 nM siRNA mixture was possible in order to avoid effects on proliferation and proteasome activity already in the absence of aspartate (Semren et al., 2015). Silencing efficiency was analyzed by Western blot analysis of the respective subunits (Figure 6.2). Next, the effect of assembly factor silencing on aspartate induced proteasome assembly was analyzed by native gel analysis. While knockdown of p27 had no influence on proteasome activity and assembly after aspartate supplementation (Figure 6.2, middle panel), silencing of p28 and Rpn6 prevented the full induction of proteasome assembly by aspartate (Figure 6.2, left and right panel). Quantification of native gel blots confirmed the significant lower levels of assembled 26S and 30S proteasome complexes upon silencing of p28 and Rpn6 in combination with aspartate treatment (Figure 6.2, lower panel). In general the effects of silencing of single assembly factors on 26S proteasome assembly was only minor indicating that the regulation of proteasome assembly might rather be a concerted action of all assembly factors.

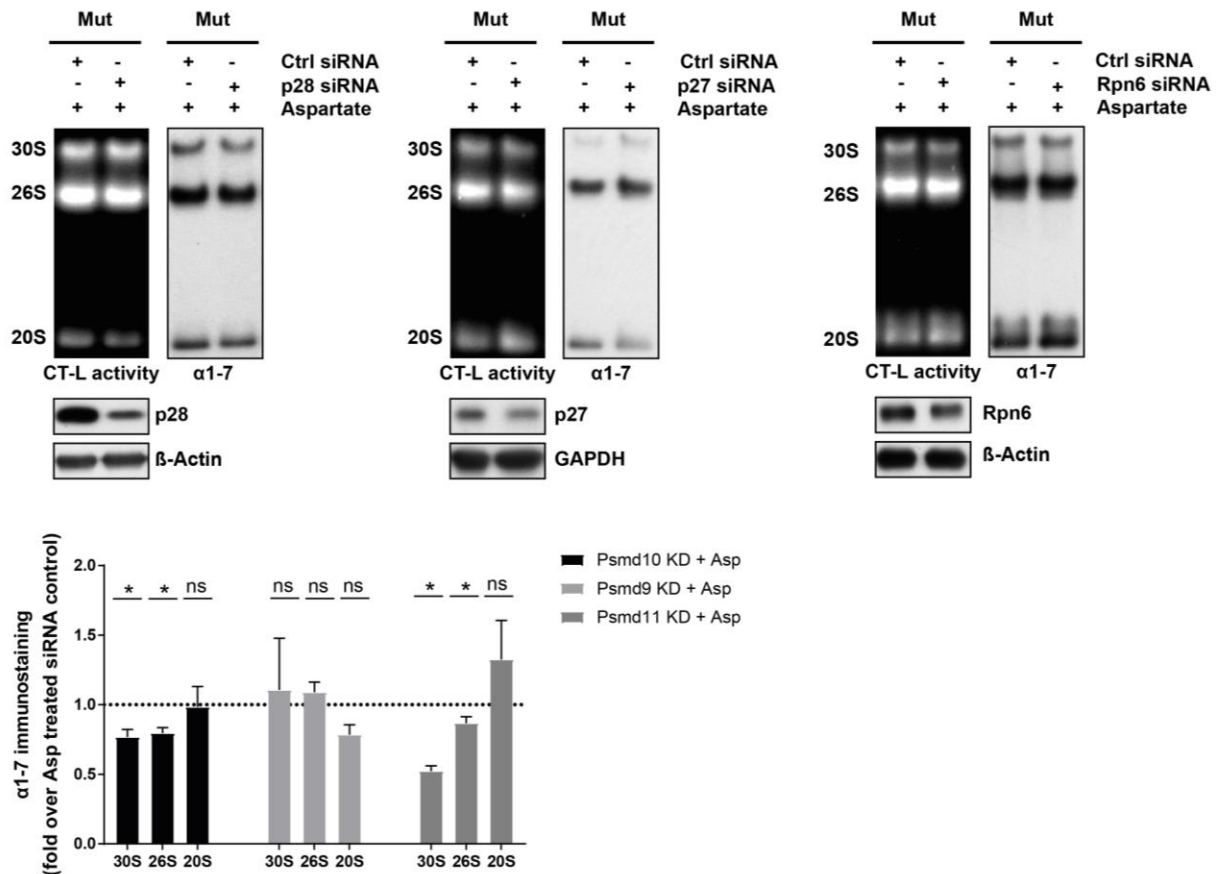


Figure 6.2 Silencing of specific proteasome assembly factors prevents aspartate induced activation of the proteasome in mutator MEFs. (A) Native gel analysis of proteasome complexes in native extracts isolated from one mutator cell line upon Rpn6 (n=5 technical replicates), p28 (n=4 technical replicates) and p27 (n=3 technical replicates) silencing treated with 10 mM aspartate for 72 h. CT-L activity and amount of proteasome complexes were determined by an in-gel substrate overlay assay followed by Western blotting and immunostaining with an antibody specific for the 20S subunits α 1-7. For control cells two different scrambled control siRNAs were used. Knockdown was confirmed via immunostaining for Rpn6, p27 and p28. Only partial knockdown of Rpn6 was used to prevent cellular stress. Quantification shows mean \pm SEM of the different aspartate treated mutator MEFs upon silencing related to the respective aspartate treated controls. Significance was determined using the one-sample t-test.

To prove that silencing of the respective assembly factors only prevented full induction of proteasome activity and assembly upon aspartate treatment and did not influence the proteasome in the absence of aspartate, proteasome complexes were analyzed by native gel electrophoresis upon knockdown of p27, p28 and Rpn6 in non-treated mutator cells. In-gel activity assay for CT-L activity followed by Western blotting and staining for the 20S subunits α 1-7 confirmed that silencing of the assembly factors had no effect neither on 26S and 30S proteasome activity (Figure 6.3, left panels) nor on the amount of these complexes (Figure 6.3, right panels).

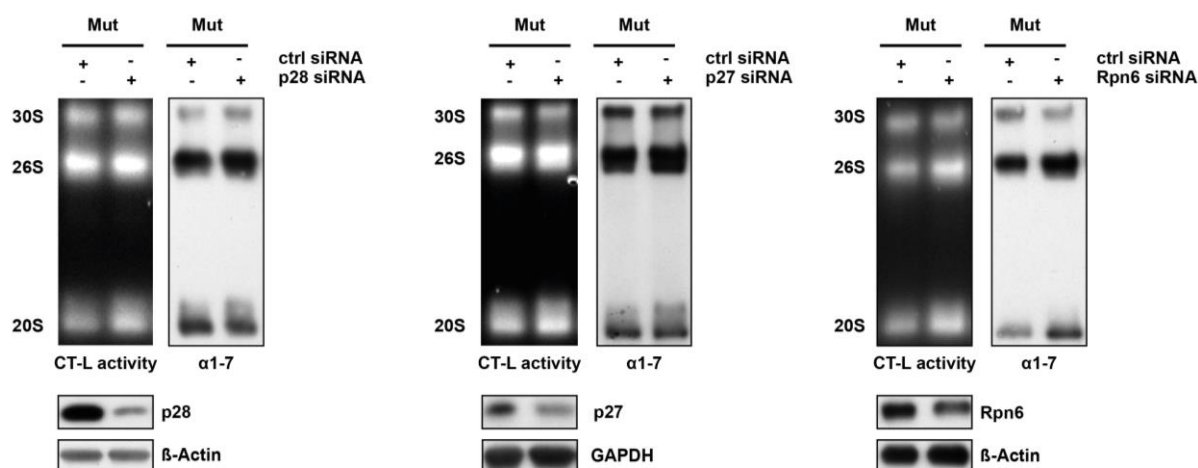


Figure 6.3 Silencing of specific proteasome assembly factors has no effect on proteasome activity and assembly in mutator MEFs. Native gel analysis of proteasome complexes in native extracts isolated from one mutator cell line upon p28 (n=4 technical replicates), p27 (n=3 technical replicates) and Rpn6 (n=5 technical replicates) silencing. CT-L activity and amount of proteasome complexes were determined by an in-gel substrate overlay assay followed by Western blotting and immunostaining with an antibody specific for the 20S subunits α 1-7. Control cells were transfected with a combination of two different control siRNAs. Successful knockdown was confirmed by immunostaining of the respective subunit.

The assembly chaperone S5b was elevated in mutator MEFs in contrast to p27, p28 and Rpn6. Therefore, silencing of S5b was performed in mutator MEFs to clarify whether this assembly factor acts as an inhibitor of proteasome activity as suggested in the literature (Levin et al., 2018). Indeed, transient knockdown of S5b led to increased proteasome activity and assembly in mutator MEFs as shown by native gel analysis using in-gel substrate overlay specific for CT-L activity and immunostaining for the 20S subunits α 1-7 (Figure 6.4A). Silencing efficiency was confirmed by immunostaining of S5b in Western blots. In-gel activity assay showed that activity of both 26S and 30S proteasome complexes was increased upon S5b knockdown (Figure 6.4A, left panel). Quantification of immunostaining for 20S proteasome complexes revealed that S5b silencing only increased the amount of assembled 30S proteasome complexes but not of 26S proteasomes (Figure 6.4A, right panel). Treatment of mutator cells with aspartate upon S5b silencing resulted in a more pronounced induction of proteasome activity and assembly compared to controls (Figure 6.4B). The obtained data indicate that S5b plays a role in the adaptive downregulation of proteasome activity in mutator MEFs by inhibiting the assembly of 30S proteasome complexes. However, proteasome inhibition by S5b seems to be only one component of the regulatory system and might work together with the specific induction of the assembly factors p27, p28 and Rpn6.

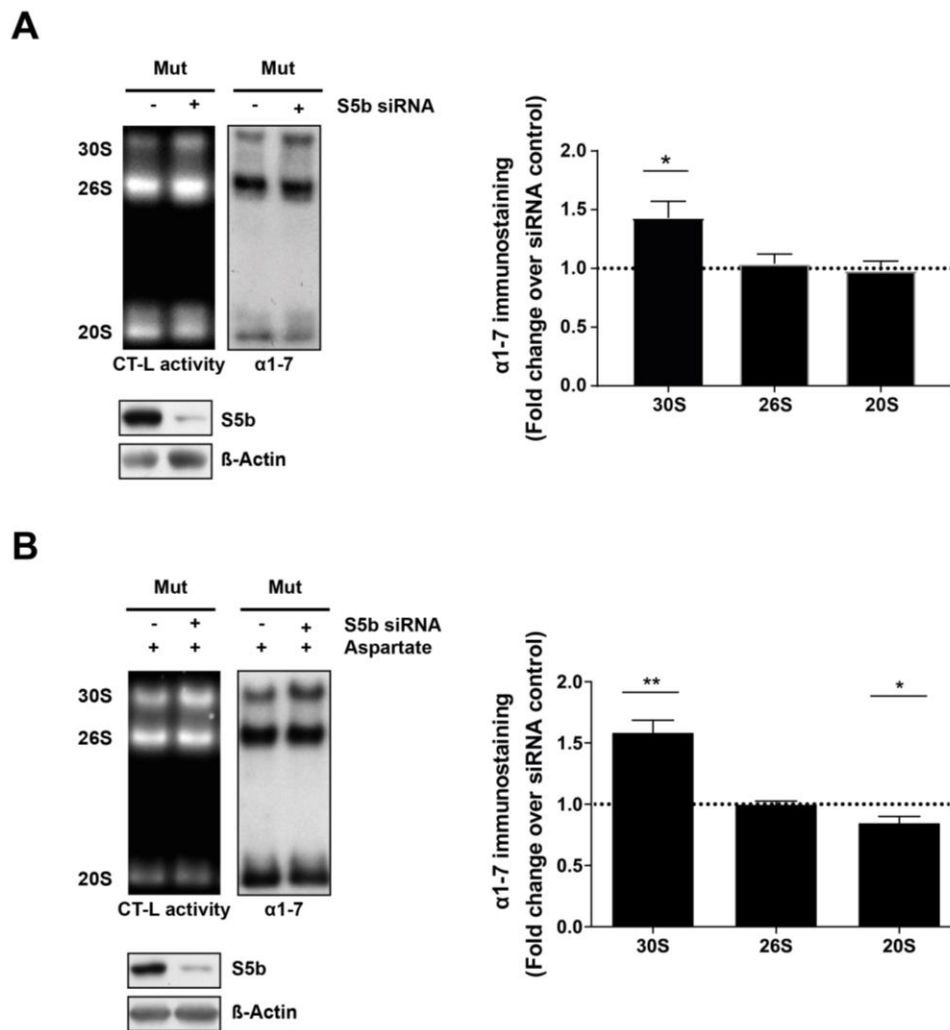


Figure 6.4 S5b silencing in mutator MEFs leads to increased proteasome activity and assembly and allows for an additional boost of proteasome activity by aspartate supplementation. (A) Representative native gel analysis of proteasome complexes in native extracts isolated from one mutator cell line upon S5b silencing for 48 h or (B) upon S5b silencing and aspartate treatment for 72 h. CT-L activity and amount of proteasome complexes were determined by an in-gel substrate overlay assay followed by Western blotting and immunostaining with an antibody specific for the 20S subunits $\alpha 1-7$. For control cells two different scrambled control siRNAs were used. Knockdown was confirmed via immunostaining for S5b. Quantification shows mean \pm SEM of the different aspartate treated mutator MEFs upon silencing related to the respective control. Significance was determined using the one-sample t-test.

5.7 Aspartate activates several signaling pathways in mutator MEFs including mTOR

To further dissect how aspartate supplementation activates proteasome assembly, an unbiased phosphoproteome screen was performed. Mutator cells were treated for four hours with or without aspartate. Phosphorylated peptides were enriched and identified by mass spec analysis according to a recently published protocol of the Mann lab (Humphrey et al., 2018). Over all replicates, almost 10.000 phosphorylation sites were identified with 233 phosphosites being significantly regulated by aspartate treatment, which

mapped to 177 proteins. Hierarchical clustering of significantly regulated phosphosites showed that about half of them were increased in abundance upon aspartate treatment (Figure 7.1A). Among these differentially phosphorylated proteins, we identified numerous key regulators of the cell cycle, DNA replication, cytoskeleton, ribosome, transcription, and growth factor signaling pathways. Phosphorylation of proteasome subunits upon aspartate treatment was visualized by a volcano plot. Phosphosites of proteasome subunits are displayed as red dots and were not differentially phosphorylated (Figure 7.1B) indicating that aspartate does not directly regulate 26S proteasome activity via phosphorylation of proteasomal subunits such as Rpn6, Rpt3, or Rpt6 (Guo et al., 2016, 2017; Lin et al., 2013; Lokireddy et al., 2015; VerPlank and Goldberg, 2017).

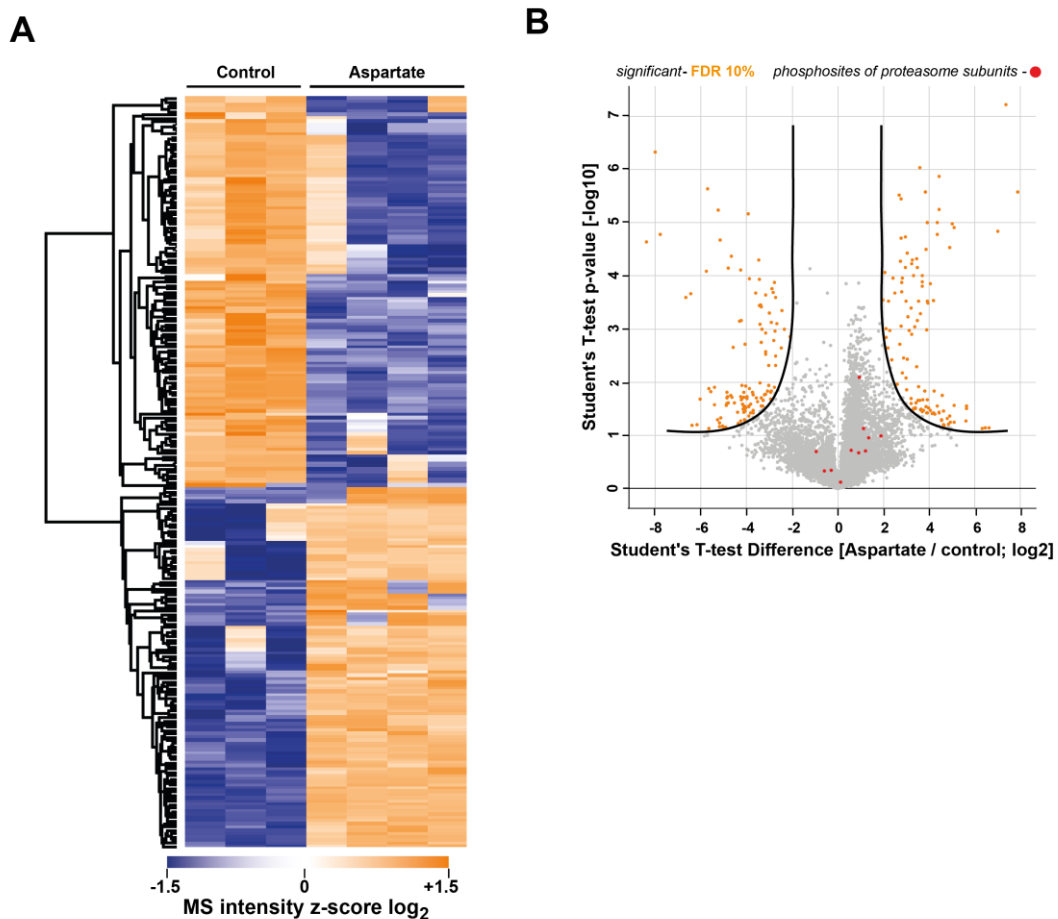


Figure 7.1 Aspartate regulates differential phosphorylation of many proteins but not of proteasome subunits. (A) Heatmap of 233 phosphosites significantly regulated by aspartate treatment compared to non-treated controls. Each row corresponds to a single distinct phosphosite. Rows are ordered according to unsupervised hierarchical clustering (Pearson correlation of z-score). (B) The depicted volcano plot shows significantly altered phosphorylation sites relative to controls with a 10 % FDR. Phosphosites of proteasome subunits are shown in red. Analysis of phosphoproteomics data was performed by Laura Mattner.

A closer inspection of the consensus motifs of the phosphorylated peptides identified several kinase motifs to be significantly enriched indicating activation of these kinases upon aspartate treatment of mutator cells (Figure 7.2A). Among these kinases were several cell cycle related kinases such as CDK1, Aurora A, GSK3, ERK1, 2, and CDK5 besides other growth factor, cell cycle and metabolic signaling kinases (Figure 7.2A). Activation of cell cycle and DNA replication related kinases by aspartate is well in line with the observed activation of proliferation as described above and observed previously (Birsoy et al., 2015; Garcia-Bermudez et al., 2018; Sullivan et al., 2015, 2018). Other most predominantly activated kinases were the p70 ribosomal S6 kinase, MAPKAP1 and 2, and AKT kinases, which are all involved in the activation of protein synthesis via the mTOR pathway (Saxton and Sabatini, 2017). These data suggest a previously unrecognized mTOR-mediated regulation of protein synthesis by aspartate. To confirm activation of mTOR signaling by aspartate in mutator MEFs phosphorylation levels of the mTOR downstream targets p70 S6 kinase and S6 ribosomal protein (Rps6) were analyzed by Western blotting. Quantification of the respective phospho signals revealed enhanced phosphorylation of mTOR downstream targets upon aspartate treatment (Figure 7.2B). In the absence of aspartate mTOR signaling was found to be downregulated in mutator MEFs compared to WT MEFs shown by decreased phosphorylation of the mTOR targets p70 S6 kinase and S6 ribosomal protein (Figure 7.2C). These observations point to a role of mTOR signaling in the adaptive regulation of proteostasis in mutator MEFs with chronic respiratory chain dysfunction.

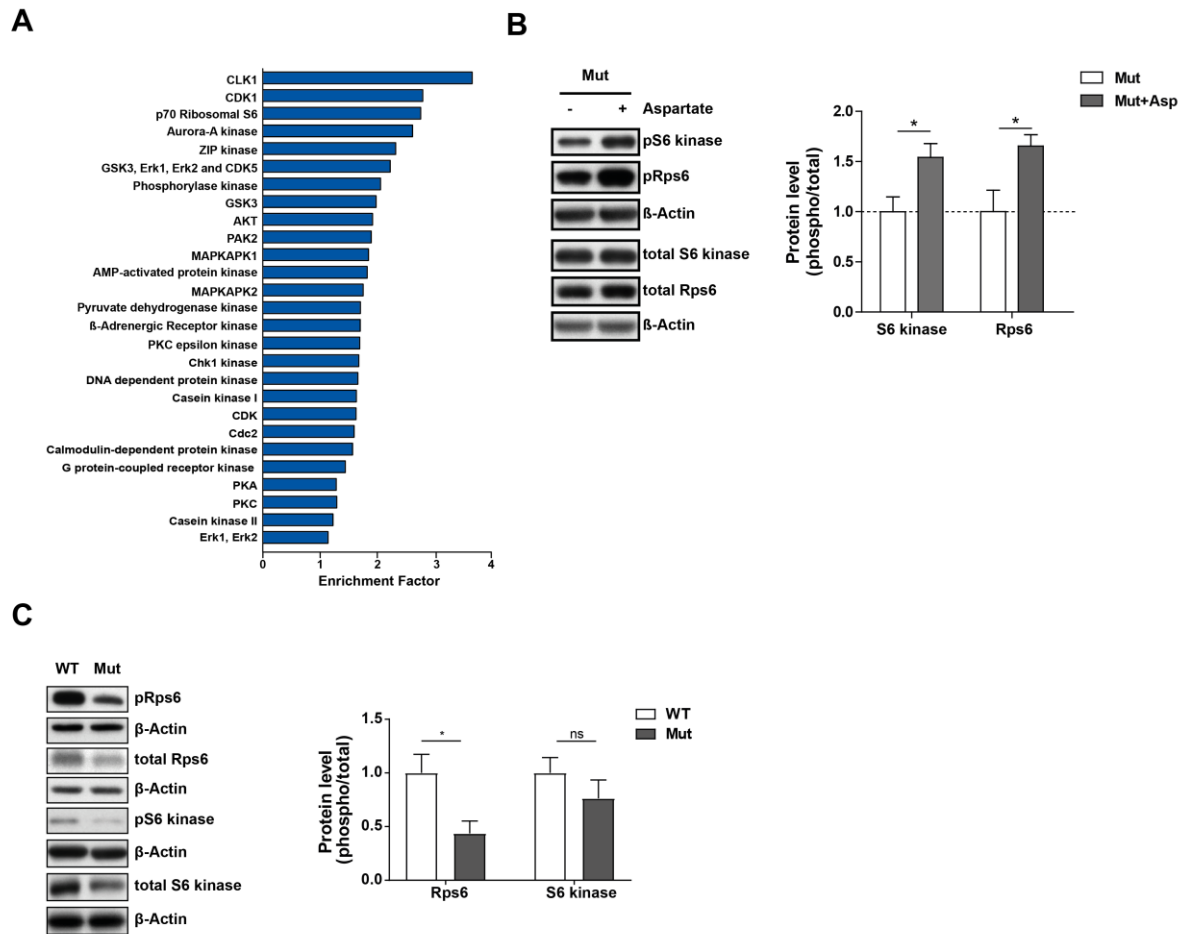


Figure 7.2 mTOR signaling is activated by aspartate supplementation but downregulated in the untreated state of mutator MEFs. (A) Enrichment analysis of phospho proteomics data for kinases predicted to be activated upon aspartate treatment using fisher exact test (False discovery rate (FDR) > 0.02). (B) Phosphoprotein levels of the mTORC1 targets p70 S6 kinase and S6 ribosomal protein (Rps6) were analyzed by Western blot analysis in mutator MEFs (n=4) treated with 10 mM aspartate for 72 h. Western blot images show one representative treated and nontreated mutator MEF cell line. β -Actin was used as a loading control. Bar graph shows the corresponding quantification of the signals obtained for the individual subunits. Phospho values were first related to the values of the total protein and then normalized to the mean of the untreated controls and illustrated as mean \pm SEM. Student's unpaired t-test was applied to determined statistical significance. (C) Analysis of mTOR signaling in WT (n=3) mutator (n=4) cells. Representative Western blots of total and phosphorylated levels of p70 S6 kinase and S6 ribosomal protein (Rps6). Bar graphs show β -Actin normalized phospho-protein levels related to total levels of the respective protein in WT and mutator cells (Mean \pm SEM). Significance was determined using student's unpaired t-test.

5.8 Aspartate induced mTOR signaling is linked to reactivation of proteasome activity and assembly in mutator MEFs

To investigate a possible link between aspartate induced mTOR signaling and the reactivation of proteasome activity and assembly in mutator MEFs, protein synthesis was blocked upon aspartate treatment by the mTORC1 specific inhibitor rapamycin. First, the effect of low doses of rapamycin (0.5 nM) on the phosphorylation of mTOR targets was

analyzed in order to exclude unspecific inhibition of the mTORC2 complex (Kang et al., 2013; Lamming, 2016; Thoreen et al., 2012). A time course experiment of rapamycin treatment followed by immunostaining for the mTOR targets p70 S6 kinase and Akt showed that phosphorylation of p70 S6 kinase was already almost completely abolished after 24 h (Figure 8.1A). In contrast, phospho levels of the mTORC2 target Akt kinase were increased upon rapamycin treatment and not inhibited indicating specific inhibition of the mTORC1 complex and a putative adaptive activation of mTORC2 signaling (Figure 8.1A). Cells of one representative mutator cell line were cotreated with 0.5 nM rapamycin and 10 mM aspartate for 72 h and Western blotting followed by immunostaining for mTORC1 downstream targets was performed. Inhibition of mTORC1 by rapamycin prevented aspartate induced activation of mTOR downstream signaling shown by strongly reduced phosphorylation of p70 S6 kinase and S6 ribosomal protein (Rps6) upon co treatment of rapamycin and aspartate (Figure 8.1B).

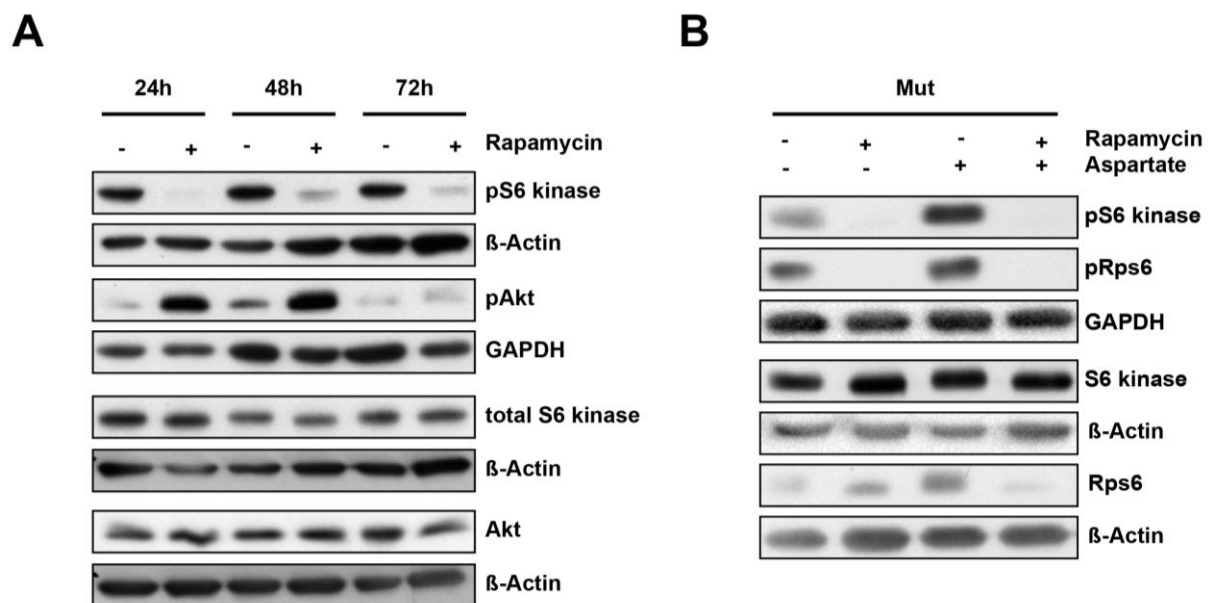


Figure 8.1 Low doses of rapamycin effectively inhibit mTORC1 but not mTORC2 downstream signaling in mutator MEFs. (A) Time course of rapamycin treatment (0.5 nM) in mutator cells showing p70 S6 kinase and Akt phosphorylation. Decreased phosphorylation of S6 kinase but not of Akt proves specificity of rapamycin treatment for mTORC1 (B) Analysis of mTOR signaling upon treatment with 0.5 nM rapamycin and 10 mM aspartate for 72 h in one mutator cell line. Representative Western blots of total and phosphorylated levels of p70 S6 kinase, S6 ribosomal protein (Rps6). GAPDH and β-Actin was used as a loading control. Data were generated together with Ayse Yazgili.

The dependency of proteasome reactivation on aspartate induced mTOR signaling was tested by native gel analysis upon co treatment of rapamycin and aspartate for 72 h.

Experiments were performed with one representative mutator cell line and technical replicates were generated in three independent treatments. Rapamycin treatment (0.5 nM) in the absence of aspartate had no effect on 26S and 30S proteasome activity and assembly in mutator MEFs as demonstrated by in-gel activity assay and immunostaining for the 20S subunits α 1-7 (Figure 8.2A). In contrast, rapamycin mediated inhibition of aspartate induced mTORC1 signaling prevented recovery of proteasome activity and assembly in mutator MEFs (Figure 8.2B). Of note, Western blot analysis showed that mTORC1 inhibition also blocked aspartate induced expression of the assembly factors Rpn6 and p28, which promoted proteasome assembly in mutator MEFs (Figure 8.2C).

To confirm the link between aspartate induced mTOR signaling and reactivation of the proteasome, raptor silencing upon aspartate treatment was performed in mutator MEFs. Raptor is a component of the mTORC1 complex and is involved in the regulation mTORC1 activity. Raptor silencing is known to specifically inhibit mTORC1 downstream signaling similar to low doses of rapamycin (Saxton and Sabatini, 2017). Cells of one representative mutator cell line were reverse silenced with either one Raptor target siRNA (10 nM) or a control siRNA (10 nM). On the next day, cells were treated with fresh medium containing 10 mM aspartate for 72 h. Technical replicates were generated in four independent silencing experiments. Successful raptor knockdown and inhibition of mTORC1 signaling was demonstrated by Western blotting. The blot in Figure 8.2C confirms raptor silencing as demonstrated by reduced raptor protein levels. Partial inhibition of mTORC1 was demonstrated by decreased phosphorylation of the mTORC1 target p70 S6 kinase (Figure 8.2C). Native gel analysis upon Raptor silencing and aspartate treatment in mutator MEFs for 72 h revealed a similar block of aspartate driven reactivation of proteasome activity as observed with rapamycin treatment (Figure 8.2D).

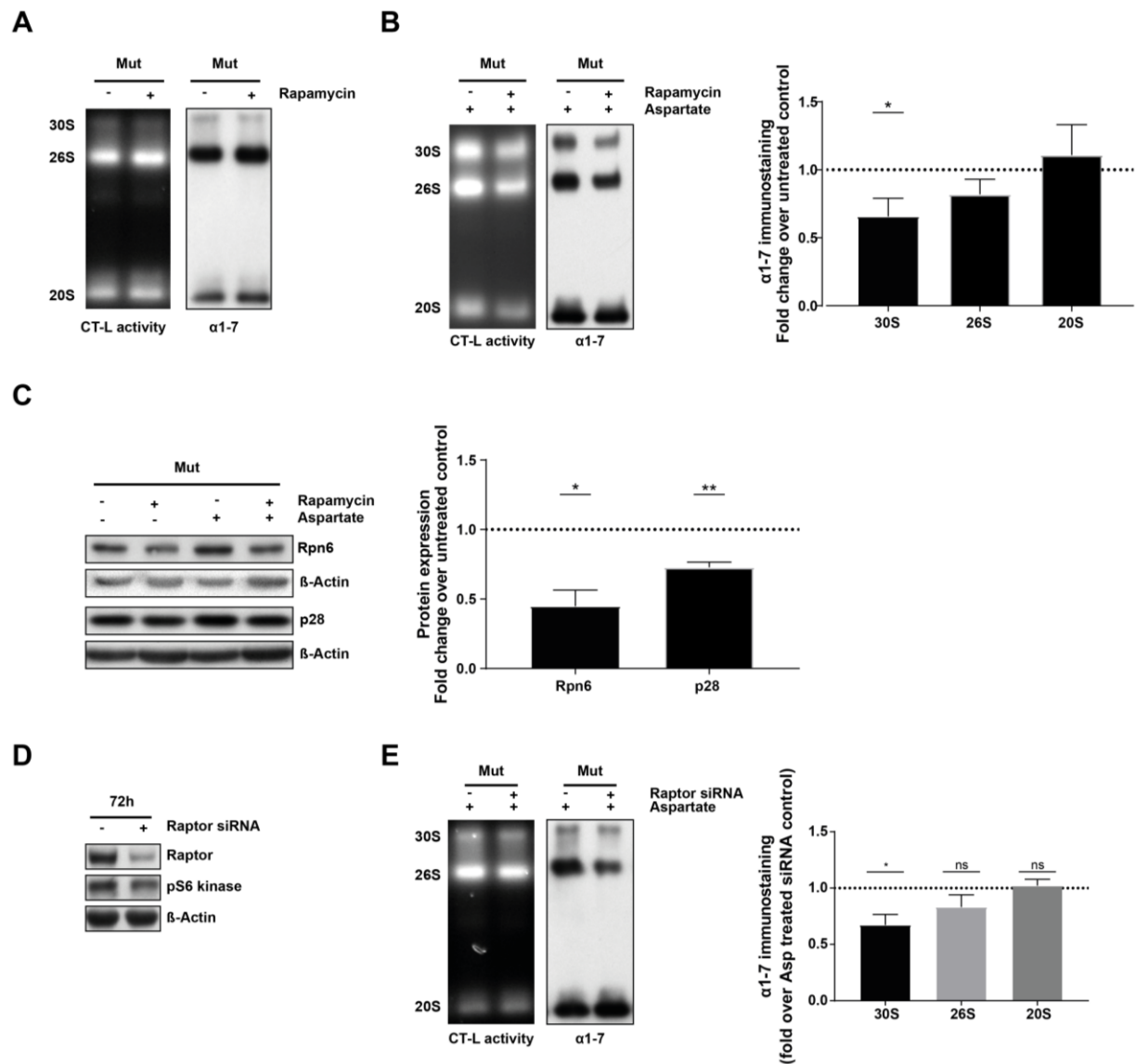


Figure 8.2 Rapamycin or raptor silencing mediated inhibition of mTOR signaling blocks aspartate induced reactivation of proteasome activity and assembly in mutator MEFs. (A) Representative native in-gel activity assay (CT-L activity) of 30S, 26S and 20S proteasome complexes separated by native gel electrophoresis from one mutator cell line upon rapamycin treatment (0.5 nM) for 72 h or (B) upon rapamycin (0.5 nM) and aspartate (10 mM) treatment for 72 h (left panel) followed by α 1-7 immunostaining of the blotted native gel (right panel). Quantification shows mean \pm SEM of the rapamycin treated mutator MEF cell line related to the respective control (n=3 technical replicates). Significance was determined using the one-sample t-test. (C) Protein levels of the proteasome subunits Rpn6 and p28 were analyzed by Western blot analysis in one representative mutator MEF cell line (n=3 technical replicates) treated with 0.5 nM rapamycin and 10 mM aspartate for 72 h. β -Actin was used as a loading control. Bar graph shows the corresponding quantification of the signals obtained for the individual subunits (mean of 3 technical replicates \pm SEM). Student's paired t-test was applied to determined statistical significance. (D) Protein levels of Raptor and phospho S6 kinase after aspartate supplementation and siRNA mediated Raptor silencing for 72 h in one mutator cell line (n=4 independent experiments). (E) Representative native in-gel activity assay (CT-L activity) of 30S, 26S and 20S proteasome complexes separated by native gel electrophoresis from one mutator cell line upon raptor silencing and aspartate (10 mM) treatment for 72 h (left panel) followed by α 1-7 immunostaining of the blotted native gel (right panel). Quantification shows mean \pm SEM of Raptor silencing and aspartate treatment in one mutator MEF cell line related to the respective control (n=4 technical replicates). Significance was determined using the one-sample t-test. Parts of the data were generated together with Ayse Yazgılı.

5.9 Defective complex I function drives metabolic adaption of the proteasome in human cells

To investigate the relevance of adaptive mitochondrial regulation of the proteasome for mitochondrial diseases, effects of mitochondrial complex I deficiency on the proteasome were assessed in human cells. Here, skin fibroblasts from human patients were used, which are characterized by a specific point mutation in the ND5 subunit of mitochondrial complex I. These cells also show a chronic respiratory chain dysfunction similar to mutator MEFs (Berschneider, 2016). Additionally, both proteasome activity and assembly were impaired in human ND5 skin fibroblasts shown by chemiluminescence based activity assay and native gel analysis (Figure 10.1A+B). When ND5 fibroblasts were treated with aspartate for 72 h not only proliferation but also proteasome activity and assembly were markedly induced (Figure 10.1C+D). These findings indicate that the novel regulation of the proteasome by mitochondrial metabolism also plays a role in human mitochondrial diseases.

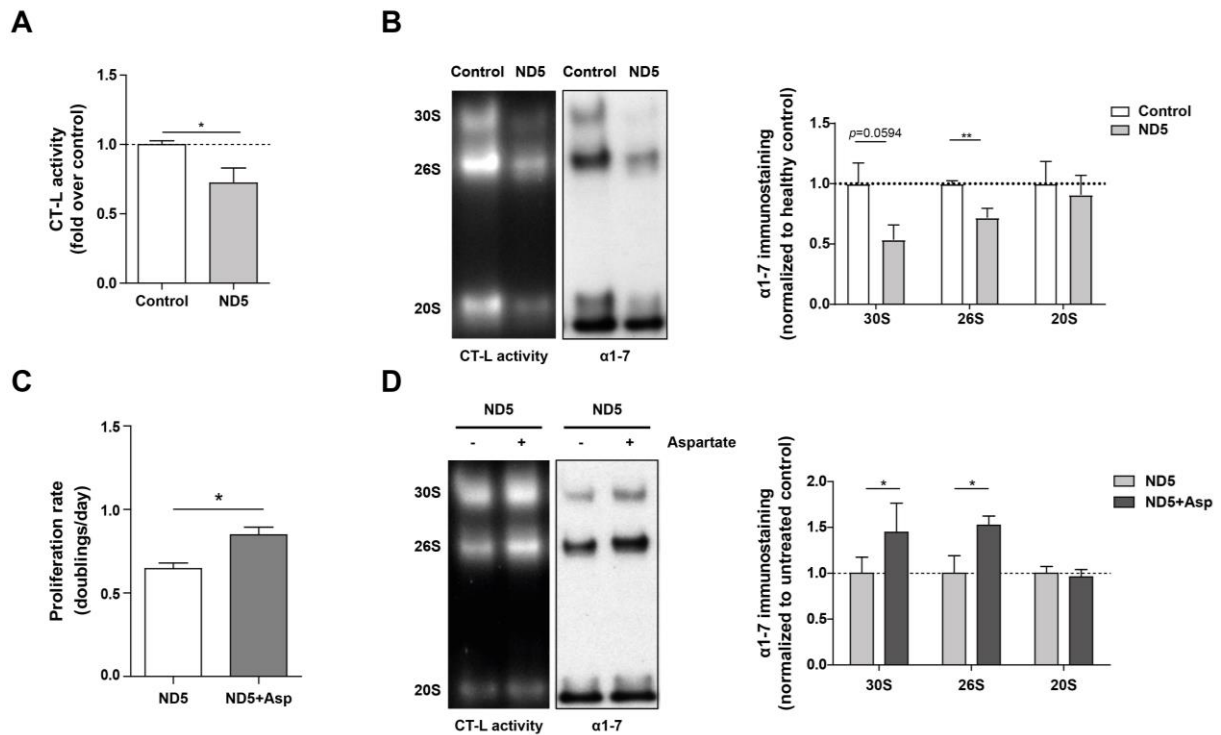


Figure 9 Human cells with ND5 mutation show decreased proteasome activity and assembly, which can be rescued by aspartate supplementation. (A) Activity of the proteasomal cleavage site chymotrypsin-like (CT-L) was determined in total cell extracts of ND5 mutant human fibroblasts and healthy controls (n=5 technical replicates) by measuring chemiluminescence generated by proteasomal cleavage of a luminogenic substrate specific for the respective active site. Bar graph shows mean±SEM. All values were normalized to the mean of the healthy control. Statistical test: student's unpaired t-test. Data were generated by Korbinian Berschneider. (B) Representative native in-gel activity assay (CT-L activity) of 30S, 26S and 20S proteasome complexes separated by native gel electrophoresis from human skin fibroblasts (healthy control and ND5 mutant) (left panel) followed by α 1-7 immunostaining of the blotted native gel (right panel). Four independent experiments were performed. Bar graphs show mean±SEM relative to healthy control. Significance was determined using student's unpaired t-test comparing healthy control vs. ND5 mutant cells. (C) Proliferation rates of ND5 mutant skin fibroblasts (n=3 independent experiments) treated with 10 mM aspartate for 72 h were determined by counting cells at day 1 and day 4 after seeding of the cells. Bar graph shows doubling rate per day for aspartate treated ND5 mutant skin fibroblasts and untreated controls. Significance was determined using student's unpaired t-test. (D) ND5 mutant patient fibroblasts were treated with 10 mM aspartate for 72 h in six independent experiments. Activity and assembly of proteasome complexes was analyzed by native gel electrophoresis with CT-L substrate overlay assay and immunoblotting for 20S α 1-7 subunits. Densitometry shows mean±SEM values of aspartate-treated relative to untreated fibroblasts. Significance was determined using student's unpaired t-test.

5.10 Pharmacological inhibition of respiratory chain complex I in murine and human cells phenocopies chronic conditions in mutator cells

To dissect whether the regulation of proteasome activity and assembly is a specific feature of impaired respiratory chain complex I activity, we tested pharmacological inhibitors of complex I in WT MEFs. Therefore, WT MEFs were treated with 5 mM metformin, which is usually used for treatment of diabetes but was recently found to specifically inhibit respiratory chain complex I without inducing ROS levels (Vial et al., 2019). After 72 h of

metformin treatment effects on proliferation and proteasome activity were assessed. Complex I inhibition by metformin led to reduced doubling rates in WT MEFs (Figure 9.1A). This observation was in line with the diminished proliferation in mutator MEFs caused by mitochondrial complex I deficiency. Of note, co treatment with aspartate or pyruvate could partially rescue diminished proliferation caused by complex I inhibition in WT MEFs (Figure 9.1A). Native gel analysis confirmed that pharmacological inhibition of complex I by metformin in WT MEFs also phenocopies the decreased proteasome activity and assembly found in mutator MEFs (Figure 9.1B). Aspartate and pyruvate supplementation in metformin treated WT MEFs reactivated proteasome assembly similar to the effects observed in mutator MEFs (Figure 9.1B). These data indicate that the regulation of proteasome activity and assembly by mitochondrial complex I is a general mechanism, that can be switched on and off by complex I inhibition and supplementation of aspartate or pyruvate.

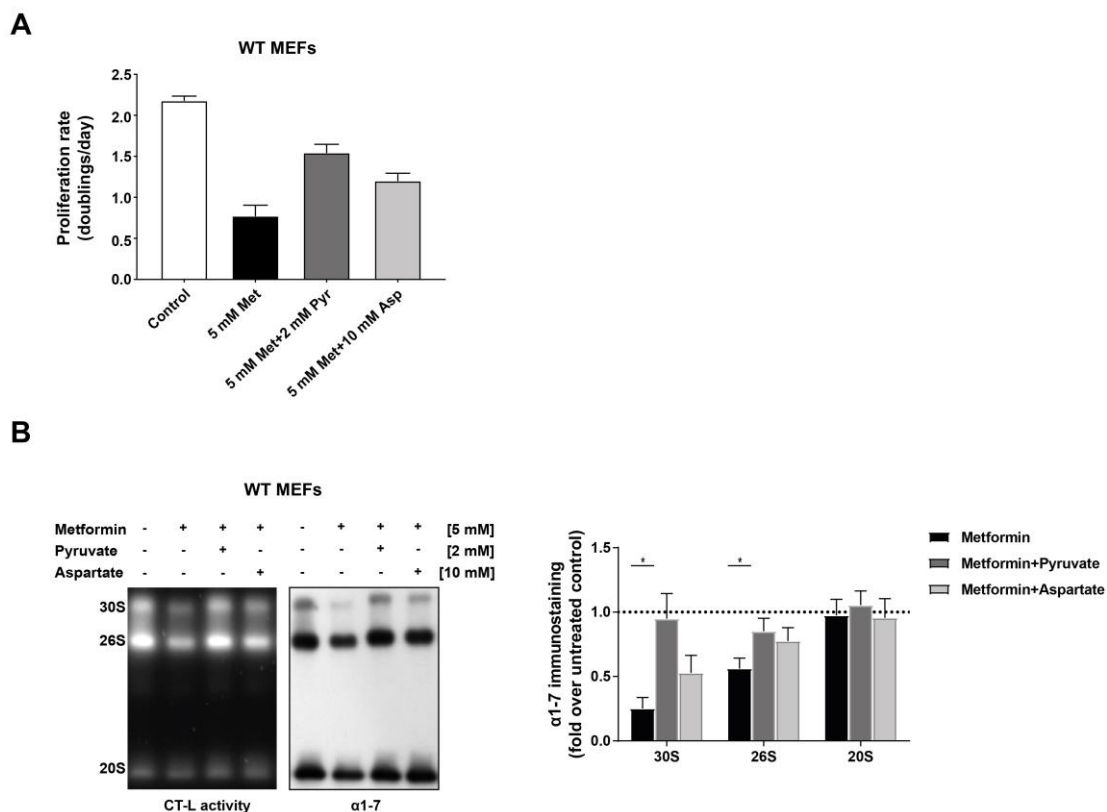


Figure 10.1 Metformin mediated complex I inhibition in WT MEFs phenocopies conditions in mutator MEFs, which can be rescued with pyruvate and aspartate supplementation. (A) Proliferation rates of one mutator cell line cotreated with 5 mM metformin and 2 mM pyruvate or 10 mM aspartate were determined by counting cells at day 1 and day 5 after seeding of the cells. Doublings per day were then calculated as explained in the methods part. Bar graph shows doubling rates of 4 independent experiments. (B) Representative native in-gel activity assay (CT-L activity) of 30S, 26S and 20S proteasome complexes separated by native gel electrophoresis from one WT MEF cell line cotreated with 10 mM aspartate or 2 mM pyruvate together with 5 mM metformin for 72 h (left panel) followed by α 1-7 immunostaining of the blotted native gel (right panel). Bar graphs represent mean \pm SEM relative to respective untreated WT MEF cell line (n=4 independent experiments). Significance was determined using one sample t-test.

To further dissect the role of aspartate and pyruvate for the reactivation of 26S proteasome activity and assembly driven by complex I inhibition in WT MEFs the downstream effect of metformin treatment was mimicked with the transaminase inhibitor aminooxyacetate (AOA). This compound has been shown to block the reversible conversion of oxaloacetic acid and glutamic acid to aspartate (Antti and Sellstedt, 2018) and the regeneration of NAD⁺ by the mitochondrial malate-aspartate shuttle (Alkan et al., 2018). Therefore, first the effect of 300 nM AOA on proliferation was tested in WT MEFs. The doubling rate per day was clearly reduced after 72 h of AOA treatment (Figure 9.2A). However, the treatment only led to decelerated proliferation but had no effect on cell viability (data not shown). Pyruvate supplementation rescued the effect of AOA on proliferation by functioning as an electron acceptor for the oxidation of NADH while aspartate treatment provided the missing precursors for nucleotide synthesis in WT MEFs (Sullivan et al., 2015) (Figure 9.2A). Of note, AOA treatment in WT MEFs reduced proteasome activity and assembly in the same way as metformin as demonstrated by native gel analysis (Figure 9.2B). While pyruvate supplementation fully restored AOA induced reduction of proteasome activity and assembly aspartate only reactivated the 30S proteasome complexes in WT MEFs (Figure 9.2B, quantification). Data from metformin and AOA treatment show that complex I driven regulation of proteasome activity and assembly can be also acutely induced in WT cells.

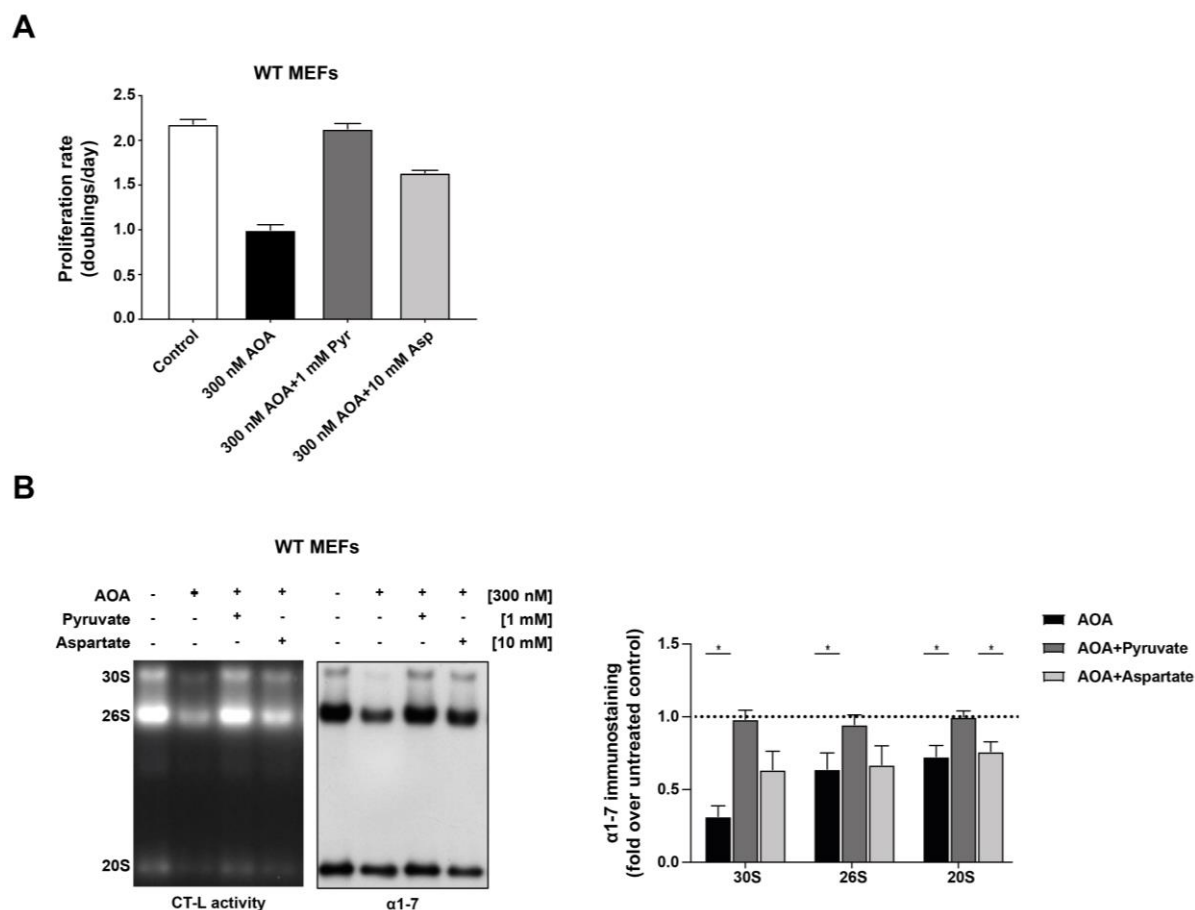
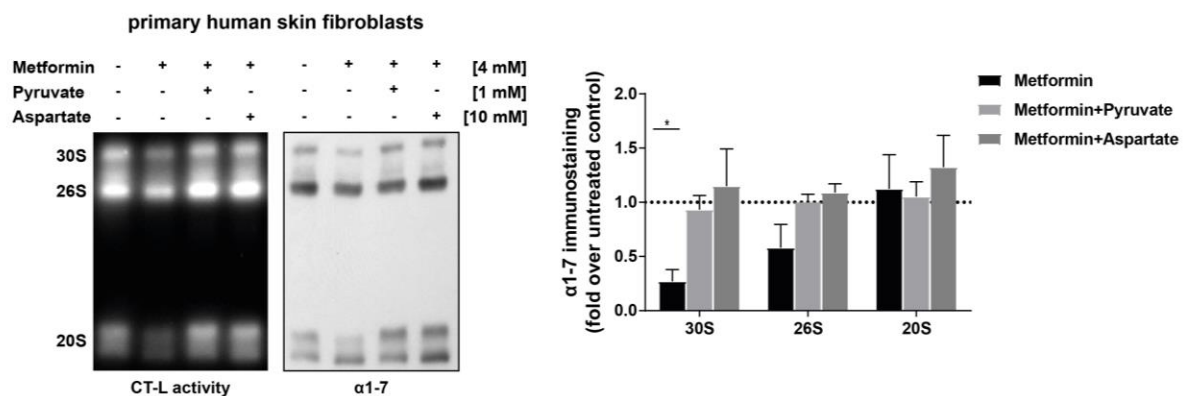


Figure 10.2 Pharmacological inhibition of aminotransferases with AOA in WT MEFs leads to effects comparable to Metformin treatment. (A) Proliferation rates of one mutator cell line cotreated with 300 nM AOA and 1 mM pyruvate or 10 mM aspartate were determined by counting cells at day 1 and day 5 after seeding of the cells. Bar graph shows doubling rates of 4 independent experiments. (B) Representative native in-gel activity assay (CT-L activity) of 30S, 26S and 20S proteasome complexes separated by native gel electrophoresis from one WT MEF cell line cotreated with 1 mM pyruvate or 10 mM aspartate or together with 300 nM AOA for 72 h (left panel) followed by α 1-7 immunostaining of the blotted native gel (right panel). Bar graphs represent mean \pm SEM relative to respective untreated WT MEF cell line (n=4 independent experiments). Significance was determined using one sample t-test.

To show the effects of pharmacological complex I inhibition on proteasome activity and assembly also in healthy human cells, both primary human skin and lung fibroblasts from healthy donors were treated with the complex I inhibitor metformin (4 mM or 2 mM) for 72 h and native gel analysis was performed. In-gel activity assay and immunoblotting of native extracts isolated from these cells revealed a clear reduction of proteasome activity and assembly after 72 h compared to untreated controls (Figure 10.2A+B). In contrast, 26S and 30S proteasome activity was distinctly increased upon cotreatment of metformin with 1 mM pyruvate or 10 mM (1 mM) aspartate for 72 h compared to the metformin only treated cells (Figure 10.2A+B, left panels). Additionally, quantification of immunostaining for 20S subunits α 1-7 showed elevated assembly of 26S and 30S proteasome complexes in cells cotreated

with metformin and aspartate or pyruvate (Figure 10.2A+B, right panels+quantification). These data indicate a reactivation of 26S proteasome assembly and activity similar to the results obtained in WT MEFs and substantiate the earlier described hypothesis of a so far unknown regulation of the proteasome by mitochondrial metabolism both in murine and human cells.

A



B

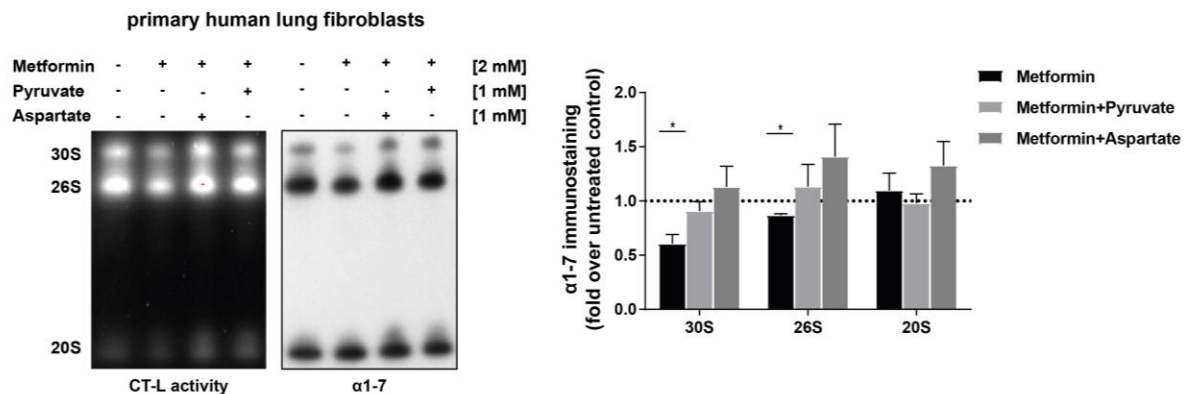


Figure 10.3 Complex I inhibition in human cells decreases proteasome activity and assembly, which can be reactivated by pyruvate or aspartate supplementation. (A) Representative native in-gel activity assay (CT-L activity) of 30S, 26S and 20S proteasome complexes separated by native gel electrophoresis from healthy primary human skin fibroblasts cotreated with 10 mM aspartate or 1 mM pyruvate together with 4 mM metformin for 72 h (left panel) followed by α 1-7 immunostaining of the blotted native gel (right panel). Quantification shows mean \pm SEM of the treated skin fibroblasts related to the respective controls. Significance was determined using the one-sample t-test. (B) Representative native in-gel activity assay (CT-L activity) of 30S, 26S and 20S proteasome complexes separated by native gel electrophoresis from healthy primary human lung fibroblasts (pHLF) cotreated with 1 mM aspartate or 1 mM pyruvate together with 2 mM metformin for 72 h (left panel) followed by α 1-7 immunostaining of the blotted native gel (right panel). Quantification shows mean \pm SEM of the treated skin fibroblasts related to the respective controls. Significance was determined using the one-sample t-test. Parts of the data were generated together with Xinyuan Wang.

5.11 Immunoproteasome dependent antigen presentation is induced in mutator MEFs with complex I deficiency

We here demonstrated regulation of proteasome activity by metabolic dysfunction, which was driven by reduced assembly of 26S proteasome complexes. The catalytic activity of the proteasome can also be regulated on the level of catalytic subunit incorporation. As outlined in the introduction, the standard catalytic proteasome subunits β 1, β 2 and β 5 can be replaced by inducible immunoproteasome subunits, which then assemble into the immunoproteasome. To investigate, whether mitochondrial dysfunction induces such shift in catalytic subunits, we thus investigated the presence of immunoproteasome subunits in mutator cells on expression and activity level. Western blot analysis and immunodetection for the immunoproteasome subunits Lmp2 and Lmp7 revealed pronounced induction of these two active sites in mutator MEFs compared to WT cells (Figure 11.1A). The immunoproteasome associated regulator Psme1 was also increased on protein level in mutator MEFs (Figure 11.1B). Upregulation of immunoproteasome subunits in mutator MEFs was confirmed on mRNA level using quantitative RT-PCR (Figure 11.1C). Psmb8 and Psmb9 mRNA level were 10 to 15 fold induced in mutator MEFs whereas the increase of Psmb10 expression was rather small. Induction of Psme1 mRNA was also comparable to protein level in mutator MEFs. Immunoproteasome activity was checked by using fluorescently labelled activity based probes (ABPs). ABPs are fluorescently labelled inhibitors, which bind irreversibly to the respective 20S active sites in native and assembled proteasomes. MV151 binds to all standard and immunoproteasome active sites. LW124 is targeted specifically against β 1 and Lmp2 and MVB127 detects only β 5 and Lmp7. The measured fluorescence intensity of the different ABPs reflects the activity of the respective active sites. The catalytic activity of the subunits MECL-1 and Lmp2 was strongly induced in mutator MEFs (Figure 11.1D, MV151+LW124). As murine Lmp7 did not separate from the β 5 subunit on the ABP gel, the activity could not be quantified in this case (Figure 11.1D, MVB127).

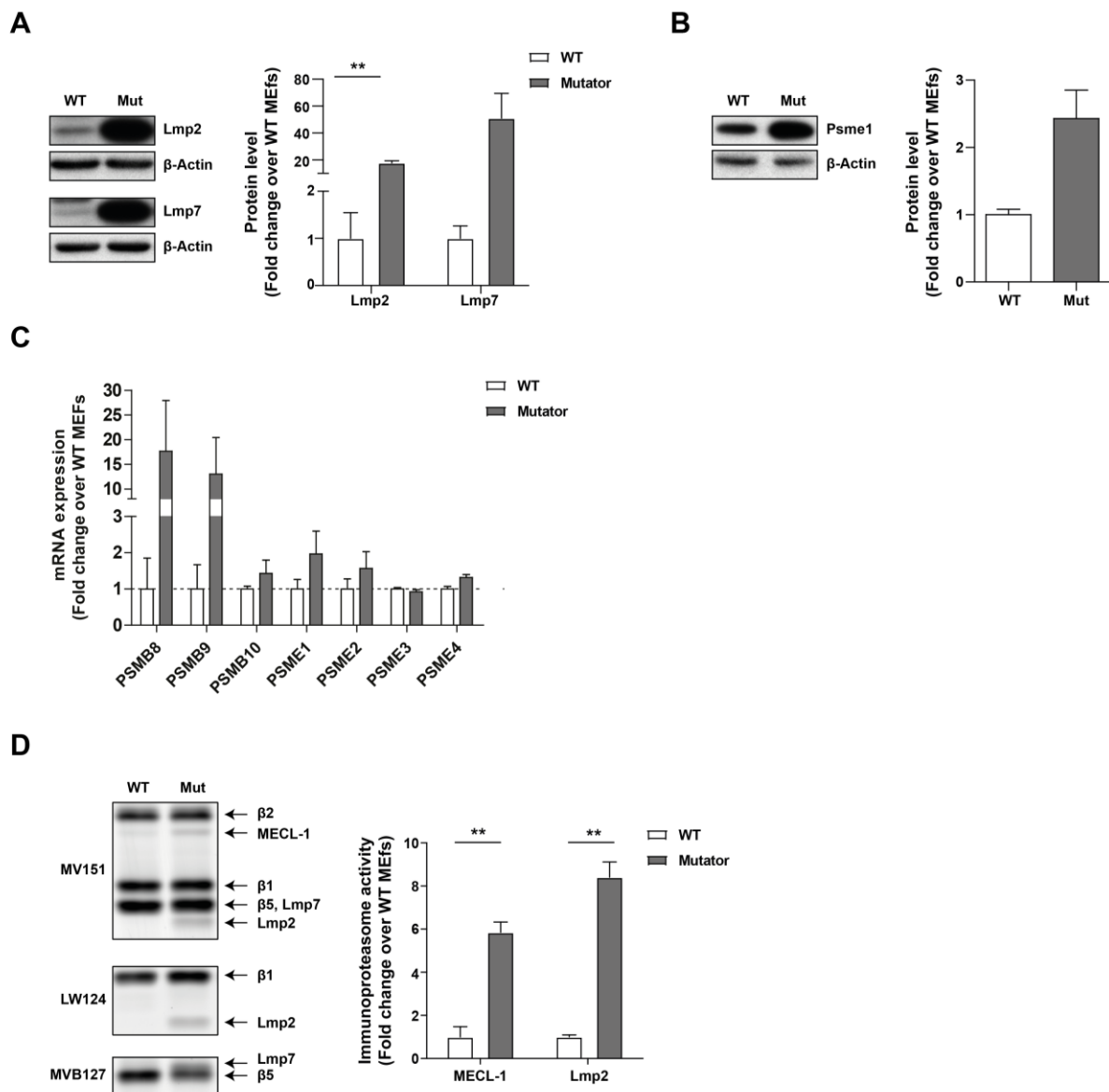


Figure 11.1: Immunoproteasome activity and expression is strongly upregulated in mutator MEFs. (A+B) Analysis of immunoproteasome expression in mutator MEFs shown by representative Western blots of immunoproteasome subunits Lmp2 and Lmp7 and Psme1 in mutator (n=3) and WT (n=3) cell lines. The bar graphs show β -Actin normalized protein levels normalized to WT controls (Mean \pm SEM). Significance was determined using student's unpaired t-test. (C) RT-qPCR analysis of proteasome subunit mRNA expression in WT (n=3) and mutator (n=3) MEFs. Data represent mean \pm SEM relative to WT controls. Significance was determined using student's unpaired t-test. (D) Representative labelling of active proteasomal cleavage sites with the Activity Based Probes (ABPs) MV151, LW124 and MVB127 in WT (n=3) mutator cells (n=4). Densitometric analysis shows activity of MECL-1 and Lmp2 (mean \pm SEM) between WT and mutator cells. Significance was determined using student's unpaired t-test.

As the immunoproteasome plays an important role for the generation of peptides, which are presented on the cell surface via MHC I, a possible regulation of MHC I antigen processing and presentation was analyzed in mutator MEFs. The scheme in Figure 11.2A shows the general pathway of MHC I antigen processing and presentation in the cell. Peptides, which fit

the MHC I complex, are generated either by the standard or the immunoproteasome. However, peptides generated by the immunoproteasome fulfil the binding requirements of MHC I complexes much better than peptides derived from standard proteasomes (Groettrup et al., 2001). Peptides are imported into the endoplasmic reticulum (ER) via so-called TAP transporters. In the ER, the peptide MHC I complex is assembled. Finally, the complex is transported to the cell surface and presented to the immune system. Proteomics data from WT and mutator MEFs, which have been generated before, were analyzed with regard to regulation of cellular antigen processing and presentation pathways. The unsupervised/unbiased 1D annotation enrichment analysis of mass spectrometry data revealed a concerted upregulation of antigen presentation related pathways (Figure 11.2). Here, the most prominent GO terms were "Adaptive immunity", "Antigen processing and presentation" and "TAP" complex. The TAP complex is crucial for the transport of peptides in the endoplasmic reticulum, where the formation of MHC I complexes takes place (Groettrup et al., 2010). Increased protein levels of components, which are involved in adaptive immunity and MHC I antigen presentation, clearly point to an activation of immune responses in mutator cells.

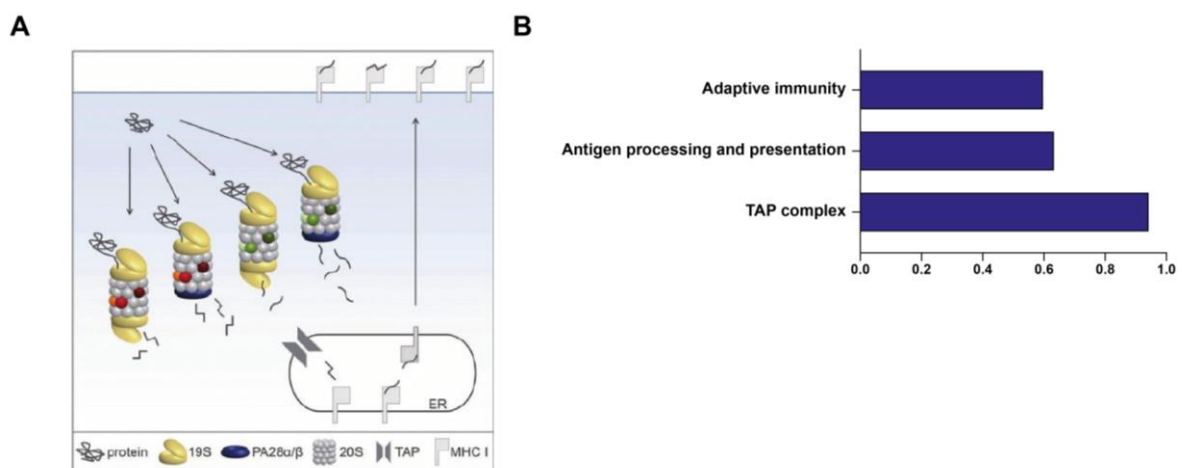


Figure 11.2 1D enrichment analysis of proteomics data identifies enriched pathways related to MHC I antigen presentation in mutator MEFs. (A) Schematic representation of MHC I antigen processing and presentation in the cell. Peptides are generated by both the standard- and immunoproteasome, transported into the ER via TAP transporter and fitted to MHC I receptors, which are then presented on the cell surface (taken from Meiners et al., 2014). (B) Bar graph shows the normalized annotation enrichment score of UniProt keyword and Gene Ontology (GO) annotations for a selection of antigen presentation related processes that were significantly regulated (FDR < 5%) between WT and mutator MEFs in the respective proteomics data set.

To further investigate the effects of chronic mitochondrial dysfunction on MHC I antigen processing and presentation in mutator cells, a signature in form of a gene list was manually curated based on the description of the pathway made by Groettrup et al. (2010) (Groettrup et al., 2010). Only the central components of MHC I antigen processing and presentation were included in the gene list to keep the analysis simple. This signature was then applied to the above mentioned proteomics and to bulk mRNA sequencing data from WT and mutator MEFs and heatmaps with significantly regulated proteins and genes from this GO term were generated. As proteomics data from WT and mutator MEFs matched with only 7 proteins from the signature, proteome analysis from isolated mitochondria was used. Here, an endoplasmic reticulum (ER) enriched fraction was prepared by differential centrifugation. The isolation procedure for mitochondria is described in the methods section. The ER rich fraction was taken in the last step before mitochondria were purified via a density gradient. This fraction still contained almost all cellular proteins and especially enriched endoplasmic reticulum, the organelle where the formation of MHC I takes place. The ER rich fraction was generated after cell lysis using first centrifugation steps. This fraction was not applied to density gradient purification. The procedure is described in detail in the methods section. The heatmap in Figure 11.3A shows all proteins from the dirty fraction of the mitochondria isolation contained in the GO term MHC I antigen processing and presentation. All identified proteins were strongly upregulated in the ER enriched fraction isolated from mutator (n=1, 4 technical replicates) MEFs compared to WT (n=1, 4 technical replicates) cells. Many more components of MHC I antigen presentation signature were identified in the RNA sequencing data from WT (n=1, 5 technical replicates) and mutator (n=1, 5 technical replicates) MEFs shown in the heatmap of Figure 11.3B. Similar to the proteomics data, most of the genes were uniformly upregulated in mutator MEFs. All three immunoproteasome subunits were found to be upregulated on mRNA level, which fits the already shown Western blot and qPCR data. Stat1, which is a common transcription factor involved in both immunoproteasome and MHC I induction (Barton et al., 2002), was not detected in the omics and therefore checked by Western blot analysis. This upstream regulator of immunoproteasome and MHC I expression was strongly upregulated in mutator MEFs (Figure 11.3C). To confirm our omics data, which indicate an upregulation of MHC I antigen presentation in mutator MEFs, a functional assay for MHC I presentation on the cell surface was performed. Therefore, WT (n=3) and mutator (n=4) MEFs were stained with a

fluorescently labelled antibody, which specifically detects MHC I receptors on the cell surface. Fluorescence signals were then measured using flow cytometry analysis (Figure 11.3D, left panel). Quantification of mean fluorescence intensity showed an almost 8 fold increase in the amount of MHC I complexes presented on the cell surface of mutator MEFs compared to WT MEFs (Figure 11.3D, right panel). The evaluated omics data together with Stat1 induction and detection of MHC I surface presentation indicate that chronic mitochondrial dysfunction in mutator MEFs induces an inside-outside alarm response to signal to the immune system that there is a severe problem with mitochondrial function in these cells.

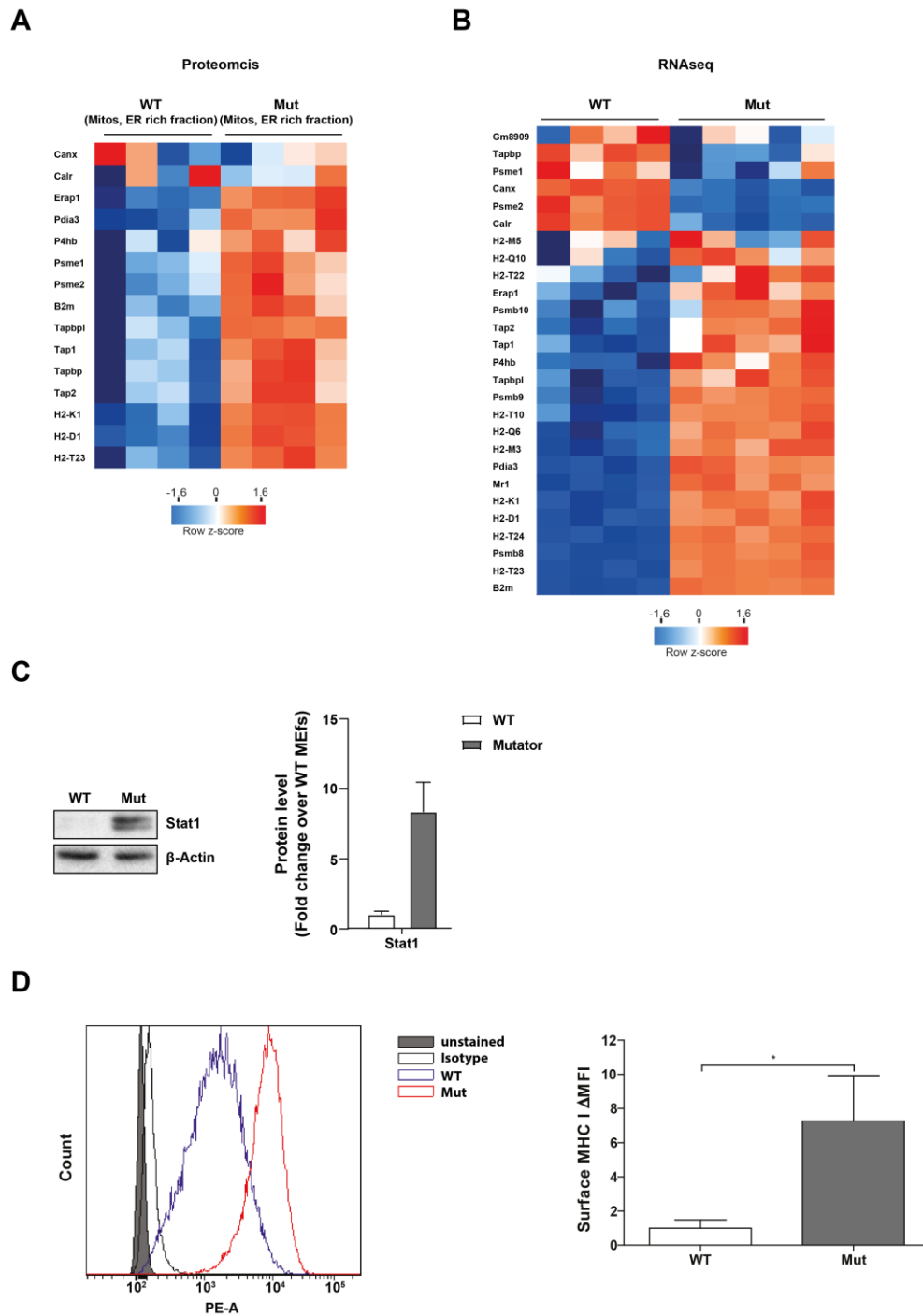


Figure 11.3: MHC I antigen processing and presentation pathway is upregulated in mutator MEFs. (A) Heatmap shows proteins detected by mass spectrometry and generated from ER rich fractions matched with the manually generated signature “MHC I antigen processing and presentation”. Technical replicates were generated for one WT and one mutator MEF cell line in 4 independent isolation experiments. (B) Heatmap of genes from bulk mRNA sequencing in WT and mutator MEFs, which were identified in the GO term “MHC I antigen processing and presentation”. 5 technical replicates were generated for one WT and one mutator MEF. One replicate for WT MEFs was excluded based on the principal component analysis. (C) Western blot analysis of Stat1 levels in WT and mutator MEFs. (D) Flow cytometry analysis of MHC I surface expression in WT (n=3) and mutator (n=4) MEFs. MHC I was stained with a fluorescently labelled antibody specific for murine MHC I receptors. Bar graph shows quantification of the mean fluorescence intensity for WT and mutator MEFs.

6 Discussion

So far several stress signals such as increased ROS levels or ATP depletion have been identified, which are sent out by mitochondria with dysfunctional respiratory chain and negatively affect activity and function of the ubiquitin-proteasome system (see Paragraph 1.4). In the present study a novel and so far unknown pathway for adaptive metabolic regulation of the proteasome by dysfunctional mitochondria was identified. Of note, this adaptive regulation is independent of ROS and ATP. Respiratory chain complex I deficiency in the mtDNA mutator mouse model caused metabolic reprogramming with altered biosynthesis of important TCA cycle products such as aspartate and reduced regeneration of electron acceptors in form of NAD⁺. This altered mitochondrial metabolism impaired 26S proteasome activity and assembly and reduced cellular protein synthesis. Downregulation of proteasome assembly and activity was also found in human skin fibroblasts with mutation of the mitochondrial ND5 protein of respiratory complex I and upon pharmacological inhibition of complex I by metformin in human lung and skin fibroblasts. Importantly, downregulation of cellular proteostasis could be reversed by supplementation of aspartate or pyruvate thus demonstrating adaptive metabolic fine-tuning of 26S proteasome function, which may also have therapeutic implications. In contrast to diminished 26S proteasome assembly and activity in mutator MEFs, immunoproteasome expression and activity was strongly induced under conditions of chronic respiratory chain dysfunction. Such an opposed regulation of the two proteasome systems has not been shown before in the context of mitochondrial dysfunction. Induced immunoproteasome activity was accompanied by upregulated MHC I antigen presentation.

6.1 Respiratory chain complex I deficiency causes metabolic reprogramming and impaired aspartate biosynthesis

To investigate effects of chronic mitochondrial dysfunction on the proteasome, three different models for respiratory chain complex I deficiency were used, which are all characterized by the absence of oxidative stress: mutator MEFs, primary human skin fibroblasts with a mutation in the complex I subunit ND5 and pharmacological inhibition of complex I by the drug metformin in murine and human cells. Mutator MEFs derived from the mtDNA mutator mouse model show chronic respiratory chain dysfunction caused by accumulation of mtDNA mutations over time (Trifunovic et al., 2004). Primary human ND5

skin fibroblasts harbor a mutation in the gene for the mitochondrial complex I subunit ND5 (Kremer et al., 2017). Respiratory chain complex I subunits are most frequently affected by mtDNA mutations, which cause OXPHOS defects and consequently human morbidity and mortality (Rodenburg, 2016). The mt-ND5 gene of complex I has been identified to be extremely prone to mutations (Bannwarth et al., 2013) and faulty synthesis of this complex I subunit is associated with numerous clinical phenotypes such as single organ involvement (Leber hereditary optic neuropathy) or multisystem disease (mitochondrial encephalomyopathy, lactic acidosis and stroke-like episodes (MELAS)) (Howell et al., 1993; Liolitsa et al., 2003; Shanske et al., 2008). Metformin is usually applied to treat type 2 diabetes in patients (Sanchez-Rangel and Inzucchi, 2017). However, recently it has been also shown to be a specific inhibitor of respiratory chain complex I independent of increased ROS production (Fontaine, 2018; Vial et al., 2019).

While proliferation was decelerated in all three models for respiratory chain complex I deficiency, cellular morphology of mutator MEFs, ND5 skin fibroblasts and metformin treated cells showed no signs of stress and was comparable with WT and control cells (morphology data not shown for ND5 skin fibroblasts and metformin treated cells). The effect of defective mitochondrial oxidative phosphorylation on proliferation is in line with observations made by Sullivan et al. (2015) in a different model of respiratory chain dysfunction (Sullivan et al., 2015). Effects of chronic mitochondrial dysfunction on cellular stress responses were exemplary investigated in detail in mutator MEFs. Despite the severe respiratory chain dysfunction, mutator MEFs maintained processes for cell viability in the absence of any signs of cellular stress responses, which was confirmed by proteomics data of WT and mutator MEFs. Chronic respiratory chain dysfunction in mutator MEFs is not accompanied by increased ROS production (Berschneider, 2016; Trifunovic et al., 2005). Absence of elevated ROS levels was also observed in ND5 mutant patient skin fibroblasts (Berschneider, 2016). For pharmacological inhibition of complex I metformin was used because this drug does not induce increased ROS production in comparison to other complex I inhibitors such as rotenone and is therefore perfectly suited to investigate the proteasome system under conditions of acute respiratory chain dysfunction in the absence of oxidative stress (Vial et al., 2019).

ATP production, which is compromised by the lack of electron transfer within the respiratory chain in mitochondria, is maintained by a shift towards upregulated glycolysis in mutator

MEFs (Berschneider, 2016; Saleem et al., 2015). This was shown by determining ATP levels and by measuring the extracellular acidification rate (ECAR) in mutator MEFs compared to WT MEFs. ATP production in cells with chronic respiratory chain dysfunction was exemplarily analysed in mutator and WT MEFs. As ND5 mutant skin fibroblasts show the same mitochondrial phenotype as mutator MEFs, a shift towards glycolysis is also very likely in these cells. Acute inhibition of the respiratory chain by supra-pharmacological metformin concentrations has been shown to reduce ATP levels and leads to an activation of the ATP sensor AMPK (Wang et al., 2019). Influences on glycolysis have not been shown so far.

Thorough characterization of mitochondria from WT and mutator MEFs revealed a severe complex I deficiency in mutator MEFs whereas overall structure and mitochondrial network were not altered. Proteomics and Western blot analysis showed that also other complexes of the respiratory chain such as complex III and IV were affected by random accumulation of mtDNA mutations in mutator MEFs. This finding is in line with respiratory chain dysfunction in mutator mouse tissue (Edgar et al., 2009; Trifunovic et al., 2005). Although most subunits of the different complexes are encoded in the nucleus and are imported into mitochondria, the 13 proteins, which are synthesized in the mitochondria, are crucial for complex formation and mutations in the genes encoding for these subunits lead to respiratory chain dysfunction (van Gisbergen et al., 2015; Picard et al., 2016; Tuppen et al., 2010). Direct consequences of respiratory chain dysfunction are for example increased ROS production or diminished oxidative phosphorylation leading to a lack of ATP. However, complex I deficiency in mutator MEFs does not lead to increased ROS production. One explanation for the severe respiratory chain dysfunction without elevated ROS production in the mutator model could be the absence of complex I. Leakage of electrons via this complex is completely missing, which is usually observed during normal mitochondrial function and especially when chemical inhibitors of the respiratory chain are used (Chaban et al., 2014).

Complex I deficiency also feeds back to the TCA cycle because it is responsible for the regeneration of electron acceptors in form of NAD^+ . Accumulation of NADH, due to its missing oxidation by complex I, is known to inhibit central enzymes of the TCA cycle (Martínez-Reyes and Chandel, 2020). The increased NADH/ NAD^+ ratio in mutator MEFs points to an accumulation of NADH and to a lack of the electron acceptor NAD^+ leading to the inhibition of the TCA cycle. This hypothesis is supported by similar observations made by Sullivan et al. (2015). The TCA cycle is not only the engine of oxidative phosphorylation but

also a source for important cellular biomolecules. Therefore, its inhibition by respiratory chain complex I deficiency could lead to a lack of important cellular components such as nucleotides. Sullivan et al. (2015) observed that respiratory chain dysfunction results in decreased biosynthesis of the non-essential amino acid aspartate, which is an important precursor for nucleotides (Sullivan et al., 2015). The lack of nucleotides resulted in downregulated proliferation. Metabolomics analysis in mutator MEFs identified a similar lack of aspartate while overall amino acid levels were not changed. Of note, aspartate is not supplemented in the culture medium compared with the majority of the other amino acids. An explanation for the decreased aspartate *de novo* synthesis in mutator MEFs could be the lack of electron acceptors caused by complex I deficiency (Sullivan et al., 2015). Aspartate is produced in the TCA cycle via reductive and oxidative reactions, which require both α -ketoglutarate and electron acceptors such as NAD^+ (Fendt et al., 2013; Mullen et al., 2014). As the TCA cycle is most probably inhibited and NAD^+ is only present in little concentrations, aspartate biosynthesis in mutator MEFs could be blocked as a direct consequence of these events.

6.2 Downregulation of protein synthesis and impaired 26S proteasome function in respiration defective cells

Impaired proliferation due to aspartate deficiency caused by respiratory chain dysfunction has been already intensively investigated by others (Birsoy et al., 2015; Sullivan et al., 2015). In addition to decreased proliferation, a proteomics screen in mutator MEFs with defective respiration, identified downregulation of pathways mainly related to RNA processing and protein synthesis. This finding was confirmed by an overall decreased protein synthesis rate and reduced phosphorylation of mTOR downstream targets in mutator MEFs. This previously unrecognized role of aspartate in protein synthesis is best explained by the requirement of aspartate for ribosomal RNA synthesis in the biogenesis of ribosomes (Fu and Danial, 2018; Mayer and Grummt, 2006). The observed concerted downregulation of most ribosomal proteins and proteins involved in ribosomal RNA processing in mutator MEFs supports this concept. Inhibition of protein synthesis appears to be a specific feature of aspartate-deficient cells with defects in respiratory complex I and is not evident in experimental models of mitochondrial heteroplasmy (Picard et al., 2014) or upon complex III insufficiency (Ansó et al., 2017).

Cellular protein synthesis and degradation are tightly regulated in the cell. Cellular proteostasis describes the balance between newly synthesized proteins and their turnover (Mitch and Goldberg, 1996). In the present study, this general concept was for the first time confirmed in cells with respiratory chain complex I deficiency. Respiratory chain dysfunction did not only reduce protein synthesis but also decreased 26S proteasome assembly and activity, which are probably adapted to the lower protein content in the cell. This mitochondrial complex I driven adaptation of 26S proteasome function was observed in mutator MEFs with chronic mitochondrial dysfunction, ND5 mutant human skin fibroblasts and cells treated with metformin as complex I inhibitor.

Accumulation of ubiquitinated proteins and protein aggregate formation are common consequences of impaired proteasome activity (Heinemeyer et al., 1991; Hipp et al., 2012; Meiners et al., 2006). The fact that mutator MEFs did not show increased amounts of ubiquitinated proteins in the presence of lower proteasome activity is a further argument for a downregulated proteasome system adopted to cellular needs instead of a pathological impairment caused by chronic mitochondrial dysfunction. A similar observation has been made by Tsvetkov et al. (2015), who showed that mild knockdown of 19S subunits accompanied by decreased proteasome activity did not trigger a protein stress response (Tsvetkov et al., 2015).

Regarding the mechanism of adaptive downregulation of 26S proteasome function several mechanisms can be envisioned and have been studied in this thesis.

Multiple studies have shown that oxidative stress in form of increased ROS production lead to impaired 26S proteasome function (Chou et al., 2010; Farout and Friguet, 2006; Livnat-Levanon et al., 2014; Segref et al., 2014). In this context, Livnat-Levanon et al. (2014) for example observed 26S proteasome disassembly in the presence of elevated ROS levels, which were induced by chemical inhibition of respiratory chain complexes. These ROS mediated effects on 26S proteasome stability could be partially reverted by antioxidants such as N-acetyl-cysteine (NAC) (Livnat-Levanon et al., 2014). As all three models used in this study are characterized by respiratory chain dysfunction in the absence of increased ROS levels (Berschneider, 2016; Trifunovic et al., 2005; Vial et al., 2019), oxidative stress can be ruled out as the main reason for the diminished 26S proteasome function. Furthermore, oxidative stress has been shown to increase 20S subunit expression and core particle assembly and activity (Digaleh et al., 2013). However, in contrast to lower levels of 26S/30S

proteasome complexes, total amount of 20S proteasome was similar between mutator and WT MEFs and the 20S core particle assembly chaperone Pomp1 was rather downregulated in mutator MEFs. Pomp1 is involved in the formation of the 20S core particle (Wang et al., 2020). Decreased Pomp1 expression has been shown to reduce 20S assembly and activity (Zhang et al., 2015). Consequently, reduced assembly of 26S proteasome complexes in mutator MEFs is not accompanied by an oxidative stress response in form of increased 20S core assembly and activity.

It has been shown before that inhibition of mitochondrial oxidative phosphorylation leads to ATP depletion and consequently to 26S proteasome disassembly and decreased proteasome activity due to proteasomal ATP dependency (Höglinger et al., 2003; Huang et al., 2013). ATP is a key molecule for 26S proteasome complex stability and necessary for substrate degradation (Kim et al., 2012; Liu et al., 2006). In contrast to these findings, chronic respiratory chain dysfunction in mutator MEFs does not influence cellular ATP levels, which can be explained with a glycolytic shift in these cells (Berschneider, 2016; Saleem et al., 2015). Therefore, ATP could be also excluded to be causative for diminished 26S proteasome function in mutator MEFs.

Several mechanisms for transcriptional regulation of 20S and 19S subunits have been identified so far. Expression of 20S and 19S subunits is mainly driven by the stress-related transcription factor NRF1 and NRF2 (Digaleh et al., 2013; Koizumi et al., 2018). Transcriptional activation of 20S subunits via NRF1 and NRF2 has been observed during increased protein turnover by the proteasome, which can be induced by oxidative stress, starvation or oncogenic proliferation (Digaleh et al., 2013; Koizumi et al., 2018; Walerych et al., 2016; Zhang et al., 2014). Decreased activity of the catalytically active sites within the 20S core particle was not accompanied by expressional changes of most 20S and 19S subunits in mutator MEFs. Overall decreased proteasome activity in mutator MEFs was mainly caused by decreased activity and amount of 26/30S proteasome complexes whereas free 20S core particle activity and amount was only slightly increased. 26S/30S proteasome complex formation can be regulated by so-called 19S regulatory assembly chaperones (RACs), which are involved in the 19S base assembly. Decreased levels of these RACs have been shown to reduce 26S proteasome activity and assembly (Kaneko et al., 2009; Rousseau and Bertolotti, 2016). Reduced protein levels of the two RACs p27 and p28 were observed in mutator MEFs. In addition to RACs, the 19S subunit Rpn6 is critical for the assembly of 19S and 20S.

Reduced levels of Rpn6 lead to diminished 26S proteasome assembly and activity whereas overexpression of this subunit induces 26S proteasome complex formation (Semren et al., 2015; Vilchez et al., 2012). Mutator cells also showed decreased Rpn6 protein levels compared to WT MEFs. Lower expression of RACs and Rpn6 could be a possible mechanism for the lower 26S/30S proteasome assembly in mutator MEFs. Unchanged expression of most 20S and 19S subunits and lower Pomp1 levels make an involvement of NRF1/2 in the observed adaption of 26S proteasome assembly very unlikely. Together with the unchanged levels of proteasome subunits these data rather indicate that mutator MEFs have all components for 26S/30S proteasome assembly available and adapt amount and activity of singly and doubly capped proteasomes to the present cellular needs probably by expression of critical assembly factors.

A regulation of proteasome activity and assembly by the metabolic sensors AMPK or cAMP as previously suggested (Lokireddy et al., 2015; Xu et al., 2012) or by metabolic by-products such as O-GlcNAc (Zhang et al., 2003), poly ADP-ribose (Ullrich et al., 1996), or NADH (Tsvetkov et al., 2014) cannot be fully excluded. However, no consistent activation of AMPK in mutator cells (data not shown) was observed arguing against AMPK-mediated proteasome inhibition. Moreover, inhibition of proteasome activity by cAMP, poly ADP-ribose, or NADH is unlikely to take place in mutator cells as these molecules have been shown to contra wise activate and stabilize assembly of 26S proteasome complexes, respectively (Lokireddy et al., 2015; Tsvetkov et al., 2014; Ullrich et al., 1996).

6.3 26S proteasome assembly is reactivated by aspartate mediated induction of protein synthesis in cells with complex I deficiency

As a lack of aspartate caused by mitochondrial complex I deficiency led to adaptively reduced levels of 26S/30S proteasome complexes, the next aim of this study was to investigate if supplementation of the single amino acid aspartate could reactivate proteostasis in respiration defective cells. A phosphoproteomics screen in mutator MEFs showed for the first time that the supplementation of aspartate induces notable changes of the cellular phosphorylation status. Aspartate treatment led to both increased and reduced phosphorylation of numerous proteins in mutator MEFs compared to WT MEFs. Bioinformatic analysis of the phosphoproteomics data set identified activation of several

central cellular kinases by aspartate such as p70 S6 kinase, Akt or different MAP kinases. Aspartate induced activating phosphorylation of kinases involved in cell-cycle regulation has been shown for the first time in the present study and adds a new aspect to the role of aspartate for cellular proliferation, which has been already investigated by others (Birsoy et al., 2015; Sullivan et al., 2015). In addition to cell cycle kinases, aspartate also changed the phosphorylation status of p70 S6 kinase, which is a central downstream target of the mammalian target of rapamycin (mTOR). Further analysis of the mTOR pathway and especially of mTORC1 signaling revealed an activation of this pathway by phosphorylation of downstream targets such as p70 S6 kinase and S6 ribosomal protein (Ben-Sahra et al., 2013; Saxton and Sabatini, 2017) upon aspartate treatment in mutator MEFs. Activation of protein synthesis by aspartate was confirmed by increased rates of protein translation in mutator MEFs. These data suggest that the already discussed activation of protein synthesis after aspartate supplementation is mediated by mTOR signaling. The mechanism how mTOR and here especially mTORC1 is activated by amino acid sensing has recently been discovered for the amino acids leucine and arginine. mTORC1 activity is controlled via a complex mechanism, which involves different regulatory proteins such as Sestrin2, Castor1, Gator1/2 and Kikstor. Raising leucine levels for example lead to deactivation of mTORC1 inhibition by Sestrin2 and Gator2 and consequently to elevated mTORC1 signaling (Wolfson and Sabatini, 2017). However, so far such an amino acid sensing has not been described for aspartate. Most probably, the mechanism how aspartate activates mTORC1 signaling also involves central aspartate sensors and regulatory proteins, which need to be identified in future studies.

Aspartate supplementation in respiration deficient cells rescues proliferation by providing precursors for nucleotide biosynthesis (Sullivan et al., 2015). The same effect was observed in mutator MEFs treated with aspartate whereas WT cells did not react to aspartate stimulation. Proliferation could be also rescued with aspartate or pyruvate in human ND5 mutant skin fibroblasts and cells (WT MEFs, healthy primary human skin and lung fibroblasts) treated with metformin. These results were in line with aspartate activated cell-cycle kinases, which were identified in the phosphoproteomics screen.

However, activation of protein translation and 26S proteasome complex formation by aspartate has not been shown before in the context of chronic respiratory chain dysfunction. Aspartate supplementation increased 26S/30S proteasome activity and assembly in mutator

MEFs already after 24 h but the strongest activation was observed after 72 h of treatment. The amount and activity of free 20S proteasomes was not influenced by aspartate indicating a specific induction of singly and doubly capped proteasome complex assembly. WT MEFs showed no increase in 26S/30S proteasome assembly. A similar induction of 26S/30S proteasome activity and assembly was observed in aspartate treated human ND5 mutant skin fibroblasts. Metformin mediated reduction of 26S/30S proteasome complex formation could be effectively rescued with aspartate in WT MEFs as well as in healthy primary human skin and lung fibroblasts. Therefore, aspartate induced activation of proteasome assembly seems to be a unique feature of respiration deficient cells. In addition to aspartate, pyruvate supplementation also induced proteasome activity and assembly in mutator MEFs and cells treated with metformin. There are two main explanations for this observation: First, pyruvate serves as electron acceptor and NAD^+ is regenerated from NADH by lactate dehydrogenase (LDH) during glycolysis. Both events support *de novo* aspartate synthesis in the TCA cycle (Sullivan et al., 2015). Second, pyruvate fuels aspartate synthesis by the enzyme GOT1 in the cytoplasm during respiratory chain dysfunction (Birsoy et al., 2015).

To tackle cellular aspartate supply more downstream of mitochondrial metabolism and to confirm the impact of aspartate on the proteasome in WT MEFs, the transaminase inhibitor aminooxyacetate (AOA) was used to block reversible conversion of oxaloacetic acid and glutamic acid to aspartate (Antti and Sellstedt, 2018) and the regeneration of NAD^+ by the mitochondrial malate-aspartate shuttle (Alkan et al., 2018). Both, proliferation and 26S/30S proteasome activity and assembly, were downregulated by AOA. The effect was reversible as supplementation of pyruvate or aspartate reactivated proliferation and 26S/30S proteasome activity and assembly in WT MEFs. The activating effect of pyruvate on cells treated with AOA, which acts more downstream on aspartate synthesis than metformin, can be explained by its role in different pathways for aspartate biosynthesis. Here, pyruvate probably served mainly as electron acceptor for aspartate synthesis in the TCA cycle as AOA also blocks NAD^+ regeneration via mitochondrial malate-aspartate shuttle (Alkan et al., 2018). Therefore, blocking aspartate synthesis via conversion of oxaloacetic acid and glutamic acid in the cytoplasm can be probably compensated via aspartate produced in the TCA cycle. The discussed results show that the adaptive regulation of the proteasome system in murine and human models of mitochondrial complex I deficiency could be mimicked and phenocopied

in mouse and human cells by pharmacological inhibition of this complex to acutely induce aspartate deficiency in these cells, which was rescued by aspartate supplementation.

Taken together, the present study has established a novel adaptive mitochondrial regulation of proteostasis by single metabolites such as aspartate or pyruvate. Aspartate supplementation induced not only 26S/30S proteasome activity and assembly but also protein translation. In this context, a phosphoproteomics screen in aspartate treated cells has been performed for the first time and identified mTOR driven protein translation to be activated by aspartate. Adaption of 26S/30S proteasome complex formation could be observed both in chronic murine and human models of respiratory chain dysfunction and during acutely induced failure of mitochondrial complex I function by metformin.

Such a pharmacological approach of targeting the proteasome could be also of interest for future therapies of different diseases. For example, in idiopathic pulmonary fibrosis (IPF) an activation of the proteasome has been demonstrated to be crucial for myofibroblast differentiation, which is one of the key events in the pathology of this disease (Semren et al., 2015). Downregulation of the proteasome by pharmacological complex I inhibition using metformin as shown in the present study, could block or prevent myofibroblast differentiation and thereby ameliorate disease progression. Recently, metformin treatment has been successfully used to reverse lung fibrosis in a murine model of lung fibrosis by inducing lipogenic differentiation in myofibroblasts (Kheirollahi et al., 2019). As cancer is often associated with upregulated proteasome activity, metformin mediated complex I inhibition could also be used to prevent uncontrolled proliferation in tumor cells driven by upregulated proteasome activity. Metformin has already been suggested to either reduce risk of different cancers or to be beneficial for the therapy of breast and colorectal cancers (Mallik and Chowdhury, 2018).

The novel universal concept of proteasomal regulation by mitochondrial dysfunction could also help to find new therapeutic approaches for mitochondrial disorders as supplementation with aspartate increased the general fitness of ND5 mutant skin fibroblasts. Data on aspartate supplementation in humans are limited. Only few studies suggest that long term supplementation of aspartate could improve submaximal work capacity and exercise tolerance of athletes (Burtscher et al., 2005). However, these results are discussed controversially (Trudeau, 2008).

Respiratory complex I dysfunction is not only a hallmark of many mitochondrial disorders with mutations in mitochondrially encoded genes (Gorman et al., 2016) but has also been identified as a distinct contributing factor to aging (Kauppila et al., 2017) and diseases such as Parkinson (Schapira et al., 1989) and heart failure (Karamanlidis et al., 2013), amongst others. While proteasome function in hereditary mitochondrial disorders has not been systematically analyzed, impairment of proteasome activity is a hallmark of aging (López-Otín et al., 2013), and contributes to multiple neuronal and heart diseases (Ciechanover and Brundin, 2003; Drews and Taegtmeyer, 2014). Together with the data of the present study, these observations further support the concept that mitochondria and proteasome dysfunction are closely linked at conditions of metabolic reprogramming, which may contribute to disease progression. Activating 26S proteasome assembly and activity by supplementation of aspartate or pyruvate might provide a therapeutic concept to counteract imbalanced proteostasis in disease.

6.4 Aspartate activates proteasome assembly via expression of specific assembly factors

Aspartate supplementation in mutator MEFs induced assembly of 26S and 30S proteasome complexes. Reactivation of 26S/30S proteasome complex formation was accompanied by upregulation of specific proteasome subunits involved in the assembly of 20S core particle and 19S regulatory particle. The concept of 26S proteasome induction by concerted transcriptional activation of proteasomal gene expression under conditions of increased protein hydrolysis, protein stress, cell growth, and p53 signaling is well established (Meiners et al., 2003; Sha and Goldberg, 2014; Walerych et al., 2016; Zhang et al., 2014). However, aspartate mediated expression of specific subunits involved in 26S proteasome assembly for rapid and reversible adaptation of proteasome activity to altered cellular needs caused by mitochondrial dysfunction has not been shown before. So far, expression of proteasome subunits as fast regulatory mechanism for proteasome activity has been described to be too costly and time-consuming (Meiners and Ballweg, 2014; Rousseau and Bertolotti, 2018). In contrast, 26S proteasome assembly and activity can be rapidly adjusted to growth signals by posttranslational modifications of 19S and 20S subunits such as phosphorylation of Rpt3 (Guo et al., 2016; VerPlank and Goldberg, 2017), Rpn1 (Liu et al., 2020) or Rpn6 (Lokireddy et al., 2015). However, no altered phosphorylation of

proteasome subunits was found after 4 h of aspartate treatment in the phosphoproteomics screen in mutator MEFs. This is an important finding as it rules out activation of 26S/30S proteasome assembly and activity in mutator MEFs by induced phosphorylation of proteasome subunits such as Rpn1, Rpt3 or Rpn6 as shown before in several studies. As Rpn6 is involved in the assembly of 26S/30S proteasome complex formation (Lokireddy et al., 2015; Pathare et al., 2012; Semren et al., 2015; Vilchez et al., 2012), the phosphorylation status of this subunit upon aspartate treatment was also analyzed by the so-called Phos-tag SDS-PAGE technology (Kinoshita et al., 2009). Here, no difference in the phosphorylation of Rpn6 between aspartate treatment and nontreated controls was found (data not shown). While most proteasome subunits were not altered on protein level upon aspartate treatment, the 19S regulatory assembly chaperones (RACs) p27 and p28 and the 19S subunit Rpn6 were significantly upregulated. The 19S regulatory assembly chaperones p27, p28 and S5b have been also shown to be involved in 26S/30S proteasome assembly (Murata et al., 2009; Rousseau and Bertolotti, 2018). S5b was the only RAC, which was not induced by aspartate. Transcriptional activation of p27, p28 and Rpn6 was already detectable after 6 h of aspartate treatment. This indicates a fast activation of signaling pathways in response to aspartate in mutator MEFs. Of note, p27, p28 and Rpn6 were significantly downregulated at conditions of chronic respiratory dysfunction in mutator versus WT cells. Therefore, expressional regulation of these subunits seems to somehow control proteasome assembly dependent on the metabolic status of the cell. However, the mechanism how these assembly factors are transcriptionally induced by aspartate is still unclear. Most probably transcription factors are involved in the specific induction of RACs and Rpn6. The transcription factor Foxo4 has been for example described to be involved in transcriptional regulation of Rpn6 in human embryonic stem cells (Vilchez et al., 2012). However, this transcription factor was not regulated upon aspartate treatment in mutator MEFs (data not shown). As aspartate only induced the expression of specific assembly factors and not of all 20S and 19S subunits, the transcription factors NRF1 and NRF2 are most probably not involved in this so far unknown regulation of 26S/30S proteasome complex formation. To identify transcription factors involved in aspartate driven expression of the described assembly factors, a promoter analysis could be performed in future experiments. The RAC S5b was found to be upregulated in mutator MEFs compared to WT MEFs. As this RAC is known to be an inhibitor of proteasome activity (Levin et al., 2018; Murata et al., 2009; Shim

et al., 2012), its increased expression under chronic conditions and the missing induction by aspartate fit together.

Silencing of p27 (Psmid9), p28 (Psmid10) and Rpn6 (Psmid11) in WT MEFs in the presence of aspartate showed that p28 and Rpn6 play an important role for aspartate induced reactivation of 26S/30S proteasome assembly. Knockdown of p28 and Rpn6 prevented full induction of 26S/30S proteasome activity and assembly by aspartate whereas silencing of p27 had no effect on the proteasome. 19S regulatory assembly chaperones have been shown to be not essential subunits and their silencing did not influence cell viability but led to reduced 26S proteasome activity (Kaneko et al., 2009; Rousseau and Bertolotti, 2016). Silencing of RACs in WT MEFs had also no influence on cell viability. However, in contrast to already published data, knockdown of these subunits did not cause reduced proteasome activity in the absence of aspartate. Silencing of Rpn6 is known to compromise cell viability and 26S proteasome assembly and activity as this subunit is essential for the cell (Semren et al., 2015). Therefore, only a partial knockdown of Rpn6 was performed, which did not affect 26S proteasome assembly and activity in WT MEFs. In general effects of the silencing experiments on aspartate induced proteasome assembly and activity were rather mild. This indicates that these assembly factors rather act in a concerted manner and simultaneously during reactivation of 26S/30S proteasome assembly by aspartate in mutator MEFs. As already mentioned S5b (Psmid5) was differently regulated in mutator MEFs compared to the other RACs. Silencing of this subunit led to induction of 26S/30S proteasome assembly and activity, which was further promoted in the presence of aspartate. These data are in line with other studies on S5b (Levin et al., 2018; Murata et al., 2009; Shim et al., 2012). Therefore, upregulation of S5b in mutator MEFs seems to be an additional mechanism to adjust proteasome activity under conditions of chronic respiratory chain dysfunction and works together with the downregulation of other assembly chaperones and Rpn6.

6.5 Reactivation of 26S proteasome assembly and activity depends on aspartate induced mTORC1 signaling in mutator MEFs

The connection between aspartate induced mTORC1 signaling and reactivation of 26S/30S proteasome assembly and activity in mutator MEFs upon aspartate treatment was shown by specific inhibition of mTORC1 using rapamycin. Blocking mTORC1 signaling upon aspartate treatment prevented both activation of mTORC1 mediated protein synthesis and full induction of 26S/30S proteasome activity and assembly in mutator MEFs. This observation was confirmed by raptor silencing, which also led to inhibition of mTORC1 signaling and prevented full proteasome activation in the presence of aspartate. The link between mTOR mediated protein synthesis and proteasome activity has been investigated already intensively but data are partially contradictory and need to be discussed carefully. Data of the present study strongly suggest co-regulation of proteasome activity with protein synthesis. Given the fact, that proteasome degradation provides amino acids for protein synthesis, coordinated regulation of protein synthesis and proteasome activity is an intuitive cell biological concept. However, a mechanistic link for co-regulation of these two major proteostasis pathways was provided only very recently and data are conflicting (Rousseau and Bertolotti, 2016; Zhang et al., 2014; Zhao et al., 2015). The Goldberg lab reported that inhibition of the mTOR pathway induces rapid ubiquitin-mediated degradation of long-lived proteins in the absence of any changes in activity or expression of the proteasome (Zhao et al., 2015). Rousseau and Bertolotti recently showed that mTOR inhibition results in the fast upregulation of proteasome subunits and 19S regulatory particle assembly-chaperones in yeast and in Hela cells resulting in increased assembly of 26S proteasome complexes within 60 minutes after mTOR inhibition (Rousseau and Bertolotti, 2016). This mode of regulation is very similar to the well-known activation of autophagy mediated protein degradation upon mTOR inhibition and might serve to provide amino acids during conditions of fasting (Saxton and Sabatini, 2017). In contrast, the Manning lab demonstrated that genetic activation of the mTOR complex induces a global increase in the expression of proteasomal genes via Nrf1-mediated gene transcription resulting in the adjustment of 26S proteasome activity to supply substrates for sustained protein synthesis (Zhang and Manning, 2015). Such direct coupling of protein synthesis with proteasome activity is in line with recently published activation of 26S

proteasome activity during cell cycle progression (Guo et al., 2016). A similar co-regulation of protein synthesis with proteasome activity has also been shown for hypertrophic cell growth of cardiomyocytes, in ES cell differentiation and in myofibroblast differentiation (Buszczak et al., 2014; Drews et al., 2010; Semren et al., 2015; Vilchez et al., 2012). These data indicate that increased rates of protein synthesis are balanced by increased proteasomal protein turnover (Saxton and Sabatini, 2017). However, the present study suggests a completely different and novel regulation of cellular proteostasis (Figure 12). Aspartate induced mTORC1 signaling mediates rapid transcriptional activation of specific assembly factors, which upregulate assembly and activity of 26S/30S proteasome complexes in metabolically deficient mutator cells. The reversible regulation of proteostasis is used to adopt protein synthesis and turnover to cellular needs, which can be shifted from low protein translation rate and proteasome activity under chronic conditions of mitochondrial dysfunction to upregulated proteostasis when aspartate acutely stimulates cellular fitness.

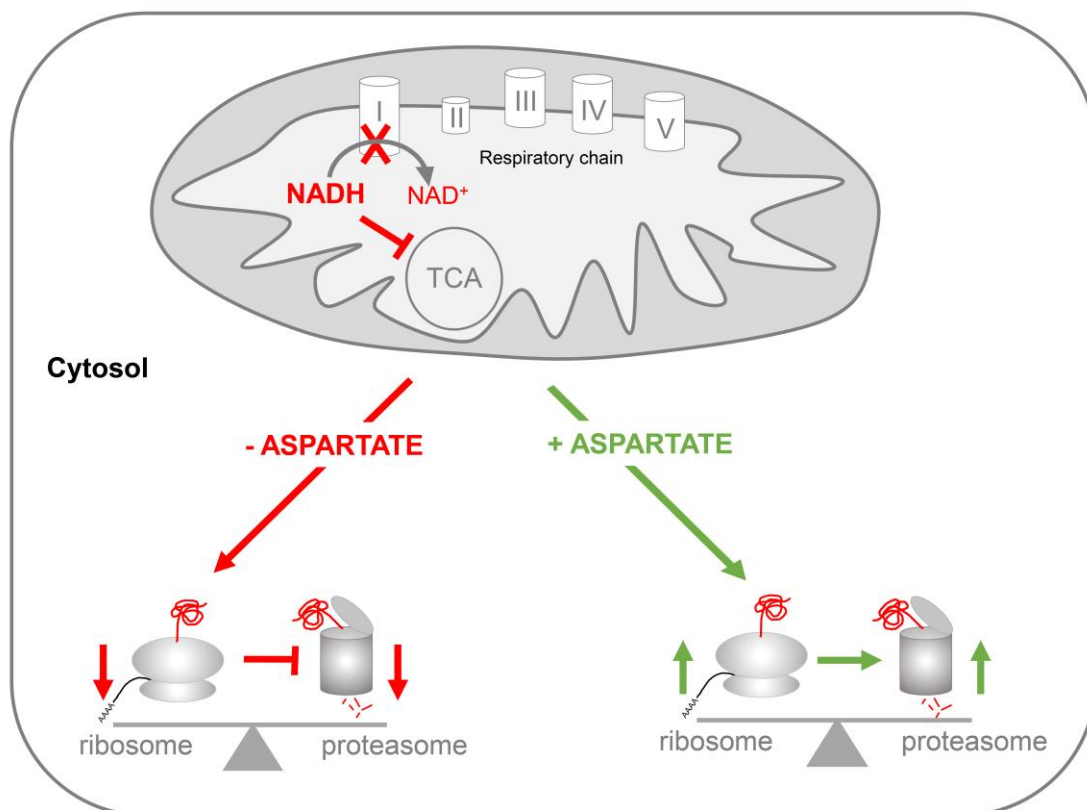


Figure 12 Proteostasis is adaptively regulated by reprogrammed mitochondrial metabolism in respiration deficient cells. Complex I deficiency leads to NADH accumulation, which inhibits the TCA cycle. As a direct consequence aspartate biosynthesis is reduced. Lack of aspartate causes downregulation of proteostasis. This phenotype can be reversed by aspartate treatment, which reactivates both protein synthesis and 26S proteasome assembly and activity.

6.6 Chronic mitochondrial dysfunction in mutator MEFs induces immunoproteasome expression and MHC I antigen presentation

In the present study the influence of chronic mitochondrial dysfunction on the proteasome has been already thoroughly investigated. However, so far, not much is known about the connection between dysfunctional mitochondria and the immunoproteasome. It has been suggested that oxidative stress, which is often induced by mitochondrial respiratory chain deficiency, leads to increased expression of immunoproteasome subunits and the degradation of oxidatively damaged proteins by the immunoproteasome. However, Nathan et al. (2013) also showed that there is no difference between constitutive and immunoproteasome in their ability to degrade ubiquitinated proteins (Launay et al., 2013; Nathan et al., 2013; Pickering and Davies, 2012; Pickering et al., 2012; Seifert et al., 2010). Of note, in mutator MEFs, which show chronic mitochondrial dysfunction in the absence of increased ROS production (Berschneider, 2016; Trifunovic et al., 2005), immunoproteasome expression and activity was strongly increased compared to WT MEFs while overall proteasome activity was reduced. This ROS independent induction of the immunoproteasome in the absence of a viral infection has not been shown before and represents a novel signaling pathway between dysfunctional mitochondria and the proteasome system. Proteomics and flow cytometry analysis revealed that the upregulation of immunoproteasome expression and activity in mutator MEFs is accompanied by a concerted induction of the whole MHC I antigen processing and presentation pathway. As Stat1 expression was also increased in mutator MEFs, this transcription factor probably regulates the concerted induction of the immunoproteasome and MHC I antigen presentation as shown before (Jongsma et al., 2019). The connection between dysfunctional mitochondria and antigen presentation response has already been shown in immune cells (Bonifaz et al., 2015). However, only one study described induced MHC I antigen presentation in response to mitochondrial dysfunction in nonimmune mitochondrial DNA deficient (ρ^0) osteosarcoma cells (Gu et al., 2003). The model of mitochondrial DNA depletion is not comparable with the mtDNA mutator mouse model and does not reflect physiological processes. In comparison, the accumulation of mitochondrial DNA mutations in the mtDNA mutator model is a process, which can be also observed for example during normal aging or in cancer (Herst et al., 2017). Therefore, the mtDNA mutator mouse model is

better suited for analysis of an adaptive immune response triggered by chronic mitochondrial dysfunction. As the mechanism how mitochondrial dysfunction induces an adaptive immune response in mutator MEFs is unclear until now, future experiments will focus on dissecting this pathway and on the effects of upregulated MHC I antigen presentation on CD8⁺ T cell activation. It has been, for example, shown that release of mitochondrial DNA activates the so-called cGAS/Sting pathway, which is involved in innate immune processes (Motwani et al., 2019). Additionally, metabolic reprogramming in mutator MEFs with chronic respiratory dysfunction, which was identified in the present study, could be involved in the activation of MHC I antigen processing and presentation. The effects of aspartate or pyruvate supplementation on the immunoproteasome and MHC I antigen presentation will be investigated in respiration deficient cells in future experiments.

7 Concluding remarks

In the present study regulation of cellular proteostasis and in particular regulation of the ubiquitin-proteasome system by metabolic reprogramming in mitochondria with respiratory chain complex I deficiency was investigated.

The first aim was to analyze the proteasome system under conditions of chronic respiratory chain dysfunction in the absence of oxidative stress. Cells with defective complex I function showed concerted downregulation of mTOR mediated protein synthesis and 26S proteasome activity and assembly. In general, these cells maintained all processes, which are required for cellular viability. While proteasome function was diminished in mutator MEFs, the immunoproteasome was found to be upregulated under conditions of chronic respiratory chain dysfunction. Increased immunoproteasome expression and activity was accompanied by higher MHC I antigen presentation. Dysfunctional mitochondria probably activate this stress response to alert the immune system.

The second aim of this study was to dissect the underlying mechanism of proteasomal regulation by reprogrammed mitochondrial metabolism in cells with complex I deficiency. Diminished aspartate biosynthesis was identified as a direct consequence of metabolic reprogramming of the TCA cycle caused by respiratory chain complex I deficiency. Treatment of respiration deficient cells with aspartate or the electron acceptor pyruvate led to reactivation of both protein synthesis and 26S proteasome function. Aspartate sensing via mTORC1 was identified to be involved in the transcriptional activation of specific assembly factors, which are important for the reactivation of 26S proteasome assembly and activity. Therefore, a so far unknown link between mitochondrial complex I deficiency, mTOR signaling, protein synthesis and 26S proteasome function was established in the present study.

The last aim of this study was to establish adaptive mitochondrial regulation as a general model in murine and human cells. Primary human ND5 mutant skin fibroblasts and metformin treated cells showed a similar downregulation of 26S proteasome function as observed in mutator MEFs. This phenotype was also reversible when aspartate was supplemented in these cells.

In conclusion, the present study could significantly contribute to the current knowledge about adaptive mitochondrial regulation of the proteasome and establish a novel signaling

pathway between mitochondria and the proteasome. However, different aspects of the mechanistic details are still unknown and need further experiments. It remains for example unclear how aspartate is sensed by mTOR and how this signal then activates transcriptional upregulation of specific assembly factors, which are involved in reactivation of 26S proteasome function. In this context, a promoter analysis of the induced assembly factors could help to identify possible transcription factors, which are probably activated by mTOR signaling. Furthermore, the therapeutic benefit of an adaptive regulation of cellular proteostasis for example in fibrosis or cancer needs to be tested in future studies. The mechanistic insights of induced immunoproteasome function and MHC I antigen presentation in cells with dysfunctional mitochondria are also still unclear. Here, especially the specific signaling pathway between dysfunctional mitochondria and the immunoproteasome and the effects of upregulated MHC I antigen presentation on the immune system require further analysis.

References

- Acosta-Alvear, D., Cho, M.Y., Wild, T., Buchholz, T.J., Lerner, A.G., Simakova, O., Hahn, J., Korde, N., Landgren, O., Maric, I., Choudhary, C., Walter, P., Weissman, J.S., and Kampmann, M.** (2015). Paradoxical resistance of multiple myeloma to proteasome inhibitors by decreased levels of 19S proteasomal subunits. *Elife* 4.
- Aiken, C.T., Kaake, R.M., Wang, X., and Huang, L.** (2011). Oxidative stress-mediated regulation of proteasome complexes. *Mol. Cell. Proteomics* 10, R110.006924.
- Alkan, H.F., Walter, K.E., Luengo, A., Madreiter-Sokolowski, C.T., Stryeck, S., Lau, A.N., Al-Zoughbi, W., Lewis, C.A., Thomas, C.J., Hoefler, G., Graier, W.F., Madl, T., Vander Heiden, M.G., and Bogner-Strauss, J.G.** (2018). Cytosolic Aspartate Availability Determines Cell Survival When Glutamine Is Limiting. *Cell Metab.* 28, 706-720.e6.
- Ansó, E., Weinberg, S.E., Diebold, L.P., Thompson, B.J., Malinge, S., Schumacker, P.T., Liu, X., Zhang, Y., Shao, Z., Steadman, M., Marsh, K.M., Xu, J., Crispino, J.D., and Chandel, N.S.** (2017). The mitochondrial respiratory chain is essential for haematopoietic stem cell function. *Nat. Cell Biol.*
- Antti, H., and Sellstedt, M.** (2018). Metabolic effects of an aspartate aminotransferase-inhibitor on two T-cell lines. *PLoS One* 13.
- Arnould, T., Michel, S., and Renard, P.** (2015). Mitochondria Retrograde Signaling and the UPRmt: Where Are We in Mammals? *Int. J. Mol. Sci.* 16, 18224–18251.
- Bajorek, M., Finley, D., and Glickman, M.H.** (2003). Proteasome disassembly and downregulation is correlated with viability during stationary phase. *Curr. Biol.* 13, 1140–1144.
- Balch, W.E., Sznajder, J.I., Budinger, S., Finley, D., Laposky, A.D., Cuervo, A.M., Benjamin, I.J., Barreiro, E., Morimoto, R.I., Postow, L., Weissman, A.M., Gail, D., Banks-Schlegel, S., Croxton, T., and Gan, W.** (2014). Malfolded protein structure and proteostasis in lung diseases. *Am. J. Respir. Crit. Care Med.* 189, 96–103.
- Bannwarth, S., Procaccio, V., Lebre, A.S., Jarde, C., Chaussonot, A., Hoarau, C., Maoulida, H., Charrier, N., Gai, X., Xie, H.M., Ferre, M., Fragaki, K., Hardy, G., de Camaret, B.M., Marlin, S., Dhaenens, C.M., Slama, A., Rocher, C., et al.** (2013). Prevalence of rare mitochondrial DNA mutations in mitochondrial disorders. *J. Med. Genet.* 50, 704–714.
- Bard, J.A.M., Goodall, E.A., Greene, E.R., Jonsson, E., Dong, K.C., and Martin, A.** (2018). Structure and Function of the 26S Proteasome. *Annu. Rev. Biochem.* 87, 697–724.
- Barton, L.F., Cruz, M., Rangwala, R., Deepe, G.S., and Monaco, J.J.** (2002). Regulation of Immunoproteasome Subunit Expression In Vivo Following Pathogenic Fungal Infection. *J. Immunol.* 169, 3046–3052.
- Basler, M., Dajee, M., Moll, C., Groettrup, M., and Kirk, C.J.** (2010). Prevention of Experimental Colitis by a Selective Inhibitor of the Immunoproteasome. *J. Immunol.* 185, 634–641.
- Ben-Nissan, G., and Sharon, M.** (2014). Regulating the 20S Proteasome Ubiquitin-Independent Degradation Pathway. *Biomolecules* 4, 862–884.

- Ben-Sahra, I., Howell, J.J., Asara, J.M., and Manning, B.D.** (2013). Stimulation of de novo pyrimidine synthesis by growth signaling through mTOR and S6K1. *Science (80-.)*, 339, 1323–1328.
- De Berardinis, R.J., and Chandel, N.S.** (2016). Fundamentals of cancer metabolism. *Sci. Adv.* 2.
- Berschneider, K.** (2016). Connecting the functions of the proteasome and mitochondria in the lung.
- Birsoy, K., Wang, T., Chen, W.W., Freinkman, E., Abu-Remaileh, M., and Sabatini, D.M.** (2015). An Essential Role of the Mitochondrial Electron Transport Chain in Cell Proliferation Is to Enable Aspartate Synthesis. *Cell* 162, 540–551.
- Bonifaz, L.C., Cervantes-Silva, M.P., Ontiveros-Dotor, E., López-Villegas, E.O., and Sánchez-García, F.J.** (2015). A role for mitochondria in antigen processing and presentation. *Immunology* 144, 461–471.
- Boos, F., Krämer, L., Groh, C., Jung, F., Haberkant, P., Stein, F., Wollweber, F., Gackstatter, A., Zöller, E., van der Laan, M., Savitski, M.M., Benes, V., and Herrmann, J.M.** (2019). Mitochondrial protein-induced stress triggers a global adaptive transcriptional programme. *Nat. Cell Biol.* 21, 442–451.
- Borissenko, L., and Groll, M.** (2007). 20S Proteasome and Its Inhibitors: Crystallographic Knowledge for Drug Development. *Chem. Rev.* 107, 687–717.
- Burtscher, M., Brunner, F., Faulhaber, M., Hotter, B., and Likar, R.** (2005). The Prolonged Intake of L-Arginine-L-Aspartate Reduces Blood Lactate Accumulation and Oxygen Consumption During Submaximal Exercise. *J. Sports Sci. Med.* 4, 314.
- Buszczak, M., Signer, R.A.J., and Morrison, S.J.** (2014). Cellular Differences in Protein Synthesis Regulate Tissue Homeostasis. *Cell* 159, 242–251.
- Calvo, S.E., Clauser, K.R., and Mootha, V.K.** (2016). MitoCarta2.0: an updated inventory of mammalian mitochondrial proteins. *Nucleic Acids Res.* 44, D1251-7.
- Cascio, P.** (2014). PA28alphabeta: The Enigmatic Magic Ring of the Proteasome? *Biomolecules* 4, 566–584.
- Chaban, Y., Boekema, E.J., and Dudkina, N. V.** (2014). Structures of mitochondrial oxidative phosphorylation supercomplexes and mechanisms for their stabilisation. *Biochim. Biophys. Acta - Bioenerg.* 1837, 418–426.
- Chou, A.P., Li, S., Fitzmaurice, A.G., and Bronstein, J.M.** (2010). Mechanisms of rotenone-induced proteasome inhibition. *Neurotoxicology* 31, 367–372.
- Ciechanover, A.** (2015). The unravelling of the ubiquitin system. *Nat. Rev. Mol. Cell Biol.* 16, 322–324.
- Ciechanover, A., and Brundin, P.** (2003). The ubiquitin proteasome system in neurodegenerative diseases: sometimes the chicken, sometimes the egg. *Neuron* 40, 427–446.
- Ciechanover, A., and Kwon, Y.T. a.** (2015). Degradation of misfolded proteins in neurodegenerative diseases: therapeutic targets and strategies. *Exp. Mol. Med.* 47, e147.
- Collins, G.A., and Goldberg, A.L.** (2017). The Logic of the 26S Proteasome. *Cell* 169, 792–806.

- Cox, J., and Mann, M.** (2012). 1D and 2D annotation enrichment: a statistical method integrating quantitative proteomics with complementary high-throughput data. *BMC Bioinformatics* *13 Suppl 1*, S12.
- Digaleh, H., Kiaei, M., and Khodagholi, F.** (2013). Nrf2 and Nrf1 signaling and ER stress crosstalk: implication for proteasomal degradation and autophagy. *Cell. Mol. Life Sci.* *70*, 4681–4694.
- Domingues, A.F., Arduíno, D.M., Esteves, A.R., Swerdlow, R.H., Oliveira, C.R., and Cardoso, S.M.** (2008). Mitochondria and ubiquitin-proteasomal system interplay: Relevance to Parkinson's disease. *Free Radic. Biol. Med.* *45*, 820–825.
- Drews, O., and Taegtmeyer, H.** (2014). Targeting the Ubiquitin-Proteasome System in Heart Disease: The Basis for New Therapeutic Strategies. *Antioxid. Redox Signal.* *21*, 2322–2343.
- Drews, O., Tsukamoto, O., Liem, D., Streicher, J., Wang, Y., and Ping, P.** (2010). Differential regulation of proteasome function in isoproterenol-induced cardiac hypertrophy. *Circ. Res.* *107*, 1094–1101.
- Dyson, H.J., and Wright, P.E.** (2005). Intrinsically unstructured proteins and their functions. *Nat. Rev. Mol. Cell Biol.* *6*, 197–208.
- Edgar, D., Shabalina, I., Camara, Y., Wredenberg, A., Calvaruso, M.A., Nijtmans, L., Nedergaard, J., Cannon, B., Larsson, N.-G., and Trifunovic, A.** (2009). Random Point Mutations with Major Effects on Protein-Coding Genes Are the Driving Force behind Premature Aging in mtDNA Mutator Mice. *Cell Metab* *10*, 131–138.
- Estrin, E., Lopez-Blanco, J.R., Chacón, P., and Martin, A.** (2013). Formation of an intricate helical bundle dictates the assembly of the 26S proteasome Lid. *Structure* *21*, 1624–1635.
- Fabre, B., Lambour, T., Garrigues, L., Ducoux-Petit, M., Amalric, F., Monsarrat, B., Burlet-Schiltz, O., and Bousquet-Dubouch, M.-P.** (2014). Label-free quantitative proteomics reveals the dynamics of proteasome complexes composition and stoichiometry in a wide range of human cell lines. *J. Proteome Res.* *13*, 3027–3037.
- Farout, L., and Friguet, B.** (2006). Proteasome Function in Aging and Oxidative Stress: Implications in Protein Maintenance Failure. *Antioxid. Redox Signal.* *8*, 2005–2216.
- Fendt, S.M., Bell, E.L., Keibler, M.A., Davidson, S.M., Wirth, G.J., Fiske, B., Mayers, J.R., Schwab, M., Bellinger, G., Csibi, A., Patnaik, A., Blouin, M.J., Cantley, L.C., Guarente, L., Blenis, J., Pollak, M.N., Olumi, A.F., Vander Heiden, M.G., et al.** (2013). Metformin decreases glucose oxidation and increases the dependency of prostate cancer cells on reductive glutamine metabolism. *Cancer Res.* *73*, 4429–4438.
- Finley, D.** (2009). Recognition and Processing of Ubiquitin-Protein Conjugates by the Proteasome. *Annu. Rev. Biochem.* *78*, 477–513.
- Fontaine, E.** (2018). Metformin-Induced Mitochondrial Complex I Inhibition: Facts, Uncertainties, and Consequences. *Front. Endocrinol. (Lausanne)*. *9*, 753.

- Förster, F., Lasker, K., Beck, F., Nickell, S., Sali, A., and Baumeister, W.** (2009). An atomic model AAA-ATPase/20S core particle sub-complex of the 26S proteasome. *Biochem. Biophys. Res. Commun.* *388*, 228–233.
- Fu, A., and Danial, N.N.** (2018). Grasping for aspartate in tumour metabolism. *Nat. Cell Biol.* *20*, 738–739.
- Garcia-Bermudez, J., Baudrier, L., La, K., Zhu, X.G., Fidelin, J., Sviderskiy, V.O., Papagiannakopoulos, T., Molina, H., Snuderl, M., Lewis, C.A., Possemato, R.L., and Birsoy, K.** (2018). Aspartate is a limiting metabolite for cancer cell proliferation under hypoxia and in tumours. *Nat. Cell Biol.* *20*, 775–781.
- van Gisbergen, M.W., Voets, A.M., Starmans, M.H.W., de Coo, I.F.M., Yadak, R., Hoffmann, R.F., Boutros, P.C., Smeets, H.J.M., Dubois, L., and Lambin, P.** (2015). How do changes in the mtDNA and mitochondrial dysfunction influence cancer and cancer therapy? Challenges, opportunities and models. *Mutat. Res. - Rev. Mutat. Res.* *764*, 16–30.
- Gorman, G.S., Chinnery, P.F., DiMauro, S., Hirano, M., Koga, Y., McFarland, R., Suomalainen, A., Thorburn, D.R., Zeviani, M., and Turnbull, D.M.** (2016). Mitochondrial diseases. *Nat. Rev. Dis. Prim.* *2*, 1–23.
- Goto, Y.I., Nonaka, I., and Horai, S.** (1990). A mutation in the tRNA^{Leu}(UUR) gene associated with the MELAS subgroup of mitochondrial encephalomyopathies. *Nature* *348*, 651–653.
- Gray, M.W., Burger, G., and Lang, B.F.** (1999). Mitochondrial evolution. *Science (80-.)*, *283*, 1476–1481.
- Groettrup, M., Khan, S., Schwarz, K., and Schmidtke, G.** (2001). Interferon- γ inducible exchanges of 20S proteasome active site subunits: Why? In *Biochimie*, (Elsevier Masson SAS), pp. 367–372.
- Groettrup, M., Kirk, C.J., and Basler, M.** (2010). Proteasomes in immune cells: more than peptide producers? *Nat. Rev. Immunol.* *10*, 73–78.
- Groll, M., Ditzel, L., Löwe, J., Stock, D., Bochtler, M., Bartunik, H.D., and Huber, R.** (1997). Structure of 20S proteasome from yeast at a 2.4 Å resolution. *Nature* *386*, 463–471.
- Groll, M., Bajorek, M., Köhler, A., Moroder, L., Rubin, D.M., Huber, R., Glickman, M.H., and Finley, D.** (2000). A gated channel into the proteasome core particle. *Nat. Struct. Mol. Biol.* *7*, 1062–1067.
- Gu, Y., Wang, C., Roifman, C.M., and Cohen, A.** (2003). Role of MHC Class I in Immune Surveillance of Mitochondrial DNA Integrity. *J. Immunol.* *170*, 3603–3607.
- Guo, X., Wang, X., Wang, Z., Banerjee, S., Yang, J., Huang, L., and Dixon, J.E.** (2016). Site-specific proteasome phosphorylation controls cell proliferation and tumorigenesis. *Nat. Cell Biol.* *18*, 202–212.
- Guo, X., Huang, X., and Chen, M.J.** (2017). Reversible phosphorylation of the 26S proteasome. *Protein Cell* *8*, 255–272.

- Haack, T.B., Kopajtich, R., Freisinger, P., Wieland, T., Rorbach, J., Nicholls, T.J., Baruffini, E., Walther, A., Danhauser, K., Zimmermann, F.A., Husain, R.A., Schum, J., Mundy, H., Ferrero, I., Strom, T.M., Meitinger, T., Taylor, R.W., Minczuk, M., et al.** (2013). ELAC2 mutations cause a mitochondrial RNA processing defect associated with hypertrophic cardiomyopathy. *Am. J. Hum. Genet.* *93*, 211–223.
- Hacker, C., and Lucocq, J.M.** (2014). Analysis of specificity in immunoelectron microscopy. *Methods Mol. Biol.* *1117*, 315–323.
- Heinemeyer, W., Kleinschmidt, J.A., Saidowsky, J., Escher, C., and Wolf, D.H.** (1991). Proteinase yscE, the yeast proteasome/multicatalytic-multifunctional proteinase: mutants unravel its function in stress induced proteolysis and uncover its necessity for cell survival. *EMBO J.* *10*, 555–562.
- Hensen, F., Cansiz, S., Gerhold, J.M., and Spelbrink, J.N.** (2014). To be or not to be a nucleoid protein: A comparison of mass-spectrometry based approaches in the identification of potential mtDNA-nucleoid associated proteins. *Biochimie* *100*, 219–226.
- Herst, P.M., Rowe, M.R., Carson, G.M., and Berridge, M. V.** (2017). Functional mitochondria in health and disease. *Front. Endocrinol. (Lausanne)*. *8*.
- Herzig, S., and Shaw, R.J.** (2018). AMPK: Guardian of metabolism and mitochondrial homeostasis. *Nat. Rev. Mol. Cell Biol.* *19*, 121–135.
- Hipp, M.S., Patel, C.N., Bersuker, K., Riley, B.E., Kaiser, S.E., Shaler, T. a, Brandeis, M., and Kopito, R.R.** (2012). Indirect inhibition of 26S proteasome activity in a cellular model of Huntington's disease. *J. Cell Biol.* *196*, 573–587.
- Hipp, M.S., Kasturi, P., and Hartl, F.U.** (2019). The proteostasis network and its decline in ageing. *Nat. Rev. Mol. Cell Biol.* *20*, 421–435.
- Höglinger, G.U., Carrard, G., Michel, P.P., Medja, F., Lombès, A., Ruberg, M., Friguet, B., and Hirsch, E.C.** (2003). Dysfunction of mitochondrial complex I and the proteasome: Interactions between two biochemical deficits in a cellular model of Parkinson's disease. *J. Neurochem.* *86*, 1297–1307.
- Howell, N., Halvorson, S., Burns, J., McCullough, D.A., and Paulton, J.** (1993). When does bilateral optic atrophy become Leber hereditary optic neuropathy? *Am. J. Hum. Genet.* *53*, 959.
- Huang, Q., Wang, H., Perry, S.W., and Figueiredo-Pereira, M.E.** (2013). Negative regulation of 26S proteasome stability via calpain-mediated cleavage of Rpn10 subunit upon mitochondrial dysfunction in neurons. *J. Biol. Chem.* *288*, 12161–12174.
- Huber, E.M., Basler, M., Schwab, R., Heinemeyer, W., Kirk, C.J., Groettrup, M., and Groll, M.** (2012). Immuno- and constitutive proteasome crystal structures reveal differences in substrate and inhibitor specificity. *Cell* *148*, 727–738.
- Humphrey, S.J., Karayel, O., James, D.E., and Mann, M.** (2018). High-throughput and high-sensitivity phosphoproteomics with the EasyPhos platform. *Nat. Protoc.* *13*, 1897–1916.
- Jin, S.M., and Youle, R.J.** (2013). The accumulation of misfolded proteins in the mitochondrial matrix is sensed by PINK1 to induce PARK2/Parkin-mediated mitophagy of polarized mitochondria. *Autophagy* *9*, 1750–1757.

- Jongsma, M.L.M., Guarda, G., and Spaapen, R.M.** (2019). The regulatory network behind MHC class I expression. *Mol. Immunol.* *113*, 16–21.
- Kaneko, T., Hamazaki, J., Iemura, S.-I., Sasaki, K., Furuyama, K., Natsume, T., Tanaka, K., and Murata, S.** (2009). Assembly pathway of the Mammalian proteasome base subcomplex is mediated by multiple specific chaperones. *Cell* *137*, 914–925.
- Kang, S.A., Pacold, M.E., Cervantes, C.L., Lim, D., Lou, H.J., Ottina, K., Gray, N.S., Turk, B.E., Yaffe, M.B., and Sabatini, D.M.** (2013). mTORC1 phosphorylation sites encode their sensitivity to starvation and rapamycin. *Science (80-.)*. *341*.
- Karamanlidis, G., Lee, C.F., Garcia-Menendez, L., Kolwicz, S.C., Suthammarak, W., Gong, G., Sedensky, M.M., Morgan, P.G., Wang, W., and Tian, R.** (2013). Mitochondrial complex I deficiency increases protein acetylation and accelerates heart failure. *Cell Metab.* *18*, 239–250.
- Kaufman, B.A., Durisic, N., Mativetsky, J.M., Costantino, S., Hancock, M.A., Grutter, P., and Shoubridge, E.A.** (2007). The mitochondrial transcription factor TFAM coordinates the assembly of multiple DNA molecules into nucleoid-like structures. *Mol. Biol. Cell* *18*, 3225–3236.
- Kaupila, T.E.S., Kaupila, J.H.K., and Larsson, N.-G.G.** (2017). Mammalian Mitochondria and Aging: An Update. *Cell Metab.* *25*, 57–71.
- Kheirollahi, V., Wasnick, R.M., Biasin, V., Vazquez-Armendariz, A.I., Chu, X., Moiseenko, A., Weiss, A., Wilhelm, J., Zhang, J.S., Kwapiszewska, G., Herold, S., Schermuly, R.T., Mari, B., Li, X., Seeger, W., Günther, A., Bellusci, S., and El Agha, E.** (2019). Metformin induces lipogenic differentiation in myofibroblasts to reverse lung fibrosis. *Nat. Commun.* *10*, 1–16.
- Kim, S., Nishide, A., Saeki, Y., Tanaka, K., Kato, K., and Mizushima, T.** (2012). New crystal structure of the proteasome-dedicated chaperone Rpn14 at 1.6 Å resolution. *Acta Crystallogr Sect F Struct Biol Cryst Commun.* *68*, 517–521.
- Kincaid, E.Z., Che, J.W., York, I., Escobar, H., Reyes-Vargas, E., Delgado, J.C., Welsh, R.M., Karow, M.L., Murphy, A.J., Valenzuela, D.M., Yancopoulos, G.D., and Rock, K.L.** (2012). Mice completely lacking immunoproteasomes show major changes in antigen presentation. *Nat. Immunol.* *13*, 129–135.
- Klaips, C.L., Jayaraj, G.G., and Hartl, F.U.** (2018). Pathways of cellular proteostasis in aging and disease. *J. Cell Biol.* *217*, 51–63.
- Kleijnen, M.F., Roelofs, J., Park, S., Hathaway, N.A., Glickman, M., King, R.W., and Finley, D.** (2007). Stability of the proteasome can be regulated allosterically through engagement of its proteolytic active sites. *Nat. Struct. Mol. Biol.* *14*, 1180–1188.
- Koizumi, S., Hamazaki, J., and Murata, S.** (2018). Transcriptional regulation of the 26S proteasome by Nrf1. *Proc. Jpn. Acad. Ser. B. Phys. Biol. Sci.* *94*, 325–336.
- Komander, D., and Rape, M.** (2012). The Ubiquitin Code. *Annu. Rev. Biochem.* *81*, 203–229.
- Kors, S., Geijtenbeek, K., Reits, E., and Schipper-Krom, S.** (2019). Regulation of Proteasome Activity by (Post-)transcriptional Mechanisms. *Front. Mol. Biosci.* *6*, 48.

- Kremer, L.S., Bader, D.M., Mertes, C., Kopajtich, R., Pichler, G., Iuso, A., Haack, T.B., Graf, E., Schwarzmayr, T., Terrile, C., Koňáriková, E., Repp, B., Kastenmüller, G., Adamski, J., Lichtner, P., Leonhardt, C., Funalot, B., Donati, A., et al. (2017). Genetic diagnosis of Mendelian disorders via RNA sequencing. *Nat. Commun.* 8.
- Kujoth, C.C., Hiona, A., Pugh, T.D., Someya, S., Panzer, K., Wohlgemuth, S.E., Hofer, T., Seo, A.Y., Sullivan, R., Jobling, W.A., Morrow, J.D., Van Remmen, H., Sedivy, J.M., Yamasoba, T., Tanokura, M., Weindruch, R., Leeuwenburgh, C., and Prolla, T.A. (2005). Medicine: Mitochondrial DNA mutations, oxidative stress, and apoptosis in mammalian aging. *Science (80-.)*. 309, 481–484.
- Lamming, D.W. (2016). Inhibition of the mechanistic target of rapamycin (mTOR)–Rapamycin and beyond. *Cold Spring Harb. Perspect. Med.* 6.
- Launay, N., Ruiz, M., Fourcade, S., Schlüter, A., Guilera, C., Ferrer, I., Knecht, E., and Pujol, A. (2013). Oxidative stress regulates the ubiquitin–proteasome system and immunoproteasome functioning in a mouse model of X-adrenoleukodystrophy. *Brain* 136, 891–904.
- Lee, S.Y.C., De La Mota-Peynado, A., and Roelofs, J. (2011). Loss of Rpt5 protein interactions with the core particle and Nas2 protein causes the formation of faulty proteasomes that are inhibited by Ecm29 protein. *J. Biol. Chem.* 286, 36641–36651.
- Van Der Lee, R., Buljan, M., Lang, B., Weatheritt, R.J., Daughdrill, G.W., Dunker, A.K., Fuxreiter, M., Gough, J., Gsponer, J., Jones, D.T., Kim, P.M., Kriwacki, R.W., Oldfield, C.J., Pappu, R. V., Tompa, P., Uversky, V.N., Wright, P.E., and Babu, M.M. (2014). Classification of intrinsically disordered regions and proteins. *Chem. Rev.* 114, 6589–6631.
- Lehmann, A., Niewienda, A., Jechow, K., Janek, K., and Enenkel, C. (2010). Ecm29 fulfils quality control functions in proteasome assembly. *Mol. Cell* 38, 879–888.
- Letts, J.A., and Sazanov, L.A. (2017). Clarifying the supercomplex: The higher-order organization of the mitochondrial electron transport chain. *Nat. Struct. Mol. Biol.* 24, 800–808.
- Levin, A., Minis, A., Lalazar, G., Rodriguez, J., and Steller, H. (2018). PSMD5 inactivation promotes 26S proteasome assembly during colorectal tumor progression. *Cancer Res.* 78, canres.2296.2017.
- Li, J., and Rechsteiner, M. (2001). Molecular dissection of the 11S REG (PA28) proteasome activators. *Biochimie* 83, 373–383.
- Li, D., Dong, Q., Tao, Q., Gu, J., Cui, Y., Jiang, X., Yuan, J., Li, W., Xu, R., Jin, Y., Li, P., Weaver, D.T., Ma, Q., Liu, X., and Cao, C. (2015). c-Abl regulates proteasome abundance by controlling the ubiquitin-proteasomal degradation of PSMA7 subunit. *Cell Rep.* 10, 484–497.
- Li, X., Thompson, D., Kumar, B., and DeMartino, G.N. (2014). Molecular and cellular roles of PI31 (PSMF1) protein in regulation of proteasome function. *J. Biol. Chem.* 289, 17392–17405.
- Lin, J.-T., Chang, W.-C., Chen, H.-M., Lai, H.-L., Chen, C.-Y., Tao, M.-H., and Chern, Y. (2013). Regulation of feedback between protein kinase A and the proteasome system worsens Huntington's disease. *Mol. Cell. Biol.* 33, 1073–1084.
- Liolitsa, D., Rahman, S., Benton, S., Carr, L.J., and Hanna, M.G. (2003). Is the mitochondrial complex I ND5 gene a hot-spot for MELAS causing mutations? *Ann. Neurol.* 53, 128–132.

- Liu, C.-W., Li, X., Thompson, D., Wooding, K., Chang, T., Tang, Z., Yu, H., Thomas, P.J., and DeMartino, G.N.** (2006). \textsc{ATP} Binding and \textsc{ATP} Hydrolysis Play Distinct Roles in the Function of 26S Proteasome. *Mol Cell* 24, 39–50.
- Liu, X., Xiao, W., Zhang, Y., Wiley, S.E., Zuo, T., Zheng, Y., Chen, N., Chen, L., Wang, X., Zheng, Y., Huang, L., Lin, S., Murphy, A.N., Dixon, J.E., Xu, P., and Guo, X.** (2020). Reversible phosphorylation of Rpn1 regulates 26S proteasome assembly and function. *Proc. Natl. Acad. Sci. U. S. A.* 117, 328–336.
- Livnat-Levanon, N., Kevei, É., Kleifeld, O., Krutauz, D., Segref, A., Rinaldi, T., Erpapazoglou, Z., Cohen, M., Reis, N., Hoppe, T., and Glickman, M.H.** (2014). Reversible 26S Proteasome Disassembly upon Mitochondrial Stress. *Cell Rep.* 7, 1371–1380.
- Lokireddy, S., Kukushkin, N.V., and Goldberg, A.L.** (2015). cAMP-induced phosphorylation of 26S proteasomes on Rpn6/PSMD11 enhances their activity and the degradation of misfolded proteins. *Proc. Natl. Acad. Sci.* 112, E7176–E7185.
- López-Otín, C., Blasco, M., Partridge, L., Serrano, M., and Kroemer, G.** (2013). The hallmarks of aging. *Cell* 153, 1194–1217.
- Lucocq, J.M., and Hacker, C.** (2013). Cutting a fine figure: On the use of thin sections in electron microscopy to quantify autophagy. *Autophagy* 9, 1443–1448.
- Mallik, R., and Chowdhury, T.A.** (2018). Metformin in cancer. *Diabetes Res. Clin. Pract.* 143, 409–419.
- Martínez-Reyes, I., and Chandel, N.S.** (2020). Mitochondrial TCA cycle metabolites control physiology and disease. *Nat. Commun.* 11, 1–11.
- Mayer, C., and Grummt, I.** (2006). Ribosome biogenesis and cell growth: mTOR coordinates transcription by all three classes of nuclear RNA polymerases. *Oncogene* 25, 6384–6391.
- Meiners, S., and Ballweg, K.** (2014). Proteostasis in pediatric pulmonary pathology. *Mol. Cell. Pediatr.* 1, 1–8.
- Meiners, S., Heyken, D., Weller, A., Ludwig, A., Stangl, K., Kloetzel, P.-M.M., Krüger, E., Ludwig, A., Stangl, K., Kloetzel, P.-M.M., and Krüger, E.** (2003). Inhibition of Proteasome Activity Induces Concerted Expression of Proteasome Genes and de Novo Formation of Mammalian Proteasomes. *J. Biol. Chem.* 278, 21517–21525.
- Meiners, S., Ludwig, A., Lorenz, M., Dreger, H., Baumann, G., Stangl, V., and Stangl, K.** (2006). Nontoxic proteasome inhibition activates a protective antioxidant defense response in endothelial cells. *Free Radic. Biol. Med.* 40, 2232–2241.
- Meul, T., Berschneider, K., Schmitt, S., Mayr, C.H., Mattner, L.F., Schiller, H.B., Yazgili, A., Wang, X., Lukas, C., Prehn, C., Adamski, J., Graf, E., Schwarzmayr, T., Perocci, F., Kukat, A., Trifunovic, A., Kremer, L., Prokisch, H., et al.** (2020). Adaptive mitochondrial regulation of the proteasome. *BioRxiv Cell Biol.* 2020.04.07.026161.
- Mitch, W.E., and Goldberg, A.L.** (1996). Mechanisms of disease: Mechanisms of muscle wasting: The role of the ubiquitin-proteasome pathway. *N. Engl. J. Med.* 335, 1897–1905.

- Moreno, D., Viana, R., and Sanz, P.** (2009). Two-hybrid analysis identifies PSMD11, a non-ATPase subunit of the proteasome, as a novel interaction partner of AMP-activated protein kinase. *Int J Biochem Cell Biol.* 41, 2431–2439.
- Motwani, M., Pesiridis, S., and Fitzgerald, K.A.** (2019). DNA sensing by the cGAS–STING pathway in health and disease. *Nat. Rev. Genet.* 20, 657–674.
- Mullen, A.R., Wheaton, W.W., Jin, E.S., Chen, P.H., Sullivan, L.B., Cheng, T., Yang, Y., Linehan, W.M., Chandel, N.S., and DeBerardinis, R.J.** (2012). Reductive carboxylation supports growth in tumour cells with defective mitochondria. *Nature* 481, 385–388.
- Mullen, A.R., Hu, Z., Shi, X., Jiang, L., Boroughs, L.K., Kovacs, Z., Boriack, R., Rakheja, D., Sullivan, L.B., Linehan, W.M., Chandel, N.S., and DeBerardinis, R.J.** (2014). Oxidation of alpha-ketoglutarate is required for reductive carboxylation in cancer cells with mitochondrial defects. *Cell Rep.* 7, 1679–1690.
- Murata, S., Yashiroda, H., and Tanaka, K.** (2009). Molecular mechanisms of proteasome assembly. *Nat. Rev. Mol. Cell Biol.* 10, 104–115.
- Nathan, J.A., Spinnenhirn, V., Schmidtke, G., Basler, M., Groettrup, M., and Goldberg, A.L.** (2013). Immuno- and Constitutive Proteasomes Do Not Differ in Their Abilities to Degrade Ubiquitinated Proteins. *Cell* 152, 1184–1194.
- Nunnari, J., and Suomalainen, A.** (2012). Mitochondria: In sickness and in health. *Cell* 148, 1145–1159.
- Panasenko, O.O., and Collart, M.A.** (2011). Not4 E3 Ligase Contributes to Proteasome Assembly and Functional Integrity in Part through Ecm29. *Mol. Cell. Biol.* 31, 1610–1623.
- Papa, L., and Germain, D.** (2011). Estrogen receptor mediates a distinct mitochondrial unfolded protein response. *J. Cell Sci.* 124, 1396–1402.
- Pathare, G.R., Nagy, I., Bohn, S., Unverdorben, P., Hubert, A., Korner, R., Nickell, S., Lasker, K., Sali, A., Tamura, T., Nishioka, T., Forster, F., Baumeister, W., Bracher, A., Körner, R., Nickell, S., Lasker, K., Sali, A., et al.** (2012). The proteasomal subunit Rpn6 is a molecular clamp holding the core and regulatory subcomplexes together. *Proc. Natl. Acad. Sci. U. S. A.* 109, 149–154.
- Picard, M., Zhang, J., Hancock, S., Derbeneva, O., Golhar, R., Golik, P., O’Hearn, S., Levy, S., Potluri, P., Lvova, M., Davila, A., Lin, C.S., Perin, J.C., Rappaport, E.F., Hakonarson, H., Trounce, I.A., Procaccio, V., and Wallace, D.C.** (2014). Progressive increase in mtDNA 3243A>G heteroplasmy causes abrupt transcriptional reprogramming. *Proc. Natl. Acad. Sci.* 111, E4033–E4042.
- Picard, M., Wallace, D.C., and Burrelle, Y.** (2016). The rise of mitochondria in medicine. *Mitochondrion* 30, 105–116.
- Pickering, A.M., and Davies, K.J.A.** (2012). Differential roles of proteasome and immunoproteasome regulators Pa28 α , Pa28 γ and Pa200 in the degradation of oxidized proteins. *Arch. Biochem. Biophys.* 523, 181–190.
- Pickering, A.M., Linder, R. a, Zhang, H., Forman, H.J., and Davies, K.J. a** (2012). Nrf2-dependent induction of proteasome and Pa28 α regulator are required for adaptation to oxidative stress. *J. Biol. Chem.* 287, 10021–10031.

- Powers, E.T., and Balch, W.E.** (2013). Diversity in the origins of proteostasis networks - a driver for protein function in evolution. *Nat. Rev. Mol. Cell Biol.* *14*, 237–248.
- Quinlan, C.L., Perevoshchikova, I. V., Hey-Mogensen, M., Orr, A.L., and Brand, M.D.** (2013). Sites of reactive oxygen species generation by mitochondria oxidizing different substrates. *Redox Biol.* *1*, 304–312.
- Raule, M., Cerruti, F., Benaroudj, N., Migotti, R., Kikuchi, J., Bachi, A., Navon, A., Dittmar, G., and Cascio, P.** (2014). PA28 $\alpha\beta$ reduces size and increases hydrophilicity of 20S immunoproteasome peptide products. *Chem. Biol.* *21*, 470–480.
- Ravanelli, S., den Brave, F., and Hoppe, T.** (2020). Mitochondrial Quality Control Governed by Ubiquitin. *Front. Cell Dev. Biol.* *8*, 270.
- Rock, K.L., Gramm, C., Rothstein, L., Clark, K., Stein, R., Dick, L., Hwang, D., and Goldberg, A.L.** (1994). Inhibitors of the proteasome block the degradation of most cell proteins and the generation of peptides presented on MHC class I molecules. *Cell* *78*, 761–771.
- Rodenburg, R.J.** (2016). Mitochondrial complex I-linked disease. *Biochim. Biophys. Acta - Bioenerg.* *1857*, 938–945.
- Roelofs, J., Park, S., Haas, W., Tian, G., McAllister, F.E., Huo, Y., Lee, B.-H., Zhang, F., Shi, Y., Gygi, S.P., and Finley, D.** (2009). Chaperone-mediated pathway of proteasome regulatory particle assembly. *Nature* *459*, 861–865.
- Ronnebaum, S.M., Patterson, C., and Schisler, J.C.** (2014). Minireview: Hey U(PS): Metabolic and proteolytic homeostasis linked via AMPK and the ubiquitin proteasome system. *Mol. Endocrinol.* *28*, 1602–1615.
- Rousseau, A., and Bertolotti, A.** (2016). An evolutionarily conserved pathway controls proteasome homeostasis. *Nature* *536*, 184–189.
- Rousseau, A., and Bertolotti, A.** (2018). Regulation of proteasome assembly and activity in health and disease. *Nat. Rev. Mol. Cell Biol.* *19*, 697–712.
- Saeki, Y.** (2017). Ubiquitin recognition by the proteasome. *J. Biochem.* *161*, 113–124.
- Saleem, A., Safdar, A., Kitaoka, Y., Ma, X., Marquez, O.S., Akhtar, M., Nazli, A., Suri, R., Turnbull, J., and Tarnopolsky, M.A.** (2015). Polymerase gamma mutator mice rely on increased glycolytic flux for energy production. *Mitochondrion* *21*, 19–26.
- Sanchez-Rangel, E., and Inzucchi, S.E.** (2017). Metformin: clinical use in type 2 diabetes. *Diabetologia* *60*, 1586–1593.
- Sarman, F., Antonicka, H., and Shoubridge, E.A.** (2008). The A3243G tRNA^{Leu}(UUR) MELAS mutation causes amino acid misincorporation and a combined respiratory chain assembly defect partially suppressed by overexpression of EFTu and EFG2. *Hum. Mol. Genet.* *17*, 3697–3707.
- Saxton, R.A., and Sabatini, D.M.** (2017). mTOR Signaling in Growth, Metabolism, and Disease. *Cell* *168*, 960–976.

- Schapira, A.H., Cooper, J.M., Dexter, D., Jenner, P., Clark, J.B., and Marsden, C.D.** (1989). Mitochondrial complex I deficiency in Parkinson's disease. *Lancet (London, England)* *1*, 1269.
- Schiller, H.B., Fernandez, I.E., Burgstaller, G., Schaab, C., Scheltema, R.A., Schwarzmayr, T., Strom, T.M., Eickelberg, O., and Mann, M.** (2015). Time- and compartment-resolved proteome profiling of the extracellular niche in lung injury and repair. *Mol. Syst. Biol.* *11*, 819.
- Schmidt, M., and Finley, D.** (2013). Regulation of proteasome activity in health and disease. *Biochim. Biophys. Acta* *1843*, 13–25.
- Schmitt, S., Eberhagen, C., Weber, S., Aichler, M., and Zischka, H.** (2015). Isolation of mitochondria from cultured cells and liver tissue biopsies for molecular and biochemical analyses. In *Methods in Molecular Biology*, (Humana Press Inc.), pp. 87–97.
- Segref, A., Kevei, É., Pokrzywa, W., Schmeisser, K., Mansfeld, J., Livnat-Levanon, N., Ensenaer, R., Glickman, M.H., Ristow, M., Hoppe, T., Kevei, E., Pokrzywa, W., Schmeisser, K., Mansfeld, J., Livnat-Levanon, N., Ensenaer, R., Glickman, M.H., Ristow, M., et al.** (2014). Pathogenesis of human mitochondrial diseases is modulated by reduced activity of the ubiquitin/proteasome system. *Cell Metab.* *19*, 642–652.
- Seifert, U., Bialy, L.P., Ebstein, F., Bech-Otschir, D., Voigt, A., Schröter, F., Prozorovski, T., Lange, N., Steffen, J., Rieger, M., Kuckelkorn, U., Aktas, O., Kloetzel, P.M., and Krüger, E.** (2010). Immunoproteasomes preserve protein homeostasis upon interferon-induced oxidative stress. *Cell* *142*, 613–624.
- Semren, N., Welk, V., Korfei, M., Keller, I.E., Fernandez, I.E., Adler, H., Günther, A., Eickelberg, O., Meiners, S., Gunther, A., Eickelberg, O., Meiners, S., Günther, A., Eickelberg, O., Meiners, S., Semren, A.N., Welk, V., Korfei, M., et al.** (2015). Regulation of 26S proteasome activity in pulmonary fibrosis. *Am. J. Respir. Crit. Care Med.* *192*, 1089–1101.
- Sha, Z., and Goldberg, A.L.** (2014). Proteasome-mediated processing of Nrf1 is essential for coordinate induction of all proteasome subunits and p97. *Curr. Biol.* *24*, 1573–1583.
- Shanske, S., Coku, J., Lu, J., Ganesh, J., Krishna, S., Tanji, K., Bonilla, E., Naini, A.B., Hirano, M., and DiMauro, S.** (2008). The G13513A mutation in the ND5 gene of mitochondrial DNA as a common cause of MELAS or Leigh syndrome: Evidence from 12 cases. *Arch. Neurol.* *65*, 368–372.
- Shi, C.X., Kortüm, K.M., Zhu, Y.X., Bruins, L.A., Jedlowski, P., Votruba, P.G., Luo, M., Stewart, R.A., Ahmann, J., Braggio, E., and Stewart, A.K.** (2017). CRISPR genome-wide screening identifies dependence on the proteasome subunit PSMC6 for bortezomib sensitivity in multiple myeloma. *Mol. Cancer Ther.* *16*, 2862–2870.
- Shim, S.M., Lee, W.J., Kim, Y., Chang, J.W., Song, S., and Jung, Y.K.** (2012). Role of S5b/PSMD5 in Proteasome Inhibition Caused by TNF- α /NF κ B in Higher Eukaryotes. *Cell Rep.* *2*, 603–615.
- Shiori Akabane, A., Uno, M., Tani, N., Kato, H., Kosako, H., and Oka, T.** (2016). PKA Regulates PINK1 Stability and Parkin Recruitment to Damaged Mitochondria through Phosphorylation of MIC60.
- Smith, D.M., Kafri, G., Cheng, Y., Ng, D., Walz, T., and Goldberg, A.L.** (2005). ATP binding to PAN or the 26S ATPases causes association with the 20S proteasome, gate opening, and translocation of unfolded proteins. *Mol. Cell* *20*, 687–698.

- Sousa, J.S., D’Imprima, E., and Vonck, J.** (2018). Mitochondrial respiratory chain complexes. In *Subcellular Biochemistry*, (Springer New York), pp. 167–227.
- Spinelli, J.B., and Haigis, M.C.** (2018). The multifaceted contributions of mitochondria to cellular metabolism. *Nat. Cell Biol.* *20*, 745–754.
- Stadtmueller, B.M., and Hill, C.P.** (2011). Proteasome Activators. *Mol. Cell* *41*, 8–19.
- Sullivan, L.B., Gui, D.Y., Hosios, A.M., Bush, L.N., Freinkman, E., and Vander Heiden, M.G.** (2015). Supporting Aspartate Biosynthesis Is an Essential Function of Respiration in Proliferating Cells. *Cell* *162*, 552–563.
- Sullivan, L.B., Gui, D.Y., and Van Der Heiden, M.G.** (2016). Altered metabolite levels in cancer: Implications for tumour biology and cancer therapy. *Nat. Rev. Cancer* *16*, 680–693.
- Sullivan, L.B., Luengo, A., Danai, L. V., Bush, L.N., Diehl, F.F., Hosios, A.M., Lau, A.N., Elmiligy, S., Malstrom, S., Lewis, C.A., and Vander Heiden, M.G.** (2018). Aspartate is an endogenous metabolic limitation for tumour growth. *Nat. Cell Biol.* *20*, 782–788.
- Suresh, B., Lee, J., Kim, K.-S., and Ramakrishna, S.** (2016). The Importance of Ubiquitination and Deubiquitination in Cellular Reprogramming. *Stem Cells Int.* *2016*.
- Taanman, J.W.** (1999). The mitochondrial genome: Structure, transcription, translation and replication. *Biochim. Biophys. Acta - Bioenerg.* *1410*, 103–123.
- Thoreen, C.C., Chantranupong, L., Keys, H.R., Wang, T., Gray, N.S., and Sabatini, D.M.** (2012). A unifying model for mTORC1-mediated regulation of mRNA translation. *Nature* *485*, 109–113.
- Tomko, R.J., Funakoshi, M., Schneider, K., Wang, J., and Hochstrasser, M.** (2010). Heterohexameric Ring Arrangement of the Eukaryotic Proteasomal ATPases: Implications for Proteasome Structure and Assembly. *Mol. Cell* *38*, 393–403.
- Trifunovic, A., Wredenberg, A., Falkenberg, M., Spelbrink, J.N., Rovio, A.T., Bruder, C.E., Bohlooly, Y.-M., Gidlöf, S., Oldfors, A., Wibom, R., Törnqvist, J., Jacobs, H.T., and Larsson, N.-G.** (2004). Premature ageing in mice expressing defective mitochondrial DNA polymerase. *Nature* *429*, 417–423.
- Trifunovic, A., Hansson, A., Wredenberg, A., Rovio, A.T., Dufour, E., Khvorostov, I., Spelbrink, J.N., and HT Jacobs, R.W., and Larsson, N.-G.** (2005). Somatic mtDNA mutations cause aging phenotypes without affecting reactive oxygen species production. *Proc Natl Acad Sci* *102*, 17993–17998.
- Trudeau, F.** (2008). Aspartate as an ergogenic supplement. *Sport. Med.* *38*, 9–16.
- Tsvetkov, P., Myers, N., Eliav, R., Adamovich, Y., Hagai, T., Adler, J., Navon, A., and Shaul, Y.** (2014). NADH Binds and stabilizes the 26S proteasomes independent of ATP. *J. Biol. Chem.* *289*, 11272–11281.
- Tsvetkov, P., Mendillo, M.L., Zhao, J., Carette, J.E., Merrill, P.H., Cikes, D., Varadarajan, M., van Diemen, F.R., Penninger, J.M., Goldberg, A.L., Brummelkamp, T.R., Santagata, S., and Lindquist, S.** (2015). Compromising the 19S proteasome complex protects cells from reduced flux through the proteasome. *Elife* *4*.

- Tsvetkov, P., Sokol, E., Jin, D., Brune, Z., Thiru, P., Ghandi, M., Garraway, L.A., Gupta, P.B., Santagata, S., Whitesell, L., and Lindquist, S.** (2017). Suppression of 19S proteasome subunits marks emergence of an altered cell state in diverse cancers. *Proc. Natl. Acad. Sci. U. S. A.* *114*, 382–387.
- Tuppen, H.A.L., Blakely, E.L., Turnbull, D.M., and Taylor, R.W.** (2010). Mitochondrial DNA mutations and human disease. *Biochim. Biophys. Acta - Bioenerg.* *1797*, 113–128.
- Tyanova, S., Temu, T., Sinitcyn, P., Carlson, A., Hein, M.Y., Geiger, T., Mann, M., and Cox, J.** (2016). The Perseus computational platform for comprehensive analysis of (prote)omics data. *Nat. Methods* *13*, 731–740.
- Ullrich, O., Siems, W.G., Lehmann, K., Huser, H., Ehrlich, W., and Grune, T.** (1996). Inhibition of poly(ADP-ribose) formation by 4-hydroxynonenal in primary cultures of rabbit synovial fibroblasts. *Biochem. J.* *315* (Pt 3, 705–708.
- Verdoes, M., Florea, B.I., Menendez-Benito, V., Maynard, C.J., Witte, M.D., van der Linden, W.A., van den Nieuwendijk, A.M.C.H., Hofmann, T., Berkers, C.R., van Leeuwen, F.W.B., Groothuis, T.A., Leeuwenburgh, M.A., Ovaa, H., Neefjes, J.J., Filippov, D. V., van der Marel, G.A., Dantuma, N.P., and Overkleeft, H.S.** (2006). A Fluorescent Broad-Spectrum Proteasome Inhibitor for Labeling Proteasomes In Vitro and In Vivo. *Chem. Biol.* *13*, 1217–1226.
- Verdoes, M., Willems, L.I., Van Der Linden, W.A., Duivenvoorden, B.A., Van Der Marel, G.A., Florea, B.I., Kisselev, A.F., and Overkleeft, H.S.** (2010). A panel of subunit-selective activity-based proteasome probes. *Org. Biomol. Chem.* *8*, 2719–2727.
- VerPlank, J.J.S., and Goldberg, A.L.** (2017). Regulating protein breakdown through proteasome phosphorylation. *Biochem. J.* *474*, 3355–3371.
- VerPlank, J.J.S., Lokireddy, S., Zhao, J., and Goldberg, A.L.** (2019). 26S Proteasomes are rapidly activated by diverse hormones and physiological states that raise cAMP and cause Rpn6 phosphorylation. *Proc. Natl. Acad. Sci.* *116*, 4228–4237.
- De Verteuil, D., Muratore-Schroeder, T.L., Granados, D.P., Fortier, M.H., Hardy, M.P., Bramoullé, A., Caron, É., Vincent, K., Mader, S., Lemieux, S., Thibault, P., and Perreault, C.** (2010). Deletion of immunoproteasome subunits imprints on the transcriptome and has a broad impact on peptides presented by major histocompatibility complex I molecules. *Mol. Cell. Proteomics* *9*, 2034–2047.
- Vial, G., Detaille, D., and Guigas, B.** (2019). Role of Mitochondria in the Mechanism(s) of Action of Metformin. *Front. Endocrinol. (Lausanne)*. *10*, 294.
- Viana, R., Aguado, C., Esteban, I., Moreno, D., Viollet, B., Knecht, E., and Sanz, P.** (2008). Role of AMP-activated protein kinase in autophagy and proteasome function. *Biochem Biophys Res Commun.* *369*, 964–968.
- Vilchez, D., Boyer, L., Morante, I., Lutz, M., Merkwirth, C., Joyce, D., Spencer, B., Page, L., Masliah, E., Berggren, W.T., Gage, F.H., and Dillin, A.** (2012). Increased proteasome activity in human embryonic stem cells is regulated by PSMD11. *Nature* *489*, 304–308.
- Walerych, D., Lisek, K., Sommaggio, R., Piazza, S., Ciani, Y., Dalla, E., Rajkowska, K., Gaweda-Walerych, K., Ingallina, E., Tonelli, C., Morelli, M.J., Amato, A., Eterno, V., Zambelli, A., Rosato, A., Amati, B., Wiśniewski, J.R., and Del Sal, G.** (2016). Proteasome machinery is instrumental in a common gain-of-function program of the p53 missense mutants in cancer. *Nat. Cell Biol.* *18*, 897–909.

- Wang, X., Jiang, B., and Zhang, Y.** (2016). Gankyrin regulates cell signaling network. *Tumour Biol.* 37, 5675–5682.
- Wang, X., Meul, T., and Meiners, S.** (2020). Exploring the proteasome system: A novel concept of proteasome inhibition and regulation. *Pharmacol. Ther.* 211.
- Wang, Y., An, H., Liu, T., Qin, C., Sesaki, H., Guo, S., Radovick, S., Hussain, M., Maheshwari, A., Wondisford, F.E., O'Rourke, B., and He, L.** (2019). Metformin Improves Mitochondrial Respiratory Activity through Activation of AMPK. *Cell Rep.* 29, 1511-1523.e5.
- Weidberg, H., and Amon, A.** (2018). MitoCPR—A surveillance pathway that protects mitochondria in response to protein import stress. *Science (80-.).* 360.
- Welk, V., Coux, O., Kleene, V., Abeza, C., Truembach, D., Eickelberg, O., and Meiners, S.** (2016). Inhibition of Proteasome Activity Induces Formation of Alternative Proteasome Complexes. *J. Biol. Chem.* 291, 13147–13159.
- Wolfson, R.L., and Sabatini, D.M.** (2017). The Dawn of the Age of Amino Acid Sensors for the mTORC1 Pathway. *Cell Metab.* 26, 301–309.
- Woo, D.K., Green, P.D., Santos, J.H., D'Souza, A.D., Walther, Z., Martin, W.D., Christian, B.E., Chandel, N.S., and Shadel, G.S.** (2012). Mitochondrial genome instability and ROS enhance intestinal tumorigenesis in APC Min/+ mice. *Am. J. Pathol.* 180, 24–31.
- Wrobel, L., Topf, U., Bragoszewski, P., Wiese, S., Sztolsztener, M.E., Oeljeklaus, S., Varabyova, A., Lirski, M., Chroscicki, P., Mroczek, S., Januszewicz, E., Dziembowski, A., Koblowska, M., Warscheid, B., and Chacinska, A.** (2015). Mistargeted mitochondrial proteins activate a proteostatic response in the cytosol. *Nature* 524, 485–488.
- Xie, D., Wu, X., Lan, L., Shangguan, F., Lin, X., Chen, F., Xu, S., Zhang, Y., Chen, Z., Huang, K., Wang, R., Wang, L., Song, X., Liu, Y., and Lu, B.** (2016). Downregulation of TFAM inhibits the tumorigenesis of non-small cell lung cancer by activating ROS-mediated JNK/p38MAPK signaling and reducing cellular bioenergetics. *Oncotarget* 7, 11609–11624.
- Xu, J., Wang, S., Viollet, B., and Zou, M.-H.** (2012). Regulation of the proteasome by AMPK in endothelial cells: the role of O-GlcNAc transferase (OGT). *PLoS One* 7, e36717.
- Yu, C., Wang, X., Huszagh, A.S., Viner, R., Novitsky, E.J., Rychnovsky, S.D., and Huang, L.** (2019). Probing H₂O₂-mediated Structural Dynamics of the Human 26S Proteasome Using Quantitative Cross-linking Mass Spectrometry (QXL-MS). *Mol. Cell. Proteomics.*
- Zhang, Y., and Manning, B.D.** (2015). mTORC1 signaling activates NRF1 to increase cellular proteasome levels. *Cell Cycle* 14, 2011–2017.
- Zhang, F., Su, K., Yang, X., Bowe, D.B., Paterson, A.J., and Kudlow, J.E.** (2003). O-GlcNAc modification is an endogenous inhibitor of the proteasome. *Cell* 115, 715–725.
- Zhang, X., Schulz, R., Edmunds, S., Krüger, E., Markert, E., Gaedcke, J., Cormet-Boyaka, E., Ghadimi, M., Beissbarth, T., Levine, A.J., Moll, U.M., and Dobbelstein, M.** (2015). MicroRNA-101 Suppresses Tumor Cell Proliferation by Acting as an Endogenous Proteasome Inhibitor via Targeting the Proteasome Assembly Factor POMP. *Mol. Cell* 59, 243–257.

- Zhang, Y., Nicholatos, J., Dreier, J.R., Ricoult, S.J.H., Widenmaier, S.B., Hotamisligil, G.S., Kwiatkowski, D.J., and Manning, B.D.** (2014). Coordinated regulation of protein synthesis and degradation by mTORC1. *Nature* 513, 440–443.
- Zhao, J., Zhai, B., Gygi, S.P., and Goldberg, A.L.** (2015). MTOR inhibition activates overall protein degradation by the ubiquitin proteasome system as well as by autophagy. *Proc. Natl. Acad. Sci. U. S. A.* 112, 15790–15797.
- Zhao, R.Z., Jiang, S., Zhang, L., and Yu, Z. Bin** (2019). Mitochondrial electron transport chain, ROS generation and uncoupling (Review). *Int. J. Mol. Med.* 44, 3–15.
- Zischka, H., Larochette, N., Hoffmann, F., Hamöller, D., Jägemann, N., Lichtmanegger, J., Jennen, L., Müller-Höcker, J., Roggel, F., Göttlicher, M., Vollmer, A.M., and Kroemer, G.** (2008). Electrophoretic analysis of the mitochondrial outer membrane rupture induced by permeability transition. *Anal. Chem.* 80, 5051–5058.
- Zukunft, S., Sorgenfrei, M., Prehn, C., Möller, G., and Adamski, J.** (2013). Targeted Metabolomics of Dried Blood Spot Extracts. *Chromatographia* 76, 1295–1305.

Abbreviations

A

ABP	activity-based probe
AA	Amino acid
ADP	adenosine diphosphate
AMP	adenosine monophosphate
AMPK	AMP activated protein kinase
ANOVA	Analysis of variance
ATP	adenosine triphosphate
ATP5A	ATP synthase subunit alpha

B

BCA	bicinchoninic acid
-----	--------------------

C

°C	degree Celsius
cAMP	cyclic AMP
C-L	caspase-like
<i>C. elegans</i>	<i>Caenorhabditis elegans</i>
cDNA	complementary DNA
CHX	cycloheximide
cm	centimeter
CO ₂	carbon dioxide
CP	core particle
CPC	Comprehensive Pneumology Center
CT-L	chymotrypsin-like
ctrl	control

D

Da	dalton
DAPI	4',6-diamidin-2-phenylindol
DMEM	Dulbecco's modified Eagle's medium
DMSO	dimethyl sulfoxide
DNA	deoxyribonucleic acid
DTT	dithiothreitol

E

EDTA	ethylenediaminetetraacetate
EGTA	ethyleneglycoltetraacetate
EM	electron microscopy
ER	endoplasmic reticulum
ERAD	ER associated degradation
ERAP	ER aminopeptidase
ETC	electron transport chain

F

FAD	flavin adenine dinucleotide
FBS	fetal bovine serum
FCCP	Carbonyl cyanide-4-(trifluoromethoxy)phenylhydrazone
FDR	false discovery rate
FoxO	forkhead box class O
FPKM	fragments per kilobase of exon model per million reads mapped

G

g gram
GAPDH Glyceraldehyde 3-phosphate dehydrogenase

H

h hour(s)
HEPES 4-(2-hydroxyethyl)-1-piperazineethanesulfonic acid
HMGU Helmholtz Zentrum München - Deutsches Forschungszentrum für Gesundheit und Umwelt
HRP horseradish peroxidase
HPRT hypoxanthine-guanine phosphoribosyltransferase

I

IDPs intrinsically disordered proteins
ILBD Institute for Lung Biology and Disease
ILD interstitial lung disease
INF interferon
IMS intermembrane space

K

K48 lysine 48
kDa kilodalton
kg kilogram

L

LC-MS/MS liquid chromatography tandem mass spectrometry
LDH lactate dehydrogenase
LMP low molecular mass protein
LPS Lipopolysaccharide

M

M molar
mA milliampere
MECL-1 multicatalytic endopeptidase complex-like 1
MEFs mouse embryonic fibroblasts
MDa megadalton
MHC major histocompatibility complex
µg mikrogram
mM millimolar
µL mikroliter
µm micrometer
min minute
mL milliliter
mRNA messenger ribonucleic acid
ms milliseconds
mt mitochondrial
mtUPR mitochondrial unfolded protein response
mTOR mammalian target of rapamycin
MTT 3-(4,5-dimethylthiazol-2-yl)-2,5 diphenyltetrazolium bromide

N

NAC N-acetyl cysteine
NAD Nicotinamide adenine dinucleotide
nm nanometer
ND5 NADH-ubiquinone oxidoreductase chain 5 protein
NRF-1/2 nuclear factor erythroid 2-related factor 1/2

O

O-GlcNAc	O-Linked β -N-acetylglucosamine
OPP	O-propargyl-puromycin
OXPPOS	oxidative phosphorylation

P

%	percent
PA200	proteasome activator 200 kDa
PA28	proteasome activator 28 kDa
PAC	proteasome assembly chaperone
PAGE	polyacrylamide gel electrophoresis
PARP	poly (ADP-ribose) polymerase
PBS	phosphate buffered saline
phLF	primary human lung fibroblasts
phSF	primary human skin fibroblasts
PI31	proteasome inhibitor 31 kDa
PINK	PTEN-induced kinase 1
PKA	protein kinase A
Pol G	DNA polymerase subunit gamma
Pomp	proteasome maturation protein
PSMA	proteasome subunit alpha type
PSMB	proteasome subunit alpha type
PSMC	26S proteasome ATPase regulatory subunit
PSMD	26S proteasome non-ATPase regulatory subunit
PTM	post-translational modification
PVDF	polyvinylidenedifluoride

Q

qPCR	quantitative polymerase chain reaction
------	--

R

RC	respiratory chain
RNAi	ribonucleic acid interference
ROS	reactive oxygen species
RP	regulatory particle
RPL19	ribosomal protein 19
rpm	revolutions per minute
RPN	regulatory particle non-ATPase
RPT	regulatory particle ATPase
rRNA	ribosomal RNA
RT	reverse transcriptase
RT	room temperature
RT-PCR	real time PCR

S

SDS	sodium dodecyl sulfate
SEM	standard error of the mean
siRNA	small interfering ribonucleic acid
SIRT1	NAD-dependent deacetylase sirtuin-1

T

TCA cycle	tricarboxylic acid cycle
T-L	trypsin-like
TNF	tumor necrosis factor
t-RNA	transfer RNA
Tris	Tris(hydroxymethyl)-aminomethane

U

U unit
UBIK48 proteins ubiquitinated at lysine 48
UPR unfolded protein response
UPS ubiquitin-proteasome system

V

V Volt

W

WB Western blot
WT wildtype

X

xg times gravity

Y**Z**